DISSERTATIONES PHYSICAE UNIVERSITATIS TARTUENSIS
64

DISSERTATIONES PHYSICAE UNIVERSITATIS TARTUENSIS
64

MAIT MÜNTEL

Detection of doubly charged higgs boson in the CMS detector

TARTU UNIVERSITY
PRESS

This study was carried out at the National Institute of Chemical Physics and Biophysics, Tallinn and the University of Tartu, Estonia.

The Dissertation was admitted on Okt 17, 2008, in partial fulfillment of the requirements for the degree of Doctor of Philosophy in physics (theoretical physics), and allowed for defense by the Council of Institute of Physics, University of Tartu.

Supervisor: Dr. Martti Raidal,
National Institute of Chemical Physics and Biophysics,
Tallinn, Estonia

Opponents: Dr. Oxana Smirnova
Lund University
Lund, Sweden

Dr. Margus Saal
Tartu Observatory
Tõravere, Estonia

Defense: December 5, 2008, University of Tartu, Estonia

ISSN 1406–0647
ISBN 978–9949–19–002–7 (trükis)
ISBN 978–9949–19–003–4 (PDF)

Tartu Ülikooli Kirjastus
www.tyk.ee
Tellimuse nr 495

Contents

List of related publications

This thesis consists of an introductory and linking review part, followed by five research publications [I–V]. The relevant publications are listed below.

I M. Raidal *et al.*, "Flavour physics of leptons and dipole moments," EPJ. C **57** (2008) 715 [arXiv:0801.1826].

II G. L. Bayatian *et al.* [CMS Collaboration], "CMS technical design report, volume II: Physics performance," J. Phys. G **34** (2007) 995.

III A. Hektor, M. Kadastik, M. Müntel, M. Raidal, and L. Rebane., "Testing neutrino masses in little Higgs models via discovery of doubly charged Higgs at LHC," Nucl. Phys. B **787** (2007) 198 [arXiv:0705.1495].

IV B. C. Allanach *et al.*, "Les Houches 'physics at TeV colliders 2005' beyond the standard model working group: Summary report," (2006) [arXiv:hep-ph/0602198].

V A. Hektor, M. Kadastik, K. Kannike, M. Müntel, M. Raidal, "Studying doubly charged Higgs pair production at the LHC," Estonian Acad. Sci. Phys. Math. **55(2)** (2006) 128.

Author's Contribution

In publication I, the author's contribution is section 5.1.4 "Low scale triplet Higgs neutrino mass scenarios in Litte Higgs models".
In publication II, the author's contribution is section 12.2.2, "Search for final states with τ leptons", which is based on an internal CMS Analysis Note CMS AN 2006/081 (also attached to the thesis).
In publication III, the dissertant gave the idea of handling τ leptons, derived selection rules and performed statistical analysis.
In publication IV, the author's contribution is part 28. The dissertant performed all reconstruction simulations and derived selection rules.
In publication V, the dissertant performed all MC simulations.

Other publications of the dissertant

VI S. Chatrchyan *et al.* [CMS Collaboration], "The CMS Experiment at the CERN LHC," JINST **3**, S08004 (2008).

VII F. del Aguila *et al.* [CMS Collaboration], "Collider aspects of flavour physics at high Q," Eur. Phys. J. C, (2008), [arXiv:0801.1800].

VIII D. G. d'Enterria *et al.* [CMS Collaboration], "CMS Physics Technical Design Report: Addendum on High Density QCD with Heavy Ions," J. Phys. G **34**, (2007) 2307.

IX G. L. Bayatian *et al.* [CMS Collaboration], "CMS physics: Technical design report," CERN-LHCC-2006-001, (2006).

X G. L. Bayatian *et al.* [CMS Collaboration], "CMS Physics TDR 8.2 Volume II: Physics Performance," CERN-LHCC 2006-021, (2006).

Chapter 1

Introduction

The mechanism that gives masses to the elementary particles is not known to this day. The most studied candidate is the so-called Higgs mechanism in the Standard Model of elementary particles. There is a particular extension of the Standard Model, the Littlest Higgs model.

From the collider physics point of view it is interesting because it predicts the existence of new particles and also there is an exciting connection to the neutrino physics. With the introduction of scalar triplet Higgs, the current neutrino mass problem can be solved. This thesis is dedicated to the search for the experimental signatures that can lead to the discovery of the scalar triplet component called doubly charged Higgs boson. Several Monte Carlo studies have been carried out to derive appropriate selection rules to distinguish the new particles from the Standard Model background.

This thesis is organized as follows. In the beginning there is a short overview of the Large Hadron Collider (LHC) accelerator and Compact Muon Solenoid (CMS) detector in Chapter 2. Chapter 3 discusses the electroweak symmetry breaking (EWSB) problem and conventional solutions in supersymmetry (SUSY). The Little Higgs framework as an alternative to SUSY is introduced and related to neutrino physics and experimental phenomenology at LHC. In Chapter 4 the principles of Monte Carlo (MC) simulation experiments are described in context of CMS software environment and relevant characteristics of the performance of the detector are outlined. In Chapter 5 the detection possibilities of doubly charged Higgs boson in CMS experiment are shown. Chapter 6 contains conclusions. The summaries of the related publications are given in the Chapter 7.

Chapter 2

CMS Detector at CERN

2.1 Large Hadron Collider

The Large Hadron Collider (LHC) is a circular particle accelerator at CERN (European Organization of Nuclear Research) [25] whose circumference is 27 km (Figure 2.1). A main goal for the project is expected discovery of the Higgs boson predicted by the mechanism of electroweak symmetry breaking in the SM.

The LHC is installed to the tunnel of the previous accelerator LEP (Large Electron Positron) [26] and started operation in October 2008 after more than a decade of construction. Its beam energy is designed to reach 7+7 TeV and luminosity up to $\mathcal{L} = 10^{34}$ cm^{-2}s^{-1}, that is seven-fold increase in energy and a hundred-fold increase in integrated luminosity over the current hadron collider experiments.

There are four experiments located in the LHC tunnel: CMS (Compact Muon Solenoid) [15], ATLAS (A Toroidal LHC ApparatuS) [13, 14], LHCb (Large Hadron Collider beauty) [16] and ALICE (A Large Ion Collider Experiment) [17]. CMS and ATLAS are general multipurpose detectors for investigating electroweak symmetry breaking through Higgs boson, looking for phenomena beyond the Standard Model (supersymmetry), and to study the high-Q^2 region in more detail. ALICE in designed to investigate heavy ion physics (quark-gluon plasma) and LHCb is dedicated to b-physics and CP-violation studies.

The LHC consists of several accelerator units (Figure 2.2). Two linear accelerators LINAC2 and LINAC3 are used for the initial acceleration up to 50 MeV and up to 1.4 GeV by booster. Then the beam is injected into the PS (Proton Synchrotron) where protons gain energy of 26 GeV

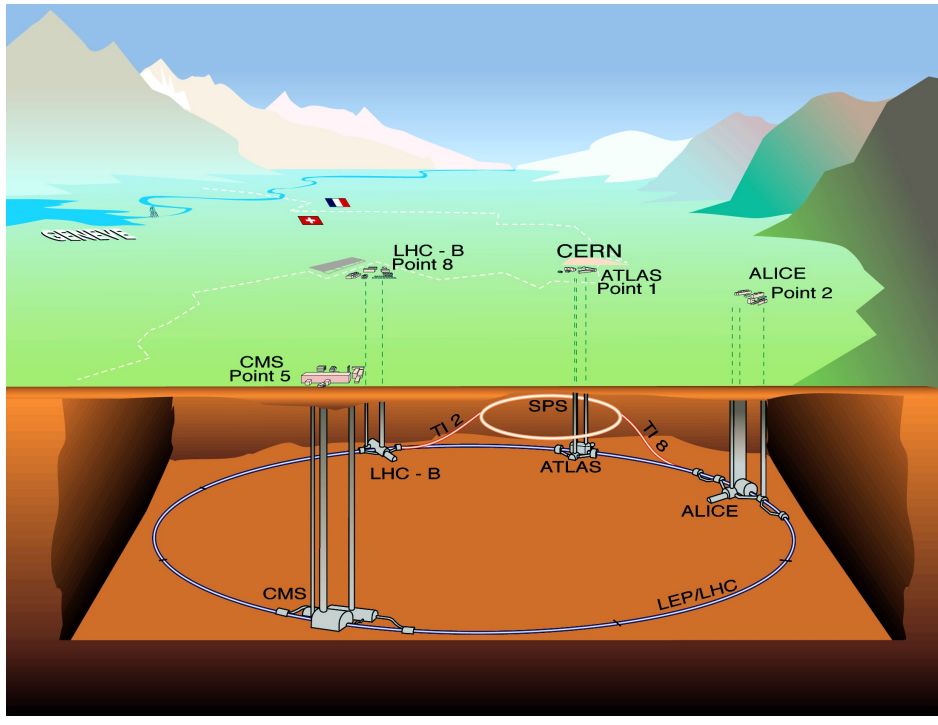

Figure 2.1: The Large Hadron Collider experimental sites above and underground, seen from the north side of the ring.

with the final bunch structure. The next stage is SPS (Super PS) and finally particles are injected into the LHC near IP2 or IP8 depending on the circulation direction. At LHC the particles are accelerated from 450 GeV to 7 TeV (for proton beam).

To achieve such an high energy new types of superconducting magnets had to be developed. The magnetic field that is needed is $B = 8.33$ T. There are 1232 main dipoles around the ring, each of 35 tons and 15 m long. Superconducting magnets are operating at superfluid He temperatures 1.9 K.

The beam consists of 2808 bunches, each bunch contains 1.14×10^{11} protons (at full luminosity $\mathcal{L} = 10^{34}$ cm^{-2}s^{-1}). At the collision point the bunch has longitudinal spread 7.5 cm. The transverse dimensions of the beam are about one millimeter, but at the collision point is is squeezed by 400 quadrupole magnets to 15 μm. The spacing of bunches in time is 25 ns and in space 7.5 m. Due to the filling scheme of the SPS, the structure

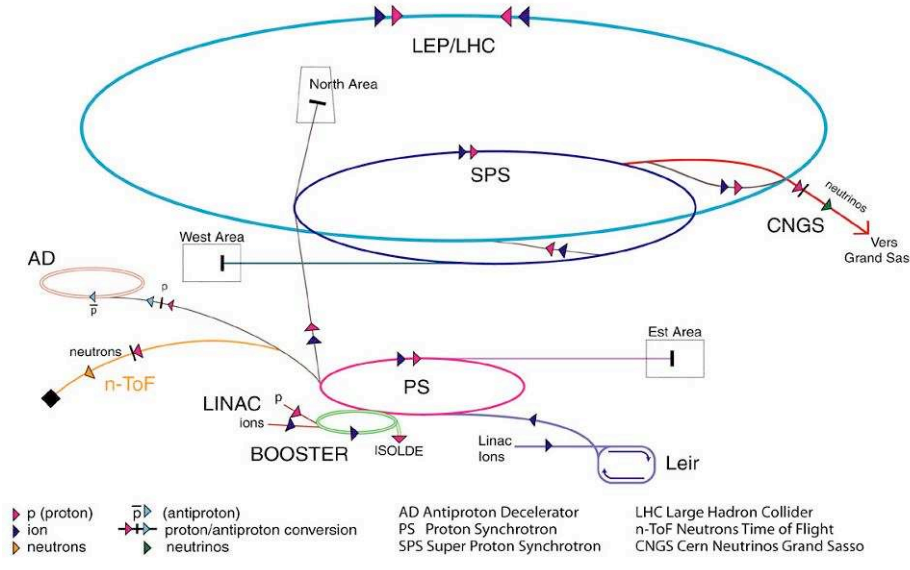

Figure 2.2: Accelerator complex at CERN, the LHC beam is prepared by several smaller facilities.

of the bunch spacing is quite complex. The gaps between bunches are used for the calibration, synchronization, and resetting the front-end electronics.

The number of interactions or event rate R can be expressed as $R = \mathcal{L} \times \sigma$, where $\mathcal{L}$ is the luminosity and σ is the cross section. For inelastic pp collision (minimum bias events) σ is 60 mb, that makes 6×10^8 events per second. This is approximately 25 collision per bunch crossing, meaning that the rare interesting events are superimposed (piled-up) by many minimum bias events.

The luminosity $\mathcal{L}$ of an accelerator is defined as

$$\mathcal{L} = f \frac{n_1 n_2}{4\pi\sigma_x\sigma_y} \tag{2.1}$$

where n_1 and n_2 are number of particles in the colliding bunches, f is frequency of the collisions, and σ_x and σ_y characterize the Gaussian transverse beam profiles. The luminosity is not constant in LHC, but decays exponentially as $\mathcal{L} = \mathcal{L}_0 e^{-i\tau\mathcal{L}}$ due to the degeneration of the beam. The decay time of the bunch intensity is written as

$$\tau_{col} = \frac{N_{tot,0}}{\mathcal{L}\sigma_{tot}k}, \tag{2.2}$$

Circumference	26 659 m
Dipole operating temperature	1.9 K (-271.3 C)
Number of dipoles	1232
Number of RF cavities	8 per beam
Nominal energy, protons	7 TeV
Energy at injection	450 GeV
Nominal energy, ions (energy per nucleon)	2.76 TeV/u
Peak magnetic dipole eld (at 7 TeV)	8.33 T
Minimum distance between bunches	7 m
Design luminosity	$10^{34} cm^{-2} s^{-1}$
Collision rate	45 MHz
Number of bunches per proton beam	2808
Number of protons per bunch (at start)	1.1×10^{11}

Table 2.1: Some of the LHC parameters [12].

where $N_{tot,0}$ describes the initial number of particles in the beam, σ_{tot} is the total cross section and k is the number of interaction points. For nominal LHC condition that makes τ_{col} ∼45 h. This is time to reach $1/e$ of the luminosity's initial value. Other effects like intra-beam scattering and beam-gas interactions make the actual luminosity lifetime even shorter $\tau_{\mathcal{L}}$ ∼15 h.

For estimating the detectors discovery potential it is important to know the integrated luminosity. Before physics data taking some time T_{fill} is needed to fill the accelerator with bunches, ramp magnets etc.. Hence the integrated luminosity could be calculated as

$$\mathcal{L}_{tot} = \frac{X \times 24}{T_{run}[h] + T_{fill}[h]} \mathcal{L}_0 \tau_{\mathcal{L}} (1 - e^{-T_{run}/\tau_{\mathcal{L}}}), \tag{2.3}$$

where X is the run time per year, T_{run} is the total length of the physics time and $\mathcal{L}_0$ is the initial luminosity. Considering the experience from SPS and HERA the filling time could be estimated from 70 minutes to 7 hours. For the designed luminosity (10^{34} cm^{-2}s^{-1}) and an estimated physics time of X = 40 days per year [18] this results in integrated luminosities between 16 fb^{-1} to 24 fb^{-1}.

The LHC parameters are summarized in Table 2.1 and the details of the LHC machine can be found in the LHC Design Report [12].

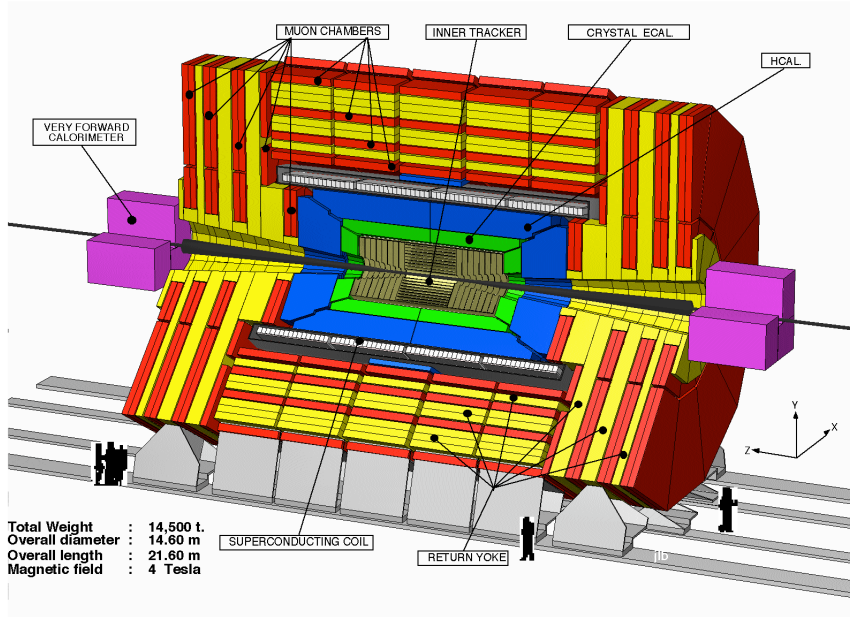

Figure 2.3: CMS detector.

2.2 CMS Detector

The CMS (Compact Muon Solenoid) is a general-purpose particle detector with a emphasis on good muon detection. An overview of the CMS detector is shown in Figure 2.3.

Its total length is approximately 21 m, the diameter is 15 m and it weighs about 12500 tons. The detector has almost 4π coverage because of its cylindrical design and planar endcaps. The CMS detector consists of many different subdetectors, which are designed to identify different physical objects.

The CMS detector has a cylindrical coordinate system with an z-axis parallel to the beam direction. In the transverse plane the geometry of CMS is described by the parameters radius (r) and angle ϕ that is the angle in the xy-plane with respect to the z-axis. In the longitudinal plane the z-coordinate along the beam axis and the angle Θ are used to specify

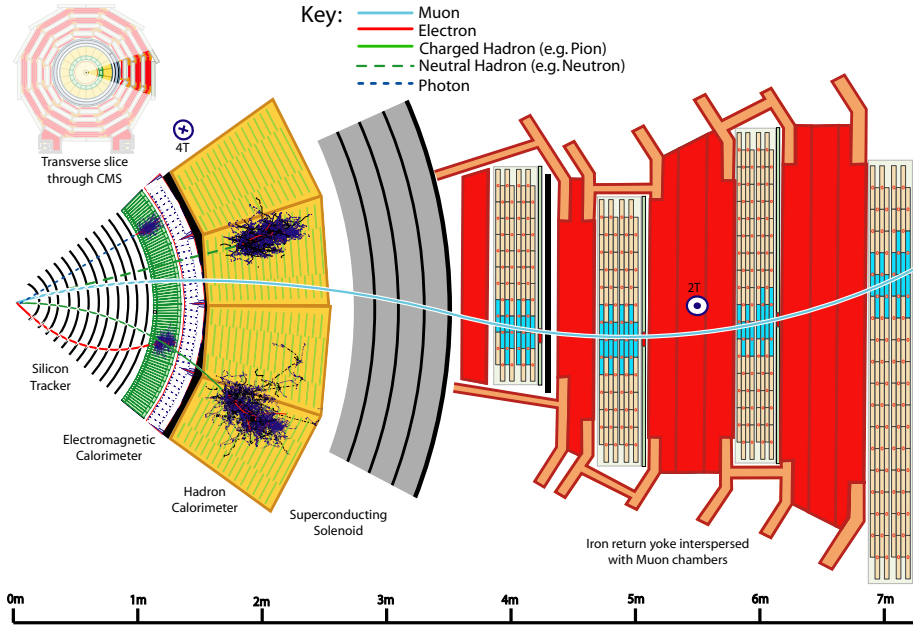

Figure 2.4: A slice of the CMS detector. The traces of particles to be detected are shown.

the detector coordinates. Instead of Θ often the pseudorapidity η is used:

$$\eta = -ln[tan(\frac{\Theta}{2})]. \tag{2.4}$$

CMS detector has a superconducting solenoid providing a 4 T magnetic field parallel to the beam direction. The field makes charged particle to bend their trajectories in the transverse plane of the detector, that enables to measure particle momentum and charge. Inside the magnetic field are the inner tracking system and the calorimeter. The muon detectors are situated outside the coil, so the muons are exposed to a lower magnetic field. The magnetic flux of the solenoid is returned by a set of iron yokes. Between of the yokes are the muon chambers.

The inner tracking system has two different detectors: the silicon pixel detector and the silicon strip detector. These are used to identify bottom quarks by so called b-tagging and to reconstruct tracks and momenta. Next layers are calorimeters: the electromagnetic (ECAL) and hadronic (HCAL)

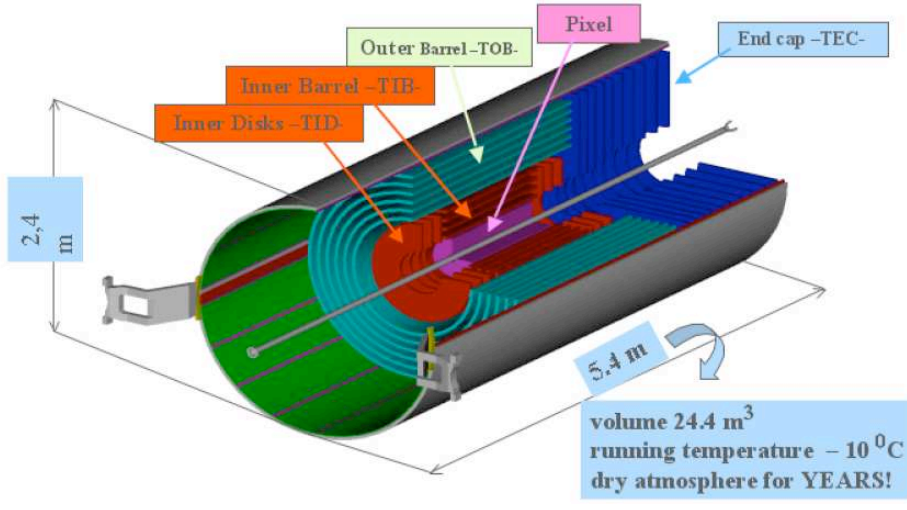

Figure 2.5: Layout of the CMS tracking detectors.

calorimeters, that measure the energies and positions of photons, electrons and hadrons respectively. The muon system measures the charge and momentum of the muons. Figure 2.4 shows how different particles can be detected in CMS detector.

In this thesis the final state to be detected consists mostly of muons. A muon passing the silicon tracker leaves a bent track due to the magnetic eld. Next it goes through the calorimeters and traverses through the muon system, where the bending direction changes because the muon is exposed to a reverse magnetic field. The muon system identifies the particle as muon. Together with data from the tracker its track and momentum can be reconstructed.

The subdetectors are described as follows in more detail starting from the innermost subdetector until outermost layers. The precise information can be found from Technical Design Reports of CMS [20–23, 27–29].

2.2.1 Tracker

The tracker is the innermost part of the CMS detector that is dedicated to the finding of tracks and vertexes. It occupies cylindrical volume with the length of about 5.4 m and diameter of 2.4 m. It is placed in the 4 T

magnetic field area that allows to measure the momentum of high energy particles accurately.

The tracker system consists of highly segmented silicon pixel and silicon strip detectors which measure the position, momenta and decay points of the charged particles from the ionization along the path of a moving particle. There is a single tracker in the barrel and one in each endcap. In the barrel part, there are ten silicon strip layers and three pixel layers. The silicon strip layers are divided to the Inner Barrel (TIB) and Outer Barrel (TOB) that are made of 4 and 6 silicon strip layers respectively. In the endcaps, there are 2 pixel layers, 3 inner disk (TID) and 9 outer forward silicon disk detectors. The silicon strip modules in the endcaps (TEC) are assembled on carbon-fiber support wedges. Layout of the CMS tracking detectors can be seen in Figure 2.5.

There are 25000 silicon strip detectors with about 200 m^2 and the signal is read out by 44 million electronic channels. The tracker coverage is up to $|\eta| = 2.5$. The spatial resolution is $\sigma_{r\phi} \sim 10$ μm and $\sigma_{rz} \sim 17$ μm. The momentum resolution of the tracker is $\Delta P/P \sim [15(P_T/\text{TeV}) \oplus 0.5]\%$ for $|\eta| < 1.6$ and becomes $[60(P_T/\text{TeV}) \oplus 0.5]\%$ as $|\eta|$ approaches 2.5. That makes for a muon with a p_T of 100 GeV the accuracy of ± 1.5 GeV for $|\eta| < 1.6$.

To protect the silicon detectors from aging because of the high radiation flux, the full silicon tracker is operating at –10°C. A thermal shield is placed outside of the tracker volume which provides insulation while a cooling system extracts 60 kW of heat dissipated by the front end electronics.

More details of the tracking system can be found in [21].

2.2.2 Electromagnetic Calorimeter

Around the tracker is placed the electromagnetic calorimeter (ECAL), which is designed to provide very good di-photon mass resolution because of one important benchmark channel for detecting Higgs ($H \to \gamma\gamma$).

The ECAL detector is a crystal-based scintillating calorimeter that offers the best performance for energy resolution from electrons and photons. The ECAL crystals are made of lead tungstate ($PbWO_4$) that has very fast light decay time and very high density (8.28 g/cm^3). After 15 ns, already 60% if the light is emitted by the crystals (for example in the LEP L3 experiment was used BGO crystals, where it took 300 ns) and 100 ns is enough to collect the emitted light. The fast scintillator crystals are needed because of the LHC very high event rate.

The crystal dimensions are 2.2 cm × 2.2 cm × 23 cm for the barrel

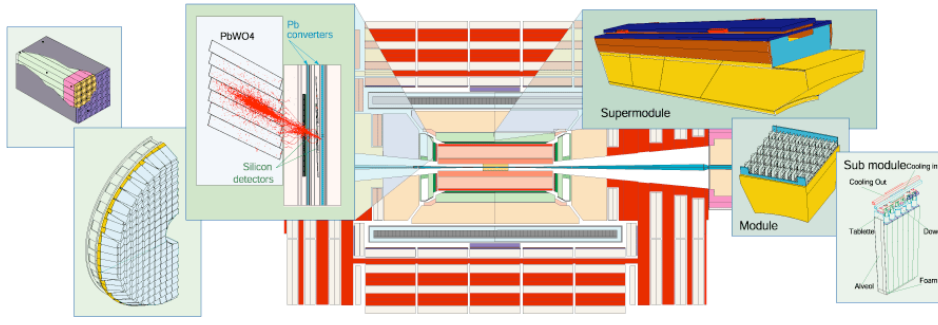

Figure 2.6: The Supermodules, Modules and Submodules of the ECAL detector.

crystals and 2.5 cm $\times$ 2.5 cm $\times$ 22 cm for the endcaps, corresponding to a granularity of $\Delta\phi \times \Delta\eta$ of 0.0175 $\times$ 0.0175 in the barrel. Electrons and photons are almost entirely absorbed by ECAL crystals because of its material has a very small Molière Radius (2.19 cm). The size of the crystals corresponds to about 26 radiation lengths. For 35 GeV electrons, 94% of the energy is absorbed by 3 $\times$ 3 crystal arrays and 97% in 5 $\times$ 5 crystal arrays. A disadvantage of the lead tungstate is its relatively low light yield, which is about 14 times smaller than the one from BGO crystals (used in LEP L3). This requires a good amplification within the photodetector at the end of the crystals. The photodiodes have to operate in a very strong radiation environment. In such a strong magnetic field photomultipliers cannot be used. In the barrel part of the calorimeters avalanche photodiodes are used and in the endcaps vacuum phototriodes are used that can operate in higher levels of radiation.

There are about 76000 individual crystals in ECAL that are mechanically organized into modules and supermodules. In the barrel, the crystals are tilted in the transverse plane by 3 degrees, in order to minimize the probability that particles pass through the inactive area between crystals. The barrel crystals are assembled into 36 supermodules, each consisting of 4 modules with 50 submodules in the first module and 40 in the remaining three modules. Those submodules are composed of 2 $\times$ 5 crystals. In total, the barrel contains 61200 crystals. The supermodules have a wedge shape and subtend an angle of 20 degrees. The overview of the ECAL modular structure can be seen from Figure 2.6.

There is a preshower detector built in front of the calorimeter ($|\eta| > 1.653$). This allows to reject high–p_T π^0s by measuring the transverse profile

of the electromagnetic shower after roughly three interaction lengths. The preshower detector is built like a sampling calorimeter with lead as the absorber and a layer of silicon strip sensors for the measurement of the charged particles created in the shower. The strips from one plane are orthogonal to these of the second plane, which gives a two-dimensional position measurement with a precision of 300 μm for a 50 GeV π^0.

The energy resolution can be expressed as a function of the energy as follows:

$$(\frac{\sigma(E)}{E})^2 = (\frac{S}{\sqrt{E}})^2 + (\frac{N}{E})^2 + C^2, \tag{2.5}$$

where the first term is the stochastic term, the second one is the noise and the C^2 is a constant term. The stochastic term includes contributions from fluctuations in the shower containment and photostatistics. The noise term comprises contributions from the electronics readout and pile-up.

2.2.3 Hadronic Calorimeter

The hadronic calorimeter (HCAL) is designed to identify hadrons and jets and to measure their energies. The hadronic calorimeter consists of four subdetectors: barrel (HB), endcap (HE), outer (HO) and forward (HF) detectors.

The HB and HE are placed between the ECAL and the magnet. These are sampling calorimeters made of plastic scintillator plates and alternating layers of brass. The HB has a coverage $|\eta| < 1.4$ and the HE covers the region between $|\eta| > 1.5$ and $|\eta| < 3.0$. Each HB tower has a projective area of $\Delta\eta \times \Delta\phi = 0.087 \times 0.087$. Wavelength-shifting (WLS) fibers are placed in the scintillator plates. The light collected from the scintillators are read out by the Hybrid Photo Diodes (HPD) detectors.

The HB detector cannot absorb the hadronic showers fully. The HO is made to catch the tails of the hadronic showers. The HO is a scintillator detector, located between the magnet and muon system. It covers the region $|\eta| < 1.26$.

The HF is located at $3.0 < |\eta| < 5.0$ outside the magnetic coil. HF calorimeters are designed to measure high energy jets with a good precision (20% to 30% at 1 TeV) [24]. It is made of steel as the absorber and quartz fibers as the active medium. Quartz fibers are chosen due to their radiation hardness, because the forward calorimeters will experience extremely hard particle fluxes. The short (1.43 m) and long (1.65 m) fibers are used. The short ones start at the depth of 22 cm from the front of the detector making it possible to distinguish showers originated from electrons and photons

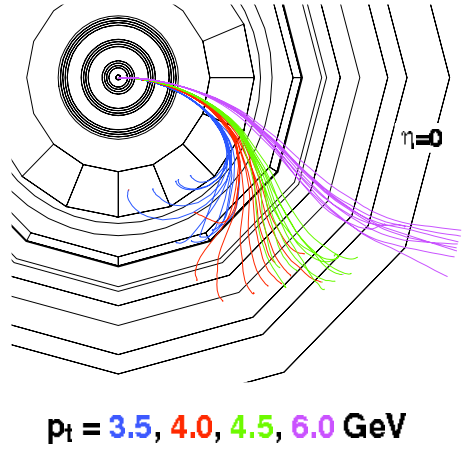

Figure 2.7: The bending od the muon tracks with different transverse momentum p_T in the magnetic field.

that deposit a large fraction of their energy in the first 22 cm. The hadrons produce signals in both segments. Test beam results yield a resolution in the range from 30 GeV to 1 TeV given by

$$\frac{\Delta E}{E} = \frac{1.22}{\sqrt{E(GeV)} + 0.05}. \tag{2.6}$$

More information about the HCAL can be found at [24].

2.2.4 Magnet System

The relative error of particle p_T measurement is inversely proportional to the magnetic field B. The compact muon solenoid design requires a very strong magnetic field in order to induce enough bending of the energetic charged particles. The basic goal is to reconstruct up to 1 TeV muons with $\sim$10% p_T resolution.

The bending of tracks with different transverse momenta p_T in a 4 T field is illustrated in Figure 2.7. At this field strength, trajectories of charged particles with $p_T > 0.7$ GeV reach the ECAL front surface (in the absence of tracker material), and muons with $p_T > 4$ GeV extend through the muon chambers.

The magnetic field is created by a superconducting coil by passing a 20 kA of current in the niobium-titanium superconductor. The magnet is

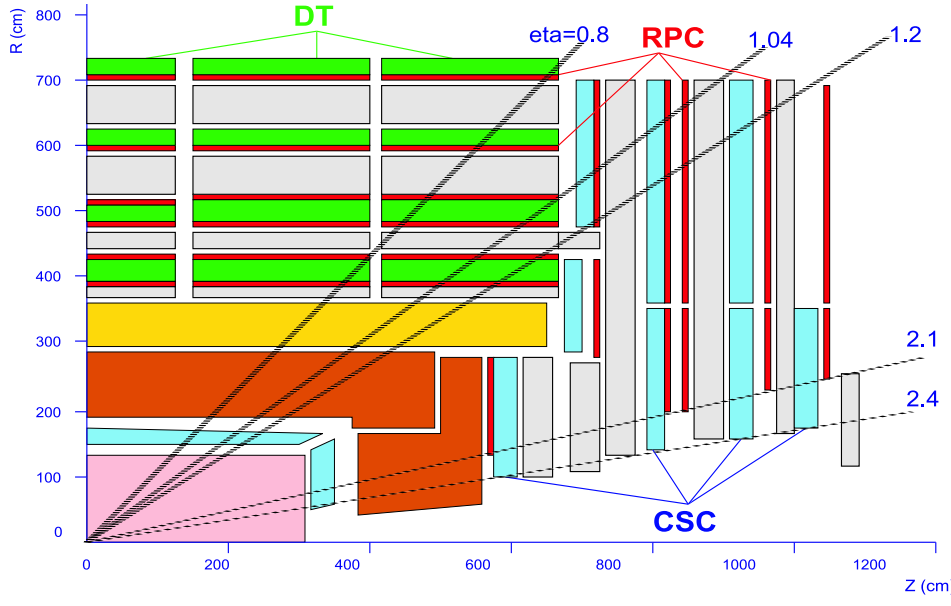

Figure 2.8: Longitudinal view of one quarter of the muon system with DTs, CSCs and RPCs

situated just outside the calorimeters at a radius of 2.9 m, and returned by 3 layers of iron yokes with a combined thickness of 1.55 m in the barrel and 1.45 m in the endcaps.

Details on the CMS magnet can be found in the Magnet TDR [19].

2.2.5 Muon System

The overview of the muon system is given in Figure 2.8. There are four muon detectors interleaved with return yoke plates and the whole muon system is divided into a barrel part and two endcaps. The iron yokes are placed between muon chambers to decelerate muons. There are approximately 16 interaction lengths before the last muon station is reached. This allows a good muon detection. Unlike electrons, muons do not emit Bremsstrahlung and they are expected to give very clear signatures. The muon chambers are in a 2 T magnetic field. There are three combined technologies: drift tubes (DT) in the barrel, cathode stripe chambers (CSC) in the endcap and resistive path chambers (RPC) in both the barrel and endcaps.

DT-s are placed in the barrel, because the magnetic field is mainly

contained by the return yoke. The DT-s are assembled in drift chambers containing 12 layers of tubes that are organized in 3 independent sub-units made up of 4 planes with parallel wires. Two of the sub-units measure the coordinate in the bending plane and the third measures the track coordinate along the beam. The measurements are combined to form an oriented segment used later on for track reconstruction. The forward environment is very different from the central one, because the high particle flux requires a better granularity and faster response. CSC-s are multiwire proportional chambers where the cathode is subdivided into strips perpendicular to the anode wires. The CSC can sustain highly varying magnetic field that is present in its region between the solenoid and the return yoke.

The resistive plate chambers (RPC) are used in both, in barrel and endcaps. RPC-s provide a lower resolution than the CSC-s and DT-s, but they have faster timing signal with a time resolution of 2-3 ns. The RPC consists of two parallel resin plates, with a high bulk of resistivity, separated by a gas-filled gap of a few millimeters. Avalanches in the gas induce a fast charge on the cathodes, that can be exploited without expensive electronics. RPS-s complement DT-s and CSC-s as an additional sensitive planes in higher trigger levels and offline reconstruction.

The reconstruction efficiency of the muon tracks is above 90% for 100 GeV muons in the pseudorapidity range covered by the muon chambers. The momentum resolution measured in the muon system depends strongly on the pseudorapidity. The muons with bigger pseudorapidity than $|\eta| > 1.5$ exit the solenoid and become therefore less bent. Using the muon detectors together with tracker the resolution is about 1 - 1.5% for 10 GeV muons and 6-17% for 1 TeV muons (depending on $|\eta|$).

2.2.6 Data Acquisition System

The LHC bunch crossing rate is 40 MHz. Each beam crossing at LHC will result more than 20 inelastic pp collisions at the full fuminosity. This corresponds to approximately $\sim$1 MB of zero-suppressed data every 25 ns. This is far too much to be handled with present day computers and the data acquisition system has to reduce it by factor of 10^5, keeping only the interesting events. The schematic view of the CMS DAQ system is depicted in Figure 2.9.

The trigger system consists of a Level-1 (L1) trigger and high level trigger (HLT) that is working completely at the software level. For Level-1 trigger it takes about 3.2 μs to come to a decision and store the data. Most of the time is consumed by the signal transfer from the front-end

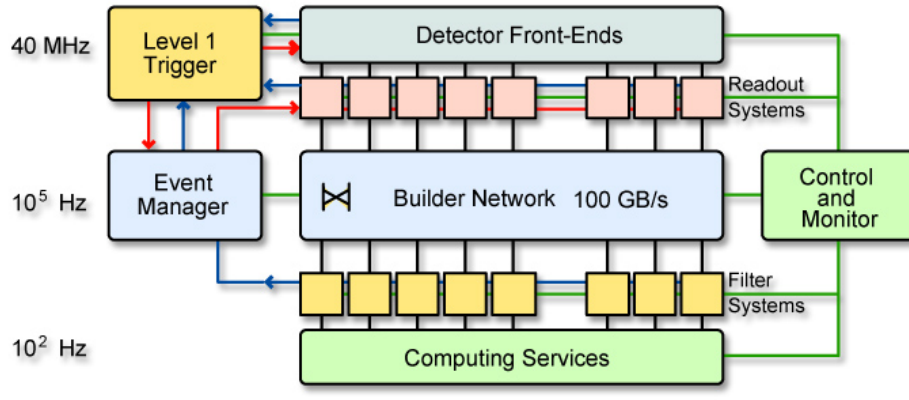

Figure 2.9: The CMS DAQ system [9].

electronics to the L1 logic system. The calculation in L1 trigger take less than 1 μs. The data has to wait in the pipe-line buffers for 3.2μs/25 ns = 128 bunch crossings before it is decided whether it is kept or not. The L1 trigger reduces the event rate to 100 kHz. The Level-1 trigger uses calorimeter, muon system and global (combination) triggers, that combine the data from calorimeters and muon system. The trigger primitive objets are constructed using the detector systems. These objects are created only if the p_T or E_T are above some thresholds.

High Level Trigger (HLT) reduces the 100 kHz Level-1 event rate to approximately 100 Hz. The calculations after Level-1 trigger are performed in a single farm of about 1000 dual-CPU computers. First the high level trigger makes a partial reconstruction using calorimeters and the muon system. This stage refines the objects that are created in Level-1. Then the results are combined with data from pixel and tracker for further rejection. There is also offline reconstruction possible in HLT trigger algorithms.

For further details, see the trigger CMS technical design reports [2, 22, 23].

Chapter 3

Doubly Charged Higgs Boson Beyond the Standard Model

3.1 Motivations

The main motivation of the LHC experiment is to reveal the secrets of electroweak symmetry breaking (EWSB) mechanism. The electroweak precision measurements predict a light Standard Model Higgs boson. However, if the Standard Model Higgs boson H will be discovered at the LHC, the question arises what stabilizes its mass against the Planck scale or some other higher scale, e.g. Grand Unified Theories (GUT), quadratically divergent radiative corrections. It is a huge gap between the natural Higgs scale (10^2 GeV) and the Planck scale (10^{19} GeV) or the GUT scale (10^{16} GeV), for example. Thus, the question is in the *naturalness* of the electroweak Higgs.

In addition, after any solution of the puzzle of EWSB some urgent question remains in particle physics: (i) cold dark matter seen in the astronomical observations, (ii) neutrino masses seen through terrestial oscillation experiments and (iii) matter-antimatter asymmetry seen in the present Universe. The questions have no definite answer in the framework of the Standard Model. Naturally, the most excellent solution would involve the EWSB mechanism, naturalness, neutrino masses, cold dark matter and matter-antimatter asymmetry in a same model.

Below a conventional solution for some of the mentioned questions, supersymmetry (SUSY), will be discussed and subsequently a possible alter-

native for SUSY, the Little Higgs framework will be introduced.

3.2 Solutions for Naturalness: Supersymmetry

First, let us present the diagrammatic view of the problem. If we add some new fields above the Higgs scale as an extrapolation of the Standard Model, quadratic divergences of the Higgs radiative corrections from the heavy fields at the higher scale will start to spoil up our Higgs physics at the lower scale. The reason is clear, there is no symmetry to protect the scalar. Figure 3.1 shows the diagrammatic view of the problem. The represented Feynman diagram is proportional to the mass squared of a (heavy) higher scale boson.

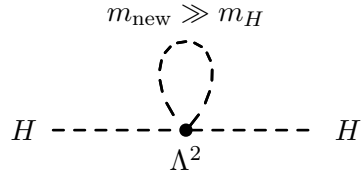

Figure 3.1: Radiative correction to the Higgs boson mass from a boson field. The new heavy fields between the electroweak and the Planck scale as an extrapolation of the Standard Model spoil up our Higgs physics at the lower scale due to the quadratic divergence of the Higgs radiative corrections.

To be more detailed, a (mass) parameter in a theory stays at a small value under radiative corrections if the radiative corrections to this quantity are multiplicative. This can happen if we set the parameter to zero and it leads the theory to exhibit a symmetry which can forbid against the radiative corrections. The symmetry "protects" the small value of the parameter and it is said to be *technically natural*. This symmetry is called a *custodial symmetry*. The Higgs boson has no custodial symmetry to protect its mass scale. This property makes fundamental scalars unnatural. Thus, any scalar boson mass is typically subject to large radiative corrections. Even in the case where the mass is set to zero initally, generally, the corrections induce a mass. The situation was diagrammatically shown in Figure 3.1.

However, there are some known possibilities to protect scalar mass:

(i) Nambu-Goldstone bosons which can have technically natural low masses due to their spontaneously broken chiral symmetry. The well-know example is the π-meson in QCD.

(ii) Composite scalars which only form at a strong scale, for example, a Λ_{QCD} in QCD. They can receive additive renormalizations in the order of the strong scale, for example, at Λ_{QCD} in QCD.

(iii) A technically natural mechanism for scalars with a low mass scale is also provided by SUSY because the scalars are then associated with fermionic superpartners. The chiral symmetries of these superpartner fermions protect the mass scale of the scalars.

First, let us start with a canonical solution to the hierarchy problem, SUSY. In particle physics, SUSY was proposed by Julius Wess and Bruno Zumino [30] in 1973. The supersymmetric algebras had been studied by Golfand and Likhtman [31] in the late 1960s. An initial idea was to find connections between the known fermion and boson fields. It turned out that the naive SUSY does not work between the Standard Model fields. Unfortunately, if we count the bosonic and fermionic fields in the Standard Model it has the 28 bosonic and the 90 fermionic (96 with massive neutrinos) degrees of freedom. In addition, the Higgs field can not be a superpartner of the fermion content, since it has nonzero vacuum expectation value (*vev*).

However, it is possible to define new SUSY fields which are supersymmetric partners of the Standard Model fields. Below we will describe some main ideas of SUSY for the Higgs physics referred from [32–35]. A possibility to save the Higgs mass in SUSY comes from the idea that the fermion corrections can cancel the bosonic ones. Figure 3.2 presents a diagram of a negative contribution to the Higgs mass. Naturally, a very exact correspondance is needed between fermionic and bosonic fields in a model. SUSY can guarantee it field-by-field using the idea of superpartner fields.

Shortly, we will describe the boson-fermion correspondance in SUSY. Let b denote a boson field and f a fermion field. We know that fermion fields anticommute, $\{f, f\} = 0$. Boson fields, on the contrary, commute, $[b, b] = 0$. *SUSY transformation* between fermion and boson fields is

$$\delta b = \varepsilon \cdot f, \tag{3.1}$$

where ε is the infinitesimal transformation generator (of the Poincare group). We see from Equation 3.1 that ε anticommutes,

$$\{\varepsilon, \varepsilon\} = 0. \tag{3.2}$$

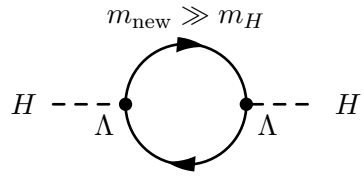

Figure 3.2: The negative radiative correction to the Higgs boson mass from a fermion field. Thus, the fermionic field is able to cancel some contributions of the positive radiative correction of boson fields.

So, all the generators of SUSY are anticommuting, therefore they are fermionic. Fermionic operator changes spin in units 1/2 and therefore it always changes the type of statistics,

$$\varepsilon : \text{Fermi-Dirac} \leftrightarrow \text{Bose-Einstein} \tag{3.3}$$

We note there exactly the same number of equal degrees of freedom of fermionic and bosonic fields in the pure SUSY models. In addition, it can be shown that due to the form of the superpotentials and the chirality of the matter superfields at least two complex chiral Higgs multiplets are presented to give masses to up and down quarks. Figure 3.3 shows the diagrammatic vied of the cancellation.

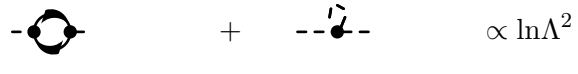

Figure 3.3: The bosonic and fermionic radiative correction to the Higgs boson mass. The radiative contribution of the fields can cancel mutually. The total contibution is $\propto \ln\Lambda^2$.

The exact cancellation of the radiative corrections takes place only in exact SUSY. Only in exact SUSY the summation of the corrections gives zero total contribution,

$$\sum_N m^2_{\text{fermion}} - \sum_N m^2_{\text{boson}} = 0, \tag{3.4}$$

where N is the order of the SUSY model. In addition to canceling the radiative contributions of the Higgs field SUSY cancels all the field contributions to the total vacuum energy. Hence, it can naturally solve the vacuum energy problem in cosmology.

SUSY offers some possible solutions in particle physics and cosmology in addition to the Higgs naturalness and the vacuum energy problem [36, 37]:

- SUSY GUT models can predict correct running of the gauge couplings of the strong and electroweak interactions.
- SUSY can unite gravitation (naturally, linearized as the gravitino spin-2 field) and the SM spin-1 vector gauge fields into an united *superalgebra* within the framework of quantum field theory.
- SUSY with *R-parity* proposes candidate(s) of cold dark matter in cosmology. The R-parity is needed to protect the light SUSY particle(s) against their decay to the SM particles.
- SUSY field(s) can be used as the cosmological inflation field(s) in the early stage of the Universe.

Unfortunately, in experiment we do not see any direct evidence of SUSY [38]. It means that if there is SUSY it is broken at some energy unreachable us. In broken SUSY the cancellation mechanism works up to the SUSY breaking scale. Equation 3.4 should be modified as

$$\sum_N m^2_{\text{fermion}} - \sum_N m^2_{\text{boson}} = M^2_{\text{SUSY}}, \tag{3.5}$$

where M^2_{SUSY} is the scale of SUSY breaking. If we believe the Higgs boson mass is at scale of 100 GeV and the Yukawa coupling is not very far from one then the SUSY breaking scale should be around 1 TeV,

$$gM_{\text{SUSY}} \propto M_H. \tag{3.6}$$

Thus, the signals of SUSY are reachable by LHC if SUSY manifests itself in the Higgs physics.

3.3 Alternatives to Supersymmetry

The SUSY breaking complicates the vacuum energy problem again. The vacuum energy should be in the scale of the SUSY symmetry breaking in a

pure SUSY theory. As we can see in cosmology observations it is not true, the observed value of the vacuum energy ($\Lambda_{\text{vacuum}} \simeq (10^{-3})$ eV^4) is many orders of magnitude smaller. If the SUSY breaking scale is $\Lambda_{\text{SUSY}} \simeq 1$ TeV then the gap between the observed vacuum energy Λ_{vacuum} in cosmology and one in the SUSY breaking remains huge, $\Lambda_{\text{SUSY}}/\Lambda_{\text{vacuum}} \simeq 10^{43}$.

The simpler SUSY models, e.g. Minimal Supersymmetric Standard Model (MSSM), suffer from the need of careful fine tuning. For example, it is needed for the unification and the dark matter predictions. Also, SUSY does not provide a natural solution for an other urgent problem in particle physics, neutrino mass. Because of that, physicists also consider alternative models. Let us list some of them below.

Top quark condensate. In this model the fundamental scalar Higgs field is replaced by a composite field composed of the top quark and its antiquark, called *top condensate* [39, 40]. The top quark is the most massive among all the SM fermions and its mass, estimated at 171 GeV, is comparable to the electroweak scale. The bound state of the condensate described by a $(1, 2, -1/2)$ composite scalar field, where the first number denotes the representation of $SU(3)_c$, the second one the rep of $SU(2)_L$ and the last one is the hypercharge. The condensate subsequently breaks the electroweak and hypercharge symmetry into electromagnetism. However, the simple versions of the top condensates fail experimentally. Only some more complicated versions of the model have survived, e.g. top see-saw. The theories will be tested soon at the LHC experiment. The simpler versions of the theory do not solve neutrino mass problem and there is no candidate of dark matter. However, there is a model to explain the masses borrowing the idea of top condensate but using the condensate of right-handed neutrinos [56].

Technicolor. The model contains no scalar field to explain the masses of fermions and heavy vector bosons. The central idea of (rather different) technicolor models is that the electroweak symmetry is broken by a new strong gauge interaction [41]. The full gauge symmetry group at high energies is $G \otimes H$, where G denotes the Standard Model gauges and H is a new gauge getting strong at lower energies. The strong behaviour of H causes chiral symmetry breaking to occur in the model. In other words, the fields of the model can acquire a *vev* dynamically. If the *vev* is not G-invariant, this leads to spontaneous breaking of G with no need for a fundamental scalar field. The masses are automatically protected agaist radiation corrections by the new gauge H.

The simpler technicolor models do not satisfy the electroweak precision tests. However, a set of new models called *walking technicolor* has been proposed [42, 43].

Little Higgs. The Little Higgs models are based on the idea that the Higgs field is a pseudo-Goldstone arising from the breaking of a global symmetry at TeV scale. The Little Higgs models borrow the results of strong dynamic, the pions in QCD etc., for the electroweak symmetry breaking. The Little Higgs models are using the idea of *dimensional deconstruction*. In these theories, the total gauge group of the model is in the form of a direct product of several copies of the same factor group. For example, $SU(2)\otimes SU(2)\ldots \equiv SU(2)^N$. Each $SU(2)$ factor group may be visualized as the $SU(2)$ group living at a particular point along an additional dimension of space. Thus, the Little Higgs models borrow some ideas of extra dimensional models even though the Little Higgs theory itself is $3+1$ dimensional.

3.4 Little Higgs

In this work we study the LHC related phenomenology of the Littlest Higgs. We are motivated by two reasons: (i) the rich spectrum of new particles reachable for the LHC experiment, (ii) the Little Higgs model can be related to neutrino physics. From collider physics point of view the model predicts the existence of new particles, such as a set of heavy gauge bosons W_H, Z_H, a vectorlike heavy quark pair T, $\bar{T}$ with charge $2/3$, and triplet Higgs bosons Φ. If the new particle masses are $\mathcal{O}(1)$ TeV, direct tests of the models are possible at the LHC experiments [52–54]. Also, there can an be a exciting connection between high energy physics at the LHC collider and lower energy physics at the neutrino experiments predicted by the Little Higgs.

In the context of this work we are interested in the Little Higgs models as a possible origin of non-zero neutrino masses [57–61]. The neutrino mass mechanism which naturally occurs in those models is the triplet Higgs mechanism [62, 63], called the *type II see-saw*. It employs a scalar with the $SU(2)_L \otimes U(1)_Y$ quantum numbers $\Phi \sim (3, 2)$. The existence of such a multiplet in some versions of the Little Higgs models is a direct consequence of global symmetry breaking which makes the SM Higgs light.

For example, in the minimal Littlest Higgs model [64], the triplet Higgs with non-zero hypercharge arises from the breaking of global $SU(5)$ down to $SO(5)$ symmetry as one of the Goldstone bosons. Its mass $M_\Phi \sim g_s f$,

where $g_s < 4\pi$ is a model dependent coupling constant in the weak coupling regime [44], is therefore predicted to be below the cut-off scale Λ, and could be within the mass reach of LHC. Although the triplet mass scale is $\mathcal{O}(1)$ TeV, the observed neutrino masses can be obtained naturally. First, non-observation of rare decays $\mu \to eee$, $\mu \to e\gamma$, $\tau \to \ell\ell\ell$, where $\ell = e, \mu$, implies that the triplet Higgs boson Yukawa couplings Y_{ij} must be small, thus suppressing also the neutrino masses. Second, the *vev* of the neutral component of triplet v_Φ contributes at tree level to the SM oblique corrections, and is therefore severely constrained by precision data. There exist additional mechanisms which can explain the smallness of v_Φ in the Little Higgs models. In this work we assume that the smallness of v_Φ is the most natural explanation of the smallness of neutrino masses in the Little Higgs models.

Let us describe shortly the type II see-saw and the relations with the Little Higgs framework. In the case of the type II see-saw the SM content is extended only by the addition of a $SU(2)$ triplet of scalar fields with the $SU(2)_L \otimes U(1)_Y$ quantum numbers $\Phi \sim (3, 2)$. Let us denote the components as

$$\vec{\Delta} \equiv (\Delta^1, \Delta^2, \Delta^3), \tag{3.7}$$

which has the physical eigenstates

$$(\Delta^{++}, \Delta^{+}, \Delta^{0}), \tag{3.8}$$

where the physical states are defined as

$$\Delta^{++} = \frac{1}{\sqrt{2}}(\Delta^1 - i\Delta^2), \quad \Delta^{+} = \Delta^3, \quad \Delta^{0} = \frac{1}{\sqrt{2}}(\Delta^1 + i\Delta^2). \tag{3.9}$$

The minimal gauge invariant Lagrangian has the Yukawa terms for the lepton and the Higgs sector as follow,

$$\begin{aligned} \mathcal{L}_Y \supset & [\bar{\tilde{L}}_L \lambda_\Delta (\vec{\sigma} \cdot \vec{\Delta}) L_L + \mu_\Delta \tilde{H}^\dagger (\vec{\sigma} \cdot \vec{\Delta})^\dagger H + h.c.] \\ & - [\vec{\Delta}^\dagger M_\Delta^2 \vec{\Delta} + \frac{1}{2}\lambda_2 (\vec{\Delta}^\dagger \cdot \vec{\Delta})^2 + \lambda_3 (H^\dagger H)(\vec{\Delta}^\dagger \vec{\Delta}) \\ & + \frac{\lambda_4}{2}(\vec{\Delta}^\dagger T^\alpha \vec{\Delta})^2 + \lambda_5 (\vec{\Delta}^\dagger T^\alpha \vec{\Delta}) H^\dagger \sigma^\alpha H], \end{aligned} \tag{3.10}$$

where $\alpha = 1, 2, 3$ is the $SU(2)$ index and the repeated indices mean summation.

In the Lagrangian 3.10 above one $d = 4$ and one $d = 5$ operator emerges. The $d = 4$ operator is

$$\mathcal{L}^{d=4} = 2\frac{|\mu_\Delta|^2}{M_\Delta^2}(H^\dagger H)^2, \tag{3.11}$$

and the $d = 5$ operator leads to the mass term of the neutrino,

$$m_\nu = -2\lambda_\Delta v^2 \frac{\mu_\Delta}{M_\Delta^2}. \tag{3.12}$$

It is a typical see-saw like term. The term has an important difference from the mass term of the type I see-saw. It depends on the Yukawa coupling Y_Δ only linearly. In this case, the left and right hand side have the same number of parameters. It differs from the type I see-saw, where there are 9 unphysical parameters. It can shed some experimental light to the neutrino parameters in this case [45].

As mentioned above, the Higgs triplet of the see-saw can be "borrowed" from the Little Higgs framework. Thus it is a junction between neutrino physics and electroweak physics of the Little Higgs models. We can study the Drell-Yan pair production of doubly charged component of the triplet [46–51] at the LHC,

$$pp \to \Phi^{++}\Phi^{--}, \tag{3.13}$$

followed by the leptonic decays,

$$\Phi \to \ell\ell. \tag{3.14}$$

Let us stress that: (i) the production cross section does not depend on any unknown model parameter but only the mass of Φ; (ii) smallness of v_Φ, related to the smallness of neutrino masses, implies that the decays $\Phi \to WW$ are negligible; (iii) the Φ leptonic decay branching fractions do not depend on the size of the Yukawa couplings but only on their ratios which are known from *neutrino oscillation experiments*. In the triplet model the *normally hierarchical* light neutrino masses predict

$$BR(\Phi \to \mu\mu) \approx BR(\Phi \to \tau\tau) \approx BR(\Phi \to \mu\tau) \approx 1/3. \tag{3.15}$$

Therefore this scenario is predictive and testable at LHC experiments. The different scenarios for the neutrino sector are carefully analysed in [11].

The LHC experiment produces Φ singly and in pairs. The cross section of the single Φ production via the WW fusion process [48] $qq \to q'q'\Phi$ scales as $\sim v_\Phi^2$. In the context of the Littlest Higgs model this process, followed by the decays $\Phi \to WW$, was studied in Refs. [52,54,55]. The detailed ATLAS simulation of this channel shows [55] that in order to observe an 1 TeV Φ, one must have $v_\Phi > 29$ GeV. This result is in conflict with the precision physics bound, $v_\Phi \leq 1.2$ GeV, as well as with the neutrino data. Therefore

the WW fusion channel is not experimentally promising at the LHC. On the other hand, the Drell-Yan pair production process $pp \to \Phi^{++}\Phi^{--}$ is not suppressed by any small coupling and its cross section is known up to next to leading order [49]. Possible additional contributions from new physics such as Z_H are strongly suppressed so we neglect those effects here. Followed by the lepton number violating decays $\Phi^{\pm\pm} \to \ell^{\pm}\ell^{\pm}$, this process allows to reconstruct $\Phi^{\pm\pm}$ invariant mass from the same charged leptons. It is known that the SM background should be very small in the signal region. If one also assumes, as it is done in this work, that neutrino masses come from the triplet Higgs interactions, one fixes the $\Phi^{\pm\pm}$ leptonic branching ratios. This allows to test the triplet neutrino mass model at LHC.

Chapter 4

Modeling the Signal at the CMS Detector

Collisions of two bunches of particles in a accelerator experiment gives a huge variety of new particles propagating through a detector. In order to interpret any measurements, these collisions must be compared with theoretical predictions using comprehensive simulations of particle interactions in the same conditions.

4.1 CMS Software Environment

The CMS experiment has put effort in building a common framework of software packages which enable perform analysis tasks of any kind in a consistent way.

The final goal is to detect all collision products as good as possible and carry out different physics analysis. While the detector is being built, the collisions are investigated using Monte Carlo (MC) simulation techniques; starting from MC generated collision events, simulating the detector response and finally performing the same physics analysis that will be used in the real experiment (Figure 4.1). The Monte Carlo simulations help to understand what will be seen in the detector, but also are very helpful to develop particle reconstruction software needed for detector readout.

There are many standalone programs in CMS software. The software components that were used in this thesis are described in following sections. As the software has been continuously updated, some of the described reconstruction programs (ORCA [65], COBRA [68]) are already obsolete and replaced with a new software framework CMSSW [66]. The details of the

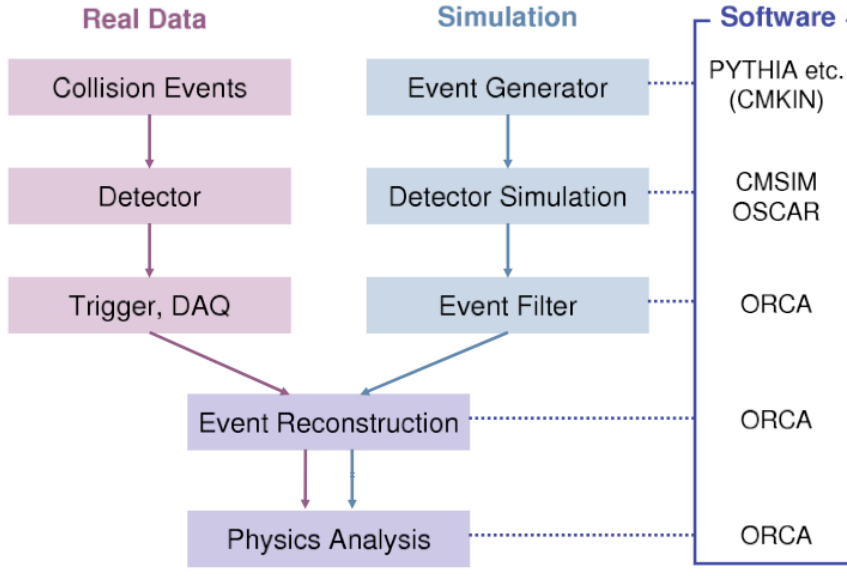

Figure 4.1: Chain of simulation and analysis stream in CMS.

CMS computing model and software architecture can be found in [67, 68].

The CMS software packaged can be divided into FORTRAN based programs (CMSIM [69], CMKIN [70]) and C++ based programs (OSCAR [71], ORCA [65], FAMOS [72]). The programs used in this thesis are FORTRAN based Monte Carlo generator PYTHIA and detector simulation and particle reconstruction programs CMSIM, ORCA, OSCAR and Objectivity/DB as an object-oriented database (OODB). The event reconstruction and analysis using simulated events and real data can be carried out in an identical manner using the same software.

4.1.1 Monte Carlo Event Generators

The first stage of testing theories in CMS detector is Monte Carlo simulation. The Monte Carlo technique is a numerical method for obtaining an estimate of the solution of a specified problem using a sequence of values of a random variable. This method is used to simulate experimental data. In high energy physics this simulation is done in two stages, event generation and detector simulation.

The event generators describe the creation of particles from a single p-p scattering event and their further decays until they reach a stable state within the scope of the experiment. The output from the generators is in the form of four-momentum vectors, assuming the primary vertex position is at (0,0,0,0), with respect to the detector frame.

There are several Monte Carlo event generators available for simulating events ranging from simple back-to-back particle production used for detector performance studies to the specific physics process arising from p-p collisions at the LHC. The standard Monte Carlo generators PYTHIA [73] and COMPHEP [74] were used to simulate the collisions between two protons at a centre of mass energy of 14 TeV.

The PYTHIA is one of the most widely used generators, which implements a few hundred different physics processes, mainly one-body (e.g. gg→H) or two-body (e.g. $q\bar{q} \rightarrow W^+W^-$) production processes. It is a leading order (LO) parton shower event generator for the description of collisions at high energies between elementary particles ($e+$, $e-$, p and $\bar{p}$). It contains theories and models for several physics aspects, including hard and soft interactions, parton distributions, initial and final state parton showers, multiple interactions, fragmentations and decays. It is based on the DGLAP evolution equations [75, 76] and provides leading order calculations of the cross sections. The formation of hadrons is simulated using the string (also called Lund) model. Simulating the LHC $p-p$ scattering process, PYTHIA simulation starts with a hard scattering process based on the parton distributions of the beams, subsequently the fragmentation and decays of particles are carried out until reaching stable particles. The radiation of initial and final states of the incoming and outgoing partons are taken account in the simulation, and also further effects that occur in high luminosity environment like multiple parton scattering and soft gluon emission from beam remnants.

In recent years, simulations of hard scattering processes have been supplemented by specialized event generators, which are based on detailed Matrix Elements (ME) calculations. The ME generators can simulate precisely the complex topology and kinematics of multi-jet (parton) production in a QCD process. However, the hadronization of the partons and the shower evolution are still best simulated by MC generators. Hence, most of the ME generators are interfaced with PYTHIA within CMKIN.

At TeV scale colliders one needs to calculate cross sections for a great number of various reactions. The COMPHEP package [74] was used in some cases in the thesis, when calculation of multiparticle final states in collision

and decay processes was needed ($t\bar{t}$, $b\bar{b}$ events). COMPHEP enables to go directly from the Lagrangian to the cross sections and distributions effectively, with the high level of automatization. The COMPHEP is interfaced to PYTHIA for further hadronization simulation.

4.1.2 Full Reconstruction Chain

The output of an event generator is used as input for a detector simulation programs. Using several software packages the MC generated particles were propagated through the detector (using CMKIN, OSCAR), simulated the digital output from the detector electronics (ORCA) and finally reconstructed (ORCA) all the particles back as they could be detected in a real CMS detector. The subsequent physics analysis could be done in ORCA or used the its output in ROOT [91] analysis skript.

CMKIN

CMKIN [70] is a FORTRAN based program, which provides a common interface between physics event generators and CMS detector simulation tools. It used to be a part of CMSIM [69] detector simulation tool that was replaced by OSCAR [69] by the time of calculating the simulations that are presented in this thesis. CMKIN was used for OSCAR and FAMOS [72] detector simulation input.

CMKIN provides an interface to a number of physics generators like PYTHIA, ISAJET and HERWIG. It also offers the possibility to use different external generators like ALPGEN, COMPHEP, MADGRAPH and TOPREX. Cosmic rays simulation is available as well. Simple particle generation is also included, i.e. single and double particles as well as simple multi particle events. The event output format follows the HEPEVT standard and additional information can be included by the user in the block MCPARAM. The generator level information of particle kinematics and the decay tree is kept as the "MC truth" which is then used to validate the various analyses.

OSCAR

OSCAR [71] (Object oriented Simulation for CMS Analysis and Reconstruction) is based on GEANT4 [77] which is a general toolkit for simulating the particle passage through matter [78]. OSCAR reads the individual events from the CMKIN ntuple and simulates the effects of energy loss,

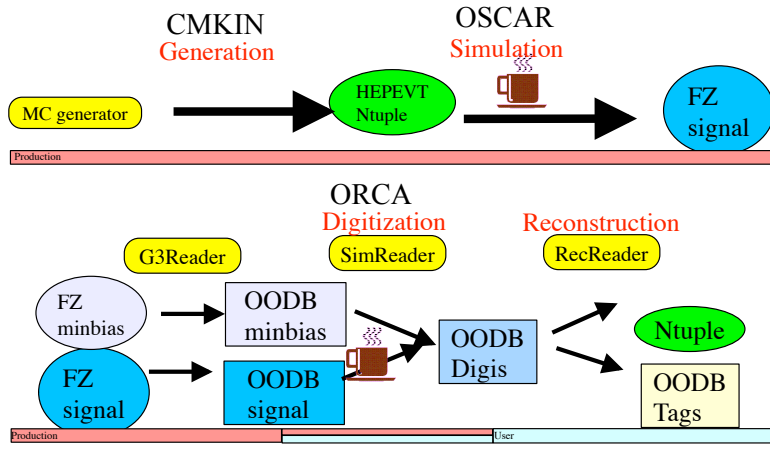

Figure 4.2: The production chain for the full simulation at CMS. The events are produced by a Monte Carlo generator (in this case PYTHIA and COMPHEP), then the simulated hits computed by CMKIN and OSCAR and finally the underlying event structure is created with the help of the full reconstruction software ORCA. The data is read out as ROOT trees.

multiple scattering and showering, etc. in the detector materials. The information is stored in the form of hits.

A simulated hit combines information about energy depositions in the detector, their magnitude, the time at which they occur and their location. In addition to the hits, OSCAR also produces simulated tracks and vertices. This is the original Monte Carlo information about the interactions and decays of particles in the detector.

OSCAR allows to have a full GEANT4 simulation of the apparatus with a simple interface and provides a full description of the subdetectors that are inside it. The package allows to run different phases of the detector simulation: generation, particle tracking in the detector with hits recording,

pile-up, signal and noise simulation, reconstruction and analysis.

The CMS detector description is taken from the Detector Description Database (DDD) [79]. It includes geometrical shapes and dimensions, material information and relative placement of each part of the detector.

ORCA

ORCA [65](Object-oriented Reconstruction for CMS Analysis) was a framework for reconstruction and was intended to be used for final detector optimisations, global detector performance evaluation of trigger studies [80].

The ORCA project covered not only reconstruction tasks, but also included code for simulating detector response and the Level-1 Trigger, as well as High-Level Trigger and analysis code.

ORCA adopted a two-level decomposition – subsystems and packages – to match the different tasks it covers. Typical subsystems were Calorimetry, Tracker, Muon or Trigger matching the hardware components of CMS. Other subsystems provided common services for several subdetectors (CommonDet, CommonReco), analysis tasks (Jets) or high-level reconstruction (TrackerReco, MuonReco, Vertex). Finally, subsystems for High-Level-Trigger selection and analysis are provided (ElectronPhoton, JetMetAnalysis, MuonAnalysis, bTauAnalysis). The subsystem Workspace is meant as a working environment for the users private code.

Other Related Projects

There are a lot of software projects that are related to the simulation tools through data formats, data transfer or specific classes needed for different projects.

- COBRA [68] (Coherent Object-oriented Base for simulation, Reconstruction and Analysis) provides basic services and utilities for analyzing the data.
- IGUANA [81] (Interactive Graphics For User Analysis) is a graphical tool for displaying events.
- SCRAM [82] (Software Configuration, Release and Management) is a configuration management tool, a distribution system, a build system and resource manager, with local resources and applications managed in a transparent way.
- CRAB [83] is the CMS remote analysis builder.

- FAMOS [72] is CMS Fast Simulation tool that provides the fast simulation takes the detector response into account by smearing the momenta of the particle. The full simulation should give results which are closer to the measurements, but the full detector simulation is sometimes too time consuming and the fast simulation is used to perform get some initial results.

4.2 Performance of the CMS Detector

4.2.1 Muons

There are two muon reconstruction algorithms in CMS detector: standalone and global muon reconstruction. Standalone muon reconstruction uses only data from the muon detectors. The global muon reconstruction extends the muon trajectories to include hits from the silicon tracker (silicon strip and silicon pixel detectors).

Standalone Muon Reconstruction

Muon reconstruction starts with the reconstruction of positions of hits in DTs, CSCs and RPCs subdetectors. The hits within each DT and CSC are matched forming segments, then the seeds are constructed by matching and combining the segments. The state vectors (track position, momentum, direction) associated with the segments found in the innermost chambers are used to seed the muon trajectories, working from inside out, using the Kalman-filter technique [84]. The predicted state vector at the next measurement surface is compared with existing measurements and updated accordingly. A suitable χ^2 cut is applied in order to reject bad hits, mostly due to showering, delta rays and pair production. The state vector is propagated from one station to the next using the GEANT4 package [85], which takes into account the muon energy loss in the material, the effect of multiple scattering, and the nonuniform magnetic field in the muon system. The procedure is iterated until the outermost measurement surface of the muon system is reached. A backward Kalman filter is then applied, working from outside in, and the track parameters are defined at the innermost muon station. Finally, the track is extrapolated to the nominal interaction point (defined by the beam-spot size: $\sigma_{xy} = 15\,\mu$m and $\sigma_z = 5.3\,$cm) and a vertex-constrained fit to the track parameters is performed. The result is a StandAloneMuon class in ORCA reconstruction frame.

Global Muon Reconstruction

The global muon reconstruction uses standalone muons as seeds. The global muon reconstruction takes muons detected in the muon chambers and extrapolates their tracks into the silicon detectors to pick up additional hits and so better define the kinematics.

The GEANT4 package is used for the propagation through the steel, the coil and the calorimeters. Silicon layers compatible with the muon trajectory are determined and a region of interest is defined in which to perform regional track reconstruction. Inside the interesting region, candidates for the muon trajectory (regional seeds) are built from pairs of reconstructed hits. The 2 hits forming a seed must come from 2 different tracker layers. All combinations of compatible pixel and double-sided silicon strip layers are used to achieve high efficiency.

The track reconstruction algorithm consists of three steps: trajectory building (recognition of seeded pattern), cleaning of the trajectory (resolution of ambiguities) and smoothing (final fitting). In the first step, the trajectory builder transforms each of the seeds into a set of trajectories. Subsequently the trajectory cleaner resolves ambiguities between multiple trajectories, that could result from a single seed. In the final step, all reconstructed tracks are fitted once again, without a beam-spot constraint, using the hits in the muon chambers from the original standalone reconstruction together with the hits in the silicon tracker. The result is a GlobalMuon class in ORCA reconstruction frame.

Performance

The muon reconstruction performance for standalone and global muon reconstruction algorithms are shown in Figure 4.3 (for $\mathcal{L} = 2 \times 10^{33}\,\mathrm{cm}^{-2}\mathrm{s}^{-1}$). In the figure is shown muon reconstruction efficiencies, (q/P_T) resolutions and charge misidentification probabilities for "Long-Term Scenario" misalignment scenario. Events are produced using the full detector simulation package (OSCAR), which simulates the particle propagation and interactions through the detector, taking into account effects from detector geometry, detector materials, magnetic field, detector misalignment and event pile-up.

4.2.2 Jets and Missing Transverse Energy

Due to the huge QCD cross section the jets will dominate high p_T physics at the LHC. Jet energy resolution is one of the key factors in separating signal

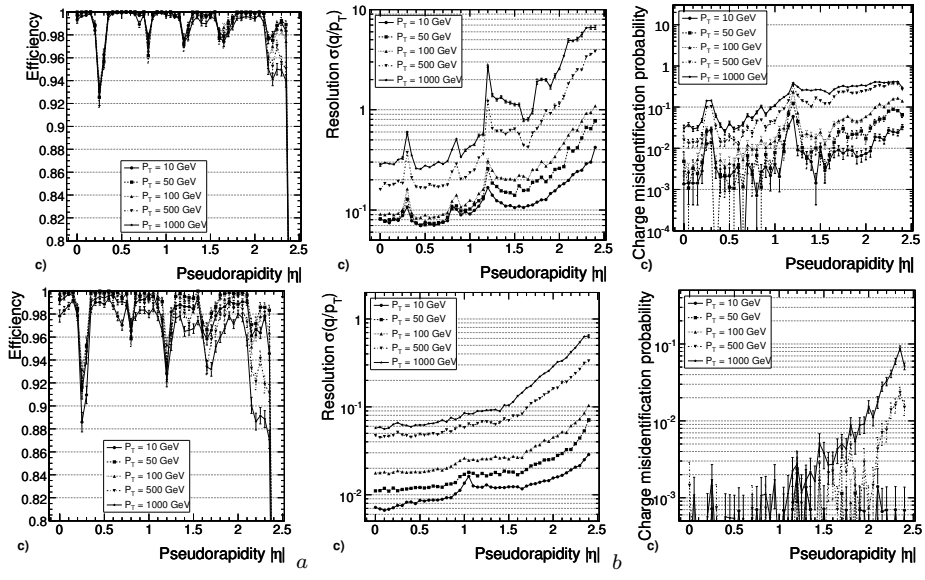

Figure 4.3: Standalone (upper panel) and global muon (lower panel) reconstruction: a) efficiencies, b) (q/P_T) resolution and c) charge misidentification probability as a function of pseudorapidity for detector misalignment "Long-Term Scenario" scenario [9].

events from background. It is also important, because the jets reconstruction is very closely related to missing transverse momentum reconstruction (E_T^{miss}), which is the only way to identify neutrinos and other undetectable particles.

Jets are searched globally, using HCAL and ECAL calorimeter towers. The energy deposition in towers are used as a seed to several jet clustering algorithms. There are three principal jet reconstruction algorithms coded for CMS: the iterative cone [86], the midpoint cone [87] and the inclusive k_T jet algorithm [88, 89]. The midpoint-cone and k_T algorithms are widely used in offline analysis in current hadron collider experiments, while the iterativecone algorithm is simpler and faster and commonly used for jet reconstruction in software-based trigger systems.

The vector sum of the transverse momenta of all final-state particles in a proton-proton collision is constrained to zero by the initial state. This constraint can be inverted and used as a means to detect and measure the total transverse momenta of all undetectable or weakly interacting par-

ticles, such as neutrinos, produced in the event. The missing transverse energy (E_T^{miss}) is a powerful tool for new physics discovery [90]. Much effort has been placed on the design of calorimeters for operation at hadron colliders to have as complete coverage as possible for the purpose of making a meaningful measurement of E_T^{miss}.

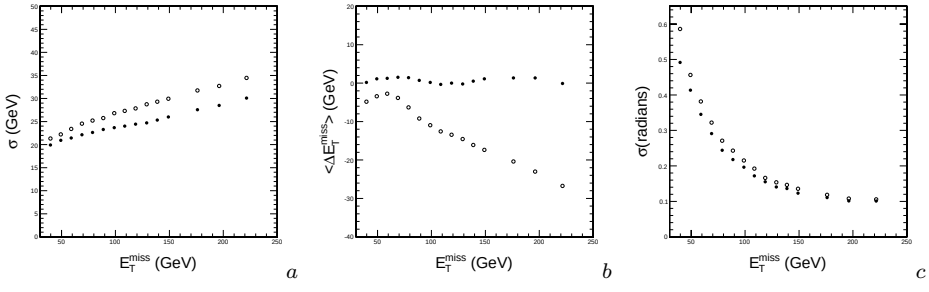

Figure 4.4: Missing transverse energy: a) energy resolution, b) error in the reconstructed E_T^{miss} scale and c) error in the direction of vector E_T^{miss} as a function of reconstructed E_T^{miss}, before (open circles) and after jet corrections (filled circles) for $t\bar{t}$ events [9].

Accurate determination of the inclusive E_T^{miss} spectrum is a difficult problem, because various detector factors contribute in subtle ways. These factors include energy resolution, limited detector coverage, non-linearity of calorimeter response, granularity of detector measurement, material in front of the calorimeter, the 4T magnetic field and its effect on low p_T charged particles, quantization of detector readout, electronic noise, event pileup, and underlying event. The energy resolution and errors of E_T^{miss} reconstruction are shown in Figure 4.4.

4.2.3 τ Tagging

The probability of τ lepton to decay hadronically is 65% (other main channels go to muons and electrons with almost equal probability ∼17%). Hadronically decayed τ leptons produce a jet-like cluster (τ-jet) containing a relatively small number of tracks. 77% of these jets consist of only one charged hadron and a number of π^0s. These are so-called one-prong decays. The probability of three-prong decay is $\sim$ 21%, and higher orders are already less important.

τ-jet finding algorithms rely on lower level objects like tracks, calorimeter clusters, jet candidates, etc. After recognizing a jet-like stucture the

main task is to distinguish it from other jets. There are huge number of QCD jets that could give a similar signature, but also muons, electrons and photons could be tagged as hadronic τ if they have other tracks in vicinity.

There are a number of methods for identifying hadronic τ-jets. These are based on τ lepton and τ-jet properties such as lifetime ($c\tau$= 87.11 μm), mass (m_τ = 1.78 GeV/c^2), small charged particle multiplicity, and the collimation and isolation of τ decay products. The optimal combination of the methods depends on the physics channel under consideration and method parameters are often a part of the physics analysis. Subsequently there is a very brief overview of the methods.

ECAL isolation method measures the localization of energy deposit in electromagnetic calorimeter. The τ-jet must be well isolated in terms of isolation parameter P_{isol} defined as

$$P_{isol} = \sum_{\Delta R<0.40} E_T - \sum_{\Delta R<0.13} E_T \tag{4.1}$$

where E_T is transverse energy deposit in electromagnetic calorimeter and ΔR is the distance in $\eta-\phi$ space from the τ-jet axis. Jets with $P_{isol} < P_{isol}^{cut}$ are considered τ candidate. The efficiency of the isolation criterion for different P_{isol}^{cut} values are given in Figure 4.5a.

Tracker isolation method reconstructs the signal cone (R_S) around leading track (tr_1) where are other tracks with similar z-impact parameters ($\Delta z_{tr} > |z_{tr} - z_{tr}^{tr1}|$). A larger isolation cone (R_i) is reconstructed where are no more new tracks and this is considered as a isolation criteria. Efficiencies for different isolation cone sizes can be seen in Figure 4.5b.

Tagging by impact parameter is considered after passing tracker isolation. The impact parameter measures if the track originates from the primary interaction vertex of from τ decay. The impact parameter can be computed in transverse plane or in three dimensions. The τ-jet must have only 1 track (3 tracks are already inefficient for QCD-jet rejection) within a significant impact parameter. The efficiencies for selecting τ and QCD jets in different bins of $E_T^M C$ can be seen in Figure 4.5c. The upper cut on the transverse impact parameter is increased starting from 100 μm (the highest cross in each point) in steps of 100 μm.

There are several other methods like tagging with flight path, tagging with mass, electron rejection, etc. (more details can be found from Ref [92]). The τ-jet energy measurement precision can be seen from Figure 4.6.

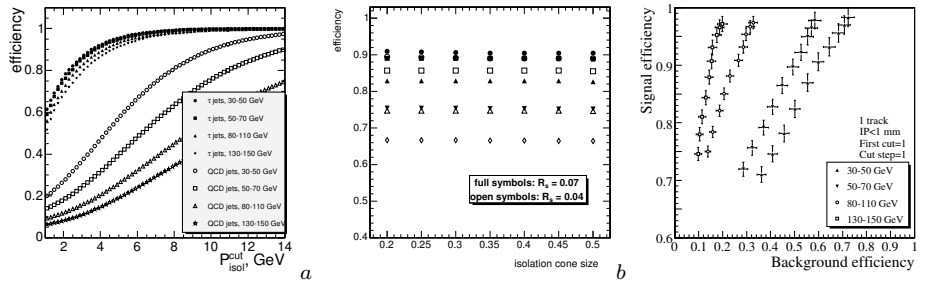

Figure 4.5: The efficiencies τ-tagging methods for: a) ECAL isolation parameter, b) tracker isolation parameter efficiency for τ-jet as a function of isolation cone for two values of signal cone R_S and c) impact parameter tagging efficiency for selecting τ and QCD-jets in different bins of E_T^{MC} when the upper cut on transverse impact parameter is increased, starting from 100 μm (highest cross in each set) in steps of 100 μm [9].

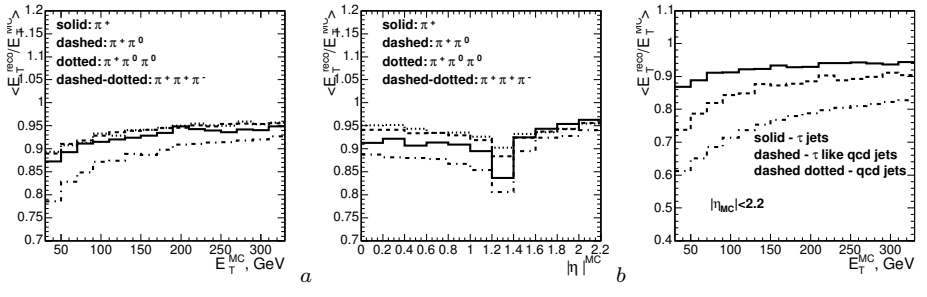

Figure 4.6: a,b) the ratio $r = E_T^{rec}/E_T^{MC}$ as a function of the E_T^{MC} (a) and τ-jet pseudorapidity (b) for different final states of hadronic decays of τ lepton. c) the ratio $r = E_T^{rec}/E_T^{MC}$ for the not preselected QCD jets (dash-dotted line), "tau-like" QCD jets (dashed line) and the real τ-jets (solid line) as a function of E_T^{MC} [9].

Chapter 5

Reconstruction and Analyses

5.1 Doubly Charged Higgs Production

At hadronic colliders like LHC and Tevatron the $\Phi^{\pm\pm}$ can be produced singly and in pairs. The main Feynman diagrams for $\Phi^{\pm\pm}$ production are shown in Figure 5.1: Drell-Yan pair production, Drell-Yan lepton production with radiative $\Phi^{\pm\pm}$ emission and WW fusion.

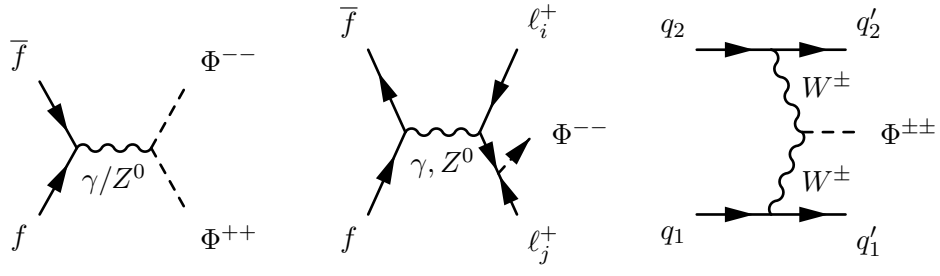

Figure 5.1: $\Phi^{\pm\pm}$ generation diagrams. From left to right: Drell-Yan pair production, Drell-Yan lepton production with radiative $\Phi^{\pm\pm}$ emission, WW fusion.

The cross section of the single $\Phi^{\pm\pm}$ production via the WW fusion process [48] $qq \to q'q'\Phi^{\pm\pm}$ scales as $\sim v_\Phi^2$. In the context of the littlest Higgs model this process, followed by the decays $\Phi^{\pm\pm} \to W^\pm W^\pm$, was studied in Ref. [52,54,55]. The detailed ATLAS simulation of this channel have shown that in order to observe 1 TeV $\Phi^{\pm\pm}$, one must have $v_\Phi > 29$ GeV [55]. This is in conflict with the precision physics bound $v_\Phi \leq 1.2$ GeV as well as with the neutrino data. Therefore the WW fusion channel is not experimentally promising for the discovery of the doubly charged Higgs.

The another single production process is Drell-Yan lepton production

with radiative $\Phi^{\pm\pm}$ emission. The coupling of this process is not known, but the primary process of electron positron scattering has a very large cross section, which could compensate for the low coupling. However this particular diagram has not been calculated yet and hence its effects cannot be estimated by the experiments.

The Drell-Yan pair production process [47, 48] $pp \to \Phi^{++}\Phi^{--}$ is not suppressed by any small coupling and its cross section is known up to next to leading order [49] (possible additional contributions from new physics such as Z' are strongly suppressed and can be neglected considering those effects here). Followed by the lepton number violating decays $\Phi^{\pm\pm} \to \ell^{\pm}\ell^{\pm}$, this process allows to reconstruct $\Phi^{\pm\pm}$ invariant mass from the same charged leptons. Assuming that the neutrino masses come from the coupling to the triplet Higgs, the $\Phi^{\pm\pm}$ leptonic branching ratios can be fixed. Due to the smallness of v_Φ the decays to WW may be neglected. The advantages of this process are the following:

1. The production cross section is known and it is independent from the unknown parameters of the model.

2. The decay $\Phi^{\pm\pm} \to \ell^{\pm}\ell^{\pm}$ is lepton number violating and allows to reconstruct $\Phi^{\pm\pm}$ invariant mass from the same charged leptons rendering the SM background very small in the signal region. Therefore it should provide a very clean detectable signature for the LHC detectors.

3. The known neutrino mixing $(m_\nu)_{ij} = (Y_\Phi)_{ij} v_\Phi$ predicts the branching ratios as $BR(\Phi^{\pm\pm} \to \mu^{\pm}\mu^{\pm}) = BR(\Phi^{\pm\pm} \to \tau^{\pm}\tau^{\pm}) = BR(\Phi^{\pm\pm} \to \mu^{\pm}\tau^{\pm}) = 1/3$. Here it is assumed that neutrinos have a normal hierarchy which implies negligible decay rates to the electron final states.

The Compact Muon Solenoid (CMS) is optimized for muon signals (in the parameter range of $p_T > 2$ GeV and $\eta < 2.4$ the discovery rate is close to 95% [20]), hence the final states that are considered are different combinations of muons, but tau leptons as well to improve discovery potential.

5.2 Invariant Mass Reconstruction

The $\Phi^{\pm\pm}$ is reconstructed using its decay products that could be muons or tau leptons. As there are two simultaneously produced Higgs bosons the final state consist of 4 leptons where the same charge leptons originate form

one Higgs boson. There are five possible signatures that can be associated to doubly charged Higgs pair.

- $\Phi^{++}\Phi^{--} \rightarrow 4\mu$: The cleanest and most simple channel.
- $\Phi^{++}\Phi^{--} \rightarrow 3\mu 1\tau$: The channel is easily reconstructable using an assumption that the neutrino originating from the τ decay is collinear with τ-jet and gives majority to the missing transverse energy (E_T^{miss}).
- $\Phi^{++}\Phi^{--} \rightarrow 2\mu 2\tau$: The signature can be reconstructed using the same assumptions for both τ-neutrinos. The whole E_T^{miss} vector has to be used here, while in the previous channel only one component was needed.
- $\Phi^{++}\Phi^{--} \rightarrow 1\mu 3\tau$: The channel can be reconstructed theoretically relying on an additional requirement that the two Higgs bosons have equal invariant masses. However, the reconstruction is very sensitive to the experimental accuracy of E_T^{miss} determination.
- $\Phi^{++}\Phi^{--} \rightarrow 4\tau$: The channel can not be reconstructed (and triggered by the single muon trigger).

Before reaching the detector, τ decays into an e, μ or a hadronic jet with branching ratios of 0.18, 0.17 and 0.65, respectively [97]. τ hadronic jets and μ-s are well visible and reconstructible in the CMS detector. The reconstruction of an energetic τ from electron decay is very sensitive to detector effects, involving sophisticated background processes [9], so its not taken account losing 31% of the total signal. Such loss is still sufficiently low and can be considered acceptable.

The reconstruction accuracy is reduced by the fact that a significant fraction of τ leptons (0.18) decays to secondary muons (μ') which cannot be distinguished from primary μ-s in the detector. Some arbitrary proportion of τ energy is carried away by neutrinos in this process. As a result there are more muons in final states. Occurrence probabilities of different reconstruction channels are presented in Table 5.1. The second column shows probabilities of Higgs decay to N μ-s and M τ-s. The following columns describe the final state after τ decay to μ'-s and/or jets. Different columns mark the number of secondary μ-s and the rows designate τ-jets in the detector recordings. The events having at least one $\tau \rightarrow e$ in a final state are not included. The proportions of reconstructible signatures are marked in a boldface. The table shows that 0...3 τ-jet channels together

with μ correction are almost equally important and overall reconstructible channels comprise 64% of total events.

Decay channel	After Higgs decay ($x = \tau$)	After τ decay ($x = jet_\tau$)				
		n=0	n=1	n=2	n=3	n=4
$\Phi^{++}\Phi^{--} \to 4\mu$	0.1111	**0.1111**	**0.0377**	**0.0107**	0.0012	0.0001
$\Phi^{++}\Phi^{--} \to 3\mu 1x$	0.2222	**0.1443**	**0.0736**	**0.0125**	0.0014	
$\Phi^{++}\Phi^{--} \to 2\mu 2x$	0.3333	**0.1407**	**0.0478**	0.0054		
$\Phi^{++}\Phi^{--} \to 1\mu 3x$	0.2222	**0.0610**	0.0207			
$\Phi^{++}\Phi^{--} \to 4x$	0.1111	0.0198				
Sum	1.0	**0.64** + 0.05				

Table 5.1: Probabilities of all possible decay channels for Φ pairs. "x" in the table marks τ or, after τ decay, τ-jet. "n" shows the number of secondary muons ($\tau \to \mu'$) in the final state. The numbers marked bold indicate possible reconstruction channels.

The invariant mass of $\Phi^{\pm\pm}$ is calculated from same charged lepton 4-momentums using the equation

$$(m_I^{\pm\pm})^2 = (p_1^{\pm} + p_2^{\pm})^2, \tag{5.1}$$

where $p_{1,2}$ is the μ or τ 4-momentum. Since the like-sign signal of μ-s or τ-s originate from a doubly charged Higgs boson, the invariant mass peak measures the mass of doubly charged Higgs, $m_I = M_\Phi$. 4-μ final state allows to obtain invariant masses directly from Eq.(5.1). In channels involving one or several τ-s, which are registered as τ-jets or secondary μ-s (marked as μ' below), the momenta of jets has to be corrected according to the equation system:

$$\mathbf{p}_\tau^i = k^i \mathbf{p}_{jet}^i, \tag{5.2}$$

$$\mathbf{p}_{Tmiss} = \sum_i \mathbf{p}_{T\nu}^i, \tag{5.3}$$

$$M_{\Phi++} = M_{\Phi--}, \tag{5.4}$$

where i counts τ-s, $\mathbf{p}$ marks 3-momentum, $\mathbf{p}_{T\nu}$ is the vector of transverse momentum of the produced neutrinos, $\mathbf{p}_{Tmiss}$ is the vector of missing transverse momentum (measured by the detector) and $k_i > 1$ are positive constants. Eq.(5.2) describes the standard approximation that the the decay products of a heavily boosted τ are collinear. Eq.(5.3) assumes missing

transverse energy only to be comprised of neutrinos from τ decays. In general, it is not a high-handed simplification, because the other neutrinos in the event are much less energetic and the detector error of E_T^{miss} is order of magnitude smaller. Using the first two formulas, it is possible to reconstruct up to two τ-s per event. Additional requirement of Eq.(5.4) allows to reconstruct the third τ per pair event, although very low measurement errors are needed.

As mentioned before the $p_{1,2}$ may also belong to secondary muons, that cannot be distinguished from primary ones. If reconstructed invariant masses of Φ^{++} and Φ^{--} are considerably different, it can be suspected that one or several μ-s originate form τ decays. In such cases the Eq.(5.2)-(5.4) has to be used to correct the 4-momenta of decay products. When only one secondary muon is present, E_T^{miss} points the same direction with its p_T. Otherwise E_T^{miss} is a superposition of neutrino transverse momenta. Such correction tightens the invariant mass peak of the signal and does not produce any artificial background.

5.3 Monte Carlo Study of $\Phi^{\pm\pm}$

The signatures of the signal are usually overwhelmed by similar final states originating form other processes. For example searching for doubly charged Higgs ($M_{\Phi^{\pm\pm}}$= 500 GeV) we are expecting 512 events during integrated luminosity 300 fb^{-1}, but only $b\bar{b}$ events produce 2.8×10^{10} similar $2\mu^+2\mu^-$ final states [4].

The main methodology is to simulate all possible background processes with Monte Carlo generators and invent several selection rules to improve signal (S) to background (B) ratio until the discovery is possible. The Monte Carlo simulations are carried out in several stages as described in Section 4. There are two levels of simulation: the physics generator level where only momentum vectors of final particles are gained for signal and background processes, and the full reconstruction level where the particles are propagated through detector simulation and reconstructed using simulated detector response. The full reconstruction is an order of magnitude more time consuming.

5.3.1 Generator Level Only Muon Final States

Four Muon Final States

The background arises mostly from the ZZ, $b\bar{b}$ and $t\bar{t}$ production and their muonic decay. Data-sets of 2.8×10^7 $b\bar{b}, t\bar{t}$ and 10^6 ZZ events for the background, and the data-sets of 5×10^5 signal events with $M_\Phi = 200, 500, 1000$ GeV were generated. Because those particles are lighter than Φ (the present bound from Tevatron is $M_\Phi \geq 136$ GeV [95, 96]) the background muons must have smaller p_T and it should not give an invariant mass peak. More details can be found from [5].

The selection rules that were applied on Monte Carlo generated particle data were:

1. *S1*: Only the muons with pseudorapidity $|\eta| < 2.4$ are detectable in the typical LHC detector, for example CMS [20]. Therefore, only the particles with $|\eta| < 2.4$ were selected from Monte Carlo generated data.

2. *S2*: All muons with transfer momentum $p_T < 25$ GeV were neglected.

3. *S3*: Only the events with at least 2 positive and 2 negative muons, the so called $2\mu^+2\mu^-$ events, were selected. The charge misidentification rate is very low for the LHC detectors, as mentioned above.

4. *S4*: The both reconstructed invariant masses with opposite charges were required to be approximately equal. This selection rule was considered with two different values: (1) a wider one, $0.5 < m_I^{++}/m_I^{--} < 1.5$ and (2) a more restrictive one, $0.9 < m_I^{++}/m_I^{--} < 1.1$, where $m_I^{\pm\pm}$ is the invariant mass of the same charged muons.

The selection rule S1 was applied first as it is a natural restriction of the real detectors at the LHC. The restriction of the detectors suppress mainly the soft energy background as it is more boosted. The S2 filter rules out all soft background particles and it saves computational resources for the next steps of the analyses. The S3 rule is natural if we are looking for two doubly charged Higgs bosons with the opposite charges and we have high charge identification rate (0.95). The final rule, S4, is based on fact that the invariant masses of same charged muon pairs have to be equal in the case of pair production of doubly charged Higgs boson. Naturally, some freedom is needed in the last condition due to decay width and experimental error of the detector. Therefore, the two versions of the rule S4 is marked as $S4_1$ and $S4_2$.

Table 5.2 describes the effect of the different selection rules. As one can see, after the last selection S4 the background is almost eliminated around the invariant mass peaks. Figure 5.2 plots the histogram for the invariant mass distribution of the like-sign muons for $M_\Phi = 500$ GeV and $M_\Phi = 1000$ GeV. The darkest histogram marks the signal left after the passage of full selection and the lightest histogram marks the signal in the detector ($|\eta| < 2.4$).

Process	Number of invariant masses			
	no cut	$p_T > 25$	$S4_1$	$S4_2$
Energy range 100...300 GeV				
$t\bar{t} \to 2\mu^+2\mu^-$	17192	875	381	86
$b\bar{b} \to 2\mu^+2\mu^-$	20196	1009	0	0
$ZZ \to 2\mu^+2\mu^-$	1313	655	345	67
M_Φ=200 GeV	4831 (3593)	3909 (3212)	3664 (3178)	3182 (2863)
Energy range 250...750 GeV				
$t\bar{t} \to 2\mu^+2\mu^-$	754	76.6	13.6	0
$b\bar{b} \to 2\mu^+2\mu^-$	0	0	0	0
$ZZ \to 2\mu^+2\mu^-$	172	81.5	26.6	3.0
M_Φ=500 GeV	151 (112)	143 (111)	129 (109)	98 (96)
Energy range 500...1500 GeV				
$t\bar{t} \to 2\mu^+2\mu^-$	18.4	1.9	0	0
$b\bar{b} \to 2\mu^+2\mu^-$	0	0	0	0
$ZZ \to 2\mu^+2\mu^-$	21.7	10.6	1.7	0
M_Φ=1000 GeV	4.52 (3.37)	4.37 (3.36)	3.87 (3.30)	2.91 (2.88)

Table 5.2: The number of $\Phi^{\pm\pm}$ candidates form $2\mu^+2\mu^-$ final states passing all the selection rules. The primary $2\mu^+2\mu^-$ events are given in the brackets. For the signal the branching ratios are $\mathrm{BR}(\Phi^{\pm\pm} \to \mu^\pm\mu^\pm) = \mathrm{BR}(\Phi^{\pm\pm} \to \mu^\pm\tau^\pm) = \mathrm{BR}(\Phi^{\pm\pm} \to \tau^\pm\tau^\pm) = 1/3$.

For the mass $M_\Phi = 1$ TeV one expects only ~ 3 doubly charged Higgs candidates although the total number of produced $\Phi^{\pm\pm}$ is ~ 33. As $\mathrm{BR}(\Phi^{\pm\pm} \to \mu^\pm\mu^\pm) = 1/3$ the strong signal suppression occurs because the probability for both $\Phi^{\pm\pm}$ to decay to two muons is $(1/3)^2 = 1/9$. The LHC can reach the Φ mass close to 1 TeV in the best case. To fully use CMS detector capacity must also be reconstructed tau leptons.

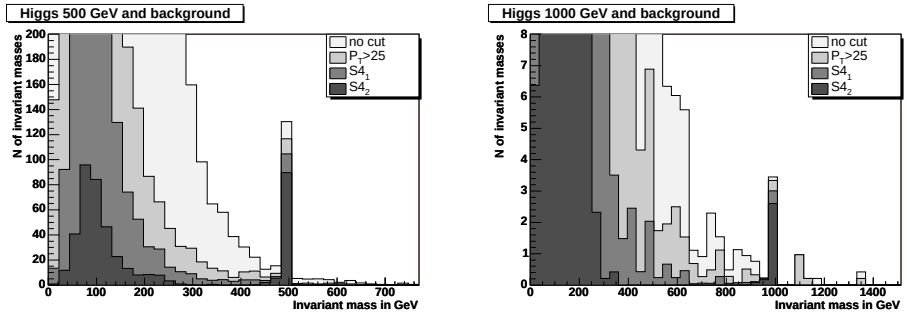

Figure 5.2: Distribution of the invariant mass of two like-sign muons. The darkest histogram marks the signal after full set of cuts for the $2\mu^+2\mu^-$ final state in the case of $M_\Phi = 500$ GeV and $M_\Phi = 1000$ GeV (the left and right panel, respectively). The background is very low around the invariant mass peak of the Higgs signal. In addition to the standard model background, the small "tail" of the self-generated $\Phi \to \tau \to \mu$ background is visible at the smaller invariant mass region close to the Higgs mass peak. The lighter histograms mark the signal with less selections applied, as indicated in the figures.

Two Muon Final States

In order to increase the LHC mass reach for $\Phi^{\pm\pm}$ discovery it was also studied the two like-sign muon final states (for details [4]). Although in this case one can identify more signal event candidates, also the background is larger. The dominant background processes giving $2\mu^\pm$ final states are listed in Table 5.3. Because the Monte Carlo generated data sets contain also additional muons from secondary decays the process like $Z^0 \to \mu^+\mu^-$ has to be added as additional background. Combining one of the Z decay products with the secondary muon one gets the fake signal which has to be eliminated. The $t\bar{t}$, $b\bar{b}$, ZZ background and the signal datasets are the same as in the 4μ study.

To minimize the background it is used the following selection rules. S1: event is counted only if it contains at least one like-sign muon pair. S2: event is rejected if it contains a quark with $p_T^{jet} > 20$ GeV. This corresponds to the jet veto and reduces the background from hadronic processes. S3: only muons with the pseudorapidity $\eta < 2.5$ are observable in CMS or ATLAS experiments. S4: it is required an opening angle between the two like-sign muons to be $\phi < 2.5$. S5: only muons with $p_T > 50$ GeV are

Process	N expected	$S1$ $2\mu^{\pm}$	$S2$ $p_T^{jet} > 20$	$S3$ $\eta < 2.5$	$S4$ $\phi < 2.5$	$S5$ $p_T > 50$
background						
$b\bar{b}$	$2.8 \cdot 10^{10}$	$9.4 \cdot 10^{8}$	$2.6 \cdot 10^{7}$	$2.5 \cdot 10^{6}$	$1.2 \cdot 10^{6}$	0
$t\bar{t}$	$1.3 \cdot 10^{8}$	$1.4 \cdot 10^{7}$	$3.6 \cdot 10^{5}$	$1.7 \cdot 10^{5}$	$1 \cdot 10^{5}$	4.4
WW	$2.7 \cdot 10^{4}$	1022	885	335	204	0
WZ	106	111	110	62	35	1.7
$Z \to 2\mu$	$1.5 \cdot 10^{7}$	$8.6 \cdot 10^{5}$	$6.6 \cdot 10^{5}$	$2.6 \cdot 10^{5}$	$1.5 \cdot 10^{5}$	12.8
$Z \to 2\tau$	$2.5 \cdot 10^{6}$	$1.4 \cdot 10^{5}$	$1.1 \cdot 10^{5}$	$4.5 \cdot 10^{4}$	$2.6 \cdot 10^{4}$	0
ZZ	177	369	363	207	115	7.5
total						26.4
signal						
$M_{\Phi} = 200$	$2 \cdot 10^{4}$	$1.6 \cdot 10^{4}$	$1.6 \cdot 10^{4}$	$1.3 \cdot 10^{4}$	8513	5832
$M_{\Phi} = 500$	512	401	389	356	225	199
$M_{\Phi} = 1000$	15	11	11	10	6	5.7

Table 5.3: The number of expected background and signal events for the integrated luminosity 300 fb^{-1}, and the number of $\Phi^{\pm\pm}$ candidates from the $2\mu^{\pm}$ final states passing each cut. For the signal events we have taken $BR(\Phi^{++} \to \mu^{+}\mu^{+}) = 1/3$.

taken and the events with at least one like-sign muon pair are selected. The number of events passing each selection rule are given in Table 5.3.

5.3.2 Full Reconstruction of μ and τ Final States

The Monte Carlo generated events were propagated through CMS detector with ORCA software to simulate the full detector response. Datasets were produced with Higgs boson mass from 200 GeV to 600 GeV and background processes that were taken account were as follows (for more details [2]):

- $t\bar{t} \to \mathrm{W^{+}W^{-}}b\bar{b}$ generated by PYTHIA, COMPHEP, ALPGEN, TOPREX and MADGRAPH with W boson decay $\mathrm{W} \to \ell\nu$ ($\ell = \mathrm{e}, \mu, \tau$) forced.
- $t\bar{t}\,\mathrm{Z} \to W^{+}W^{-}Zb\bar{b}$ generated with COMPHEP. The W and Z bosons are allowed to decay arbitrarily.

- Zb$\bar{\text{b}}$ where the Z boson decays to muons and τ leptons, generated with COMPHEP.

- ZZ generated with PYTHIA, where the Z bosons are forced to decay leptonically (e, μ, τ). The contribution of γ^* is included with m_{γ^*} >12 GeV.

The next-to-leading order (NLO) cross sections times branching ratios used for the backgrounds for $t\bar{t}$ →4l, $Zb\bar{b}$, ZZ and $t\bar{t}$ Z are accordingly $88.4 \cdot 10^3$, $52.4 \cdot 10^3$, 229.5 and 650 fb-s. The Monte Carlo statistics of the generated background exceed $30\,\text{fb}^{-1}$ except $Zb\bar{b}$ background, where it is $8\,\text{fb}^{-1}$. Therefore the results will be presented for an integrated luminosity of $10\,\text{fb}^{-1}$.

The events were triggered by the single muon trigger at Level 1 and HLT. After HLT the event was only used if it was possible to reconstruct the event primary vertex. If the primary vertex failed to be reconstructed the event was rejected.

The muons were reconstructed using Global Muon Reconstructor. The τ leptons were reconstructed using τ-jet candidates and missing transverse energy after selection cuts. The doubly charged Higgs boson invariant mass was reconstructed from the same charge lepton pairs after all selection cuts.

The selection cuts used on muons:

- the transverse momentum must be higher than 50 GeV. For background events 80% of muons have p_T less than 50 GeV while for the signal with Higgs boson mass 200 GeV it is 27% and for higher masses it reduces to around 10%.

- the distance to primary vertex in z-direction must not exceed 0.03 cm. It does not cut away any muons from the signal events but limits analysis to leptons coming from the same primary vertex.

The selection cuts used on τ jets:

- for τ jets we consider τ decays which involve 1 or 3 charged tracks. We use τ-jet candidates which passed the τ-jet filtering algorithms described in [92]. Two isolation criteria were used. Either one or three charged tracks in the signal cone and no charged tracks in the isolation cone or two tracks in signal cone and exactly one charged track in the isolation cone.

- the maximal distance to the primary vertex in the z-direction of any charged track in the τ jet must not exceed 0.2 cm.

$m_{\Phi}^{\pm\pm}$ (GeV)	200	300	400	500
N_{ev} expected at $10\,fb^{-1}$	26	10	4	2
$\sigma_{NLO} \pm$ stat $\pm$syst (fb)	$93.9^{+19.3}_{-17.5}$ ± 12.2	$19.6^{+6.6}_{-5.6}$ ± 2.5	$5.9^{+3.4}_{-2.5}$ ± 0.8	$2.2^{+1.9}_{-1.3}$ ± 0.3
Luminosity for 95% CL exclusion, fb^{-1}	1.3	3.0	7.7	16.8

Table 5.4: Expected number of events, NLO cross section with expected statistical and systematic uncertainty of the cross section measurement at $10\,fb^{-1}$, and integrated luminosity needed for exclusion at 95% CL [2]

- the transverse energy of the hottest HCAL tower of the τ jet must be higher than 2 GeV. This cut eliminates 86% of all electrons taken as τ candidates and only removes 7.5% of real τ jets.
- the transverse energy of the τ jet candidate must exceed 50 GeV. It has been chosen to be the same as the cut used on muons.
- no muon track should be in a cone with $\Delta R = 0.3$ constructed around the τ-jet candidate. If there is, then the candidate is dropped. This eliminates false τ-jet candidates which are generated when a charged muon track passes the same region as photons or hadrons. With this cut only a few real τ jets are discarded; however most of the false τ jets coming from this misidentification are rejected.

Missing transverse energy ($E_{\mathrm{T}}^{\mathrm{miss}}$) was reconstructed using calorimeter Type 1 $E_{\mathrm{T}}^{\mathrm{miss}}$ ($E_{\mathrm{T}}^{\mathrm{miss}}$ with the jet energy corrections) and p_T of muons.

Once the event leptons were reconstructed, some additional selections were performed:

- Z boson veto - if the odd sign pairing gives an invariant mass of 91 ± 5 GeV then these leptons are removed from further use.
- Same charge lepton pairs are reconstructed and only those reconstructed Higgs candidate pairs whose invariant mass difference is within 20% of each other are considered.

The reconstructed mass of doubly charged Higgs boson is shown on Figure 5.3 for the Higgs boson masses 200 and 500 GeV.

The selection rule efficiencies for signal and background processes can be found from [2]. Table 5.4 shows also the integrated luminosity needed

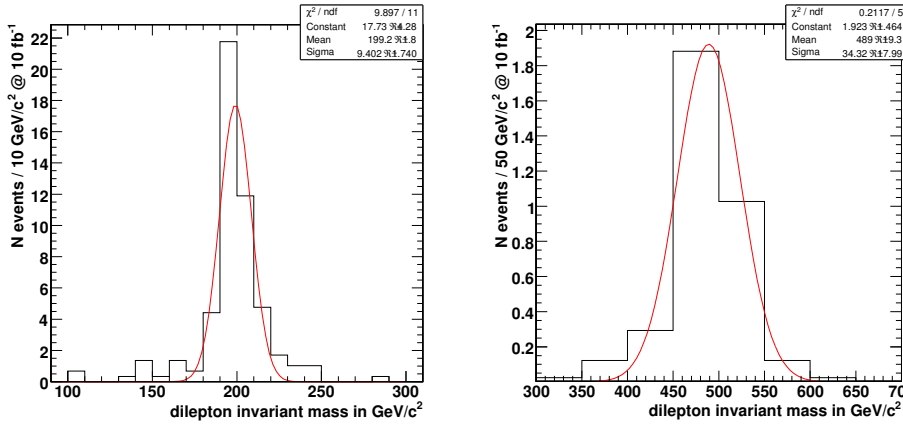

Figure 5.3: The reconstructed invariant mass for M($\Phi^{\pm\pm}$)=200 GeV and 500 GeV.

for exclusion at 95% CL and summarizes the expected number of events at $10\,\mathrm{fb}^{-1}$ with expected statistical and systematic uncertainties.

5.3.3 Generator Level of μ and τ Final States

The full detector study showed that the statistical information about events was too scarce to work out the best kinematical selection rules. Because of a big software change from ORCA, OSCAR, etc. to CMSSW framework additional production of signal and background events was impossible for almost a year. Consequently another generator level work was done on all four-lepton final states. This work was meant to be more general, not only for CMS detector. Nevertheless, the estimation of detector effects to the discovery potentials was based on the CMS performance that was predicted by the already obsolete version of CMS software.

This study comprised only the four-lepton background processes with reasonable cross-sections: $pp \to t\bar{t}$, $pp \to t\bar{t}Z$, $pp \to ZZ$ (for more details [3]). The importance of other processes was ruled out by previous studies. PYTHIA was used to generate $t\bar{t}$ and ZZ background ($t\bar{t}$ is forced to decay to $WWb\bar{b}$ and W leptonically). COMPHEP was used to generate the $Zt\bar{t}$ background via its PYTHIA interface [98, 99].

Generated particles were reconstructed within the pseudorapidity region $|\eta| < 2.4$ and with transverse momentum higher than 5 GeV. These were the natural restrictions of the CMS and ATLAS detectors at the LHC. These restrictions suppressed mainly the soft Standard Model background.

A clear signal extraction from the Standard Model background was achieved using a set of selection rules imposed on a reconstructed events in the following order.

- *S1*: events with at least 2 positive and 2 negative muons or jets which had $|\eta| < 2.4$ and $p_T > 5$ GeV were selected.

- *S2*: $\sum p_T$ (scalar) sum of 2 most energetic positive and negative μ-s or τ-jets had to be bigger than a certain value (depending on Higgs mass). The advantage compared to the widely used p_T cut for a single particle can clearly be seen from Figure 5.4.

- *S3*: Z-tagging – if invariant mass of the pair of opposite charged μ-s or τ-jets was nearly equal to Z mass (85-95 GeV), then the particles were eliminated from the analysis.

- *S4*: as Φ-s were produced in pairs, the reconstructed invariant masses (in one event) had to be equal. We used the following condition for further background suppression

$$0.8 < m_I^{++}/m_I^{--} < 1.2. \tag{5.5}$$

  If the invariant masses satisfied the condition they were included to the histogram. Otherwise it was suspected that some μ-s might originate from τ decay, and made an attempt to find corrections to their momenta according to the method described above. Figure 5.5 gives a clear picture of the behavior of signal and background under this selection rule.

While the selection rules S1, S3 and S4 are independent of the Higgs mass, the selection rule S2 ($\sum p_T$ cut) has to be optimized for a certain Higgs mass value. The cut may be set to a very high value which eliminates all background events, but inevitable loss in signal may postpone the discovery of new physics at LHC. Thus it was natural to take the minimal discovery luminosity (L_{min}) as the optimization criteria. Looking for a cut value that enables to make a discovery with the lowest luminosity, we are dealing with small signal and background expectations by definition. Simple significance estimators cannot be exploited here. The log-likelihood ratio (LLR) statistical method [100, 101] was used to demand 5σ discovery potential to be bigger than 95% ($1 - \mathrm{CL}_{s+b} > 0.95$) as for a discovery criteria. This is a rather strong requirement, because it allows to make a discovery (meaning the fluctuation of background may mimic the outcome of an experiment with probability less than $2.9 \cdot 10^{-7}$ (5σ)) during

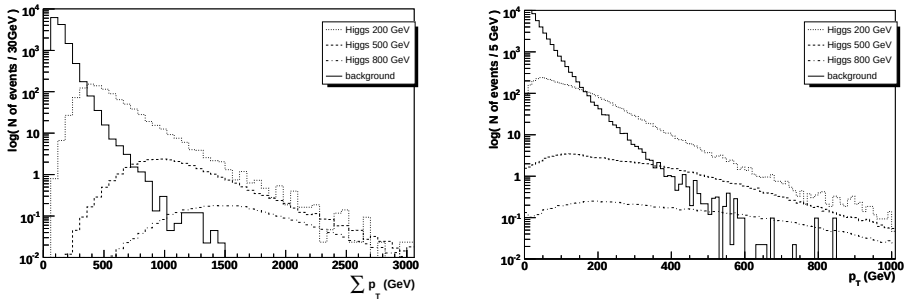

Figure 5.4: The left panel shows the distribution of events according to scalar sum of 2 most energetic (highest p_T) positively and 2 most energetic negatively charged muons or jets ($\sum p_T$). The right panel shows the distribution of events considering traditional p_T cut for single particles. Both figures correspond to luminosity $\mathcal{L} = 30 fb^{-1}$.

the specified luminosity with a probability of 95% (if s+b hypothesis is correct). The widely used convention, that significance should exceed five, gives only 50% discovery potential in Gaussian limit and diminishes to very small values when background approaches zero.

The best value for S2 cut does depend on M_Φ but is not too sensitive to it. Typically the $\sum p_T$ can be assigned a value with a precision of 100 GeV while affecting the minimum luminosity by only a couple of percent. In the Table 5.5 the approximated middle point of this value is given. As the best S2 cut is very strong, it suppresses almost entirely the generated background (being combined with the other selection rules). For Higgs masses above 500 GeV the background is totally suppressed and the discovery potential criteria meets the requirement for 3 signal events (6 invariant masses). Nevertheless we cannot infer that the background is really zero in nature. To estimate the statistical error due to final number of generated background events we have found 95% upper limit of background according to Poisson statistics [2]. Using this limit in LLR analysis we get much higher luminosities for discovery. Even a very small background expectancy ($b = 0.01$) gives some possibility to have one ($9.9 \cdot 10^{-3}$) or two ($4.9 \cdot 10^{-5}$) background events in the experiment and these outcomes cannot be interpreted as discovery anymore. This phenomenon shifts the minimal required luminocity to much higher values denoted as $\mathcal{L}_{max}$ in Table 5.5 (marked as MC).

As the full detector simulation was not possible at that time due to

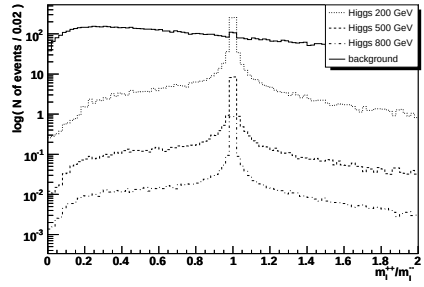

Figure 5.5: Distribution of events according to the ratio of reconstructed invariant masses ($m_{\Phi++}/m_{\Phi--}$) (no other cuts are applied). The figure corresponds to luminosity $\mathcal{L} = 30fb^{-1}$.

the big software change the detector effects were estimated using simplified smearing technique [3]. The result of such a distortion is a decrease in both signal and background approximately by factor two (Table 5.5) (marked as Det Eff). As the background and the signal decrease proportionally, the luminosity needed for discovery roughly doubles.

Mass of Φ	200	300	400	500	600	700	800	900	1000
Optimal S2	300	400	600	700	860	860	860	860	860
MC $\mathcal{L}_{min}$	0.25	0.93	2.0	3.6	8	17	34	62	120
MC $\mathcal{L}_{max}$	0.26	1.03	3.1	7.0	17	38	77	160	320
Optimal S2	300	400	600	700	860	860	860	860	860
Det Eff $\mathcal{L}_{min}$	0.526	1.20	3.0	6.6	15	30	60	111	200
Det Eff $\mathcal{L}_{max}$	0.546	2.19	6.5	16.6	39	86	190	420	900

Table 5.5: Optimal $\sum p_T$ cut for different Higgs masses and the corresponding minimal discovery luminosities: the lower ($\mathcal{L}_{min}$) corresponds to the generated background in our analyses and the higher ($\mathcal{L}_{max}$) corresponds to 95% upper limit of the background error.

Chapter 6

Conclusions

It is shown that the scalar triplet Higgs model is a very simple and promising extension to the Standard Model. It provides an interesting connection between high energy physics at the LHC collider and lower energy physics at the neutrino experiments. The neutrino mass mechanism which naturally occurs in those models can be directly tested through the detection of doubly charged Higgs boson.

There is a very pure experimental signature from the leptonic decays of Drell-Yan pair produced Higgs bosons. To investigate the detection possibilities several Monte Carlo studies were carried out, including pure physics generator level as well as full detector simulations. Appropriate selection rules and reconstruction techniques were derived for four-lepton signal using muons and τ leptons. As it is found out from the Monte Carlo simulations, the CMS experiment should be capable of detecting the Higgs boson if its mass stays below 1 TeV.

Once it is found and sufficient statistical data is collected (in lower Φ^{++} masses) about its leptonic decay branching ratios it will be possible to measure the currently unknown neutrino parameters that neutrino oscillation experiments are not sensitive to. These include the mass hierarcy, the mass of the lightest neutrino and the Majorana phases [11].

Chapter 7

Summary of the Related Publications

The thesis links the studies of five publications from the dissertant [1–5]. The work does not include the set of publication, reports and technical notes from the dissertant, which are not directly related to the topic of the current thesis. This excluded set of publications covers some experimental, detailed technical and computational topics in particle physics [6–10].

7.1 Publication I

M. Raidal *et al.*
"Flavour physics of leptons and dipole moments."
EPJ. C **57** (2008) 715 [arXiv:0801.1826].

This work has been done as a chapter of the report of the "Flavour in the era of the LHC" workshop at CERN. In general, the report discusses a wide set of theoretical, phenomenological and experimental issues related to flavour phenomena in the charged lepton sector and in flavour-conserving CP-violating processes. The current experimental limits and the main theoretical models for the flavour structure of fundamental particles are reviewed carefully. The phenomenological consequences of the available data are analyzed to setting constraints on explicit models beyond the Standard Model. The benchmarks for the discovery potential of forthcoming measurements both at the LHC and at low energy (g–2, factories etc) are presented. Some suggestions are made for possible future experiments.

In concrete, our studies in the current framework are focused on an

open issue, the origin of non-zero neutrino masses in the context of Little Higgs models. The neutrino mass occurs naturally in these models from the triplet Higgs mechanism (type-II see-saw) which employs a scalar with the $SU(2)_L \times U(1)_Y$ quantum numbers $\tilde{\Phi}(3,2)$. The existence of the triplet in some versions of the Little Higgs models is a direct consequence of global symmetry breaking. The global symmetry is needed to protect the Standard Model Higgs from the radiation corrections of higher scales. In other words, the global symmetry is a possible solution for the hierarchy problem. As an example, in the minimal Littlest Higgs model, the triplet Higgs with non-zero hypercharge occurs from the breaking of global $SU(5)$ down to $SO(5)$ symmetry as one of the Goldstone bosons. Its mass $M_\Phi \tilde{g}_s f$, where $g_s < 4\pi$, is a model dependent coupling constant in the weak coupling regime. It is therefore predicted to be below the cut-off scale Λ and it could be within the mass reach of LHC. The present lower bound for the invariant mass of Φ is set by Tevatron to $M_\Phi \geq 136$ GeV.

7.2 Publication II

G. L. Bayatian *et al.* [CMS Collaboration]
"CMS technical design report, volume II: Physics performance."
J. Phys. G **34** (2007) 995.

This report is the result of several years of work of the CMS collaboration on the preparation for physics analysis at the CERN LHC collider experiment with the CMS detector. The report includes all the subprojects in all areas (Detector, PRS, Software and Computing) in order to produce the large Monte Carlo simulation samples needed, to develop the software to analyse those samples, to perform the studies reported, and to review the findings of the collaboration.

Our work covers Section 2 in Chapter 12 of the report, p.p. 392-402. We have investigated the possibility of direct tests of little Higgs models incorporating the triplet Higgs neutrino mass mechanism at LHC experiments. We have performed Monte Carlo studies of Drell-Yan pair production of doubly charged Higgs boson Φ^{++} (in the context of LHC). After the boson is produced, it decays into leptons with the branching ratios fixed from neutrino oscillation data. We propose appropriate selection rules for the four-lepton signal, including reconstructed taus. The Standard Model background can be effectively eliminated in the context of the CMS detector, so we optimize our analysis for a small number of signal events to reach the

discovery at the lowest possible integrated luminosity. In this case, correct statistical treatment of the discovery potential is a crucial aspect. Adding detection efficiencies and measurement errors to our Monte Carlo analyses, Φ^{++} can be discovered with the integrated luminosities (exclusion at 95% CL): 1.3 fb^{-1} at $M_\Phi = 200$ GeV, 3.0 fb^{-1} at $M_\Phi = 300$ GeV, 7.7 fb^{-1} at $M_\Phi = 400$ GeV, 16.8 fb^{-1} at $M_\Phi = 500$ GeV.

7.3 Publication III

A. Hektor, M. Kadastik, M. Müntel, M. Raidal, and L. Rebane.
"Testing neutrino masses in little Higgs models via discovery of doubly charged Higgs at LHC."
Nucl. Phys. B **787** (2007) 198 [arXiv:0705.1495].

The possibility of direct tests of little Higgs models incorporating triplet Higgs neutrino mass mechanism have been studied at the CERN LHC experiments. We have used Monte Carlo techniques to study the Drell-Yan pair production of doubly charged Higgs boson Φ^{++} followed by its leptonic decays. The neutrino oscillation data fixes the branching ratios of the decays. We have proposed some selection rules for the four-lepton signal including reconstructed tau leptons. The rules are optimized for the discovery of Φ^{++} with the lowest LHC luminosity phase. We show that the Standard Model background can be effectively eliminated. An important aspect of our study is the correct statistical treatment of the LHC discovery potential in the region of small event numbers. Together with included detection efficiencies and measurement errors, in the Monte Carlo analysis Φ^{++} can be discovered up to the mass 250 GeV in the first year of LHC, and 700 GeV mass is reachable for the integrated luminosity $L = 30$ fb^{-1} of LHC.

7.4 Publication IV

B. C. Allanach *et al.*
"Les Houches 'physics at TeV colliders 2005' beyond the standard model working group: Summary report."
(2006) [arXiv:hep-ph/0602198].

This is a summary report of the fourth Workshop: "Physics at TeV Colliders" in Les Houches which brought together theorists and experi-

mentalists who were working on the phenomenology of the upcoming TeV colliders. Although the summary report is not published in any journals, it is well known and quite highly cited through electronic library servers. It comprises several Beyond the Standard Model problems (SUSY and non–SUSY) as well as some computing tool issues.

Our work covers Part 28 in the report, p.p.191-196. Motivated by predictions of the littlest Higgs model, full detector simulation Monte Carlo studies are carried out for doubly charged Higgs pair production. We assume that triplet Higgs also generates the observed neutrino masses which fixes the Φ^{++} leptonic branching ratios. This allows to test neutrino mass models at LHC. We have generated and analyzed the signal as well as the background processes for both four muon and two muon final states. Studying the invariant mass distribution of the like-sign muon pairs allows to discover the doubly charged Higgs with the mass M_Φ= 1050 GeV. Relaxing the neutrino mass assumption, and taking BR($\Phi \to \mu + \mu$) = 1, the LHC discovery reach increases to M_Φ = 1.2 TeV

7.5 Publication V

A. Hektor, M. Kadastik, K. Kannike, M. Müntel, M. Raidal
"Studying doubly charged Higgs pair production at the LHC."
Estonian Acad. Sci. Phys. Math. **55(2)** (2006) 128.

The little Higgs models predict a rich phenomenology for the future collider experiments. Our attention is focused on the littlest Higgs model. We carry out a generator level Monte Carlo study of the doubly charged Higgs pair production ($pp \to \Phi^{++}\Phi^{--}$). The branching ratios are fixed using an assumption that, in addition, the observed masses of the neutrinos are generated by triplet Higgs: BR ($\Phi^{\pm\pm} \to \mu^\pm\mu^\pm$) = BR ($\Phi^{\pm\pm} \to \mu^\pm\tau^\pm$) = BR ($\Phi^{\pm\pm} \to \tau^\pm\tau^\pm$) = 1/3. We study the invariant mass distribution of same-charged muon pairs ($\Phi^{\pm\pm} \to 2\mu^\pm$) together with the background processes from the standard model: $b\bar{b}, t\bar{t}$, and ZZ production. To suppress the background, we propose a new type of selection rule, suitable in the case of production of the pairs of equal mass particles ($\Phi^{\pm\pm}$). This selection rule ensures high significance of the signal over the background of the Standard Model and implies a very small cut of the signal under study. At the Monte Carlo level the doubly charged Higgs can be visible at the LHC in the mass range up to approximate 1 TeV.

Summary in Estonian

Topleltlaetud Higgsi Bosoni Detekteerimine CMSi Detektoril

Elementaarosakeste Standardmudel on olnud äärmiselt edukas kirjeldamaks elektromagnetilist, nõrka ja tugevat interaktsiooni osakeste vahel. Ometi on sellel ka mõned olulised puudused, mis on pannud füüsikuid otsima võimalikke täiendusi, et seletada teistest eksperimentidest teadaolevaid andmeid, mida Standardmudel ei kirjelda. Üheks selliseks ajendiks on neutriinode ostsillatsioonidest teadaolevad neutriinode massid. Kuigi Standardmudelis sisalduv Higgsi väli võimaldab sümmeetria spontaanse rikkumise kaudu seletada teiste osakeste masse, jätab see neutriinod massituks.

Lisades Standardmudelile skalaarse tripleti, millel on vastasmõju ainult leptonite ja elektronõrga sektoriga, võib ennustada uut osakest, topeltlaetud Higgsi bosonit. See on üks $SU(2)_L$ tripletse Higgsi bosoni komponent, mis on seotud elektronõrga sümmeetriarikkumise väiksema Higgsi mudeliga.

Käesolev doktoritöö ("Topeltlaetud Higgsi bosoni detekteerimine CMS-i detektoril") võtab kokku viis autori poolt doktoriõpingute perioodil avaldatud publikatsiooni, milles on uuritud topeltlaetud Higgsi bosoni avastamise võimalusi peagi käikumineval LHC kiirendil. Monte Carlo meetodiga on uuritud bosonipaaride teket ($pp \to \Phi^{++}\Phi^{--}$) ja nende järgnevaid lagunemisi leptoniteks. Erinevate lagunemiskanalite jaoks on välja töötatud analüüsialgoritmid, mis võimaldavad eristada otsitavat osakest teistest samalaadseid eksperimentaalseid jälgi andvatest Standardmudeli taustaprotsessidest. Osutub, et topeltlaetud Higgsi boson on avastatav, kui selle mass jääb alla 1 TeV.

Kui reaalses eksperimendis õnnestub topeltlaetud Higgsi boson leida ja on olemas piisav statistika selle lagunemiskanalite kohta, on võimalik määrata nende harusuhete kaudu ka mitmeid neutriinode parameetreid, mis

jäävad ostsillatsiooni eksperimentidele kättesaamatuks (neutriinode massi-de hierarhia, kergeima neutriino mass ja Majorana faasid).

Doktoritöö algab ülevaatega Suurest Hadronite Põrkurist (LHC) ja selle CMS-i eksperimendi riistvarast. Järgeb ülevaade elektronõrga sümmeetria rikkumise probleemist (EWSB) ja supersümmeetriast (SUSY) kui võimalikust lahendusest sellele. Alternatiivse võimalusena on tutvustatud väiksemat Higgsi mudelit ja näidatud, kuidas seda saab siduda neutriinode füüsikaga LHC eksperimendis. Neljas peatükk kirjeldab Monte Carlo eksperimentide põhimõtteid ja annab ülevaate vastavast CMS tarkvarast. Viies peatükk võtab kokku erinevad MC uuringud topeltlaetud Higgsi bosoni kohta. Töö lõppeb põgusa kokkuvõtte ja ülevaatega lisatud publikatsioonidest.

Bibliography

[1] M. Raidal *et al.*, "Flavour physics of leptons and dipole moments," arXiv:0801.1826 [hep-ph].

[2] G. L. Bayatian *et al.* [CMS Collaboration], J. Phys. G **34**, 995 (2007).

[3] A. Hektor, M. Kadastik, M. Muntel, M. Raidal and L. Rebane, Nucl. Phys. B **787**, 198 (2007) [arXiv:0705.1495].

[4] B. C. Allanach *et al.*, "Les Houches 'Physics at TeV colliders 2005' Beyond the standard model working group: Summary report," [arXiv:hep-ph/0602198].

[5] A. Hektor, M. Kadastik, M. Muntel, M. Raidal and L. Rebane, Est. Ac. Sci. Phys. Math. **55(2)**, 128 - 136, 2006.

[6] S. Chatrchyan, et al. [CMS Collaboration] JINST, **3**, S08004, 2008.

[7] F. del Aguila *et al.*, arXiv:0801.1800 [hep-ph].

[8] D. G. . d'Enterria *et al.* [CMS Collaboration], J. Phys. G **34**, 2307 (2007).

[9] G. L. Bayatian *et al.* [CMS Collaboration], "CMS physics: Technical design report," CERN-LHCC-2006-001, (2006)

[10] G. L. Bayatian *et al.* [CMS Collaboration], "CMS physics TDR 8.2" CERN-LHCC-2006-021, (2006)

[11] M. Kadastik, M. Raidal and L. Rebane, Phys. Rev. D **77**, 115023 (2008) [arXiv:0712.3912 [hep-ph]].

[12] O. Bruning, et al., "LHC design report. Vol. I: The LHC main ring," CERN-2004-003-V-1, (2004)

[13] "ATLAS: Detector and physics performance technical design report. Volume 1," ATLAS-TDR-14, CERN-LHCC-99-14, (1999)

[14] "ATLAS detector and physics performance. Technical design report. Vol. 2," ATLAS-TDR-15, CERN-LHCC-99-15, (1999)

[15] "CMS, the Compact Muon Solenoid: Technical proposal," CERN-LHCC-P-1, CERN-LHCC-94-38, (1994)

[16] S. Amato *et al.* [LHCb Collaboration], "LHCb technical proposal," CERN-LHCC-P-4, CERN-LHCC-98-04, (1998)

[17] "ALICE: Technical proposal for a large ion collider experiment at the CERN LHC," CERN-LHCC-P-3, CERN-LHCC-95-71, (1995)

[18] R. Bailey, *Prepared for 11th Workshop on Electronics for LHC and Future Experiments (LECC 2005), Heidelberg, Germany, 12-16 September 2005*

[19] G. Acquistapace *et al.* [CMS Collaboration], "CMS, the magnet project: Technical design report," CERN-LHCC-97-10, (1997)

[20] "CMS, the Compact Muon Solenoid. Muon technical design report," CERN-LHCC-97-32, (1997)

[21] [CMS Collaboration], "CMS, tracker technical design report," CERN-LHCC-98-06, (1998)

[22] S. Dasu *et al.* [CMS Collaboration], "CMS. The TriDAS project. Technical design report, vol. 1: The trigger systems," CERN-LHCC-2000-038, (2000)

[23] P. Sphicas [CMS Collaboration], "CMS: The TriDAS project. Technical design report, Vol. 2: Data acquisition and high-level trigger," CERN-LHCC-2002-026, (2002)

[24] G. Bayatian *et al.*, Eur. Phys. J. C **53**, 139 (2008).

[25] http://www.cern.ch/

[26] http://greybook.cern.ch/

[27] [CMS Collaboration], "Addendum to the CMS tracker TDR," CERN-LHCC-2000-016, (2000)

[28] "CMS: The electromagnetic calorimeter. Technical design report," CERN-LHCC-97-33, (1997)

[29] "CMS: The hadron calorimeter technical design report," CERN-LHCC-97-31, (1997)

[30] J. Wess and B. Zumino, Phys. Lett. B **49**, 52 (1974).

[31] Yu. A. Golfand and E. P. Likhtman, JETP Lett. **13**, 323 (1971) [Pisma Zh. Eksp. Teor. Fiz. **13**, 452 (1971)].

[32] G. Altarelli, F. Feruglio and I. Masina, JHEP **0011**, 040 (2000) [arXiv:hep-ph/0007254].

[33] A. B. Lahanas, N. E. Mavromatos and D. V. Nanopoulos, Int. J. Mod. Phys. D **12**, 1529 (2003) [arXiv:hep-ph/0308251].

[34] A. Zee, *Princeton, UK: Princeton Univ. Pr. (2003) 518 p*

[35] D. I. Kazakov, arXiv:hep-ph/0012288.

[36] H. Pagels and J. R. Primack, Phys. Rev. Lett. **48**, 223 (1982).

[37] W. de Boer, Prog. Part. Nucl. Phys. **33**, 201 (1994) [arXiv:hep-ph/9402266].

[38] S. Eidelman *et al.* [Particle Data Group], Phys. Lett. B **592**, 1 (2004).

[39] A. Hasenfratz, P. Hasenfratz, K. Jansen, J. Kuti and Y. Shen, Nucl. Phys. B **365**, 79 (1991).

[40] V. A. Miransky, M. Tanabashi and K. Yamawaki, Phys. Lett. B **221**, 177 (1989).

[41] E. Farhi and L. Susskind, Phys. Rept. **74**, 277 (1981).

[42] B. Holdom and J. Terning, Phys. Lett. B **247**, 88 (1990).

[43] A. Dobado, D. Espriu and M. J. Herrero, Phys. Lett. B **255**, 405 (1991).

[44] G. F. Giudice, C. Grojean, A. Pomarol and R. Rattazzi, JHEP **0706**, 045 (2007) [arXiv:hep-ph/0703164].

[45] A. Abada, C. Biggio, F. Bonnet, M. B. Gavela and T. Hambye, JHEP **0712**, 061 (2007) [arXiv:0707.4058 [hep-ph]].

[46] J. F. Gunion, C. Loomis and K. T. Pitts, *In the Proceedings of 1996 DPF / DPB Summer Study on New Directions for High-Energy Physics (Snowmass 96), Snowmass, Colorado, 25 Jun - 12 Jul 1996, pp LTH096* [arXiv:hep-ph/9610237].

[47] J. F. Gunion, J. Grifols, A. Mendez, B. Kayser and F. I. Olness, Phys. Rev. D **40**, 1546 (1989).

[48] K. Huitu, J. Maalampi, A. Pietila and M. Raidal, Nucl. Phys. B **487**, 27 (1997) [arXiv:hep-ph/9606311].

[49] M. Muhlleitner and M. Spira, Phys. Rev. D **68**, 117701 (2003) [arXiv:hep-ph/0305288].

[50] A. G. Akeroyd and M. Aoki, Phys. Rev. D **72**, 035011 (2005) [arXiv:hep-ph/0506176].

[51] T. Rommerskirchen and T. Hebbeker, J. Phys. G **33**, N47 (2007).

[52] T. Han, H. E. Logan, B. McElrath and L. T. Wang, Phys. Rev. D **67**, 095004 (2003) [arXiv:hep-ph/0301040].

[53] W. Kilian and J. Reuter, Phys. Rev. D **70**, 015004 (2004) [arXiv:hep-ph/0311095].

[54] T. Han, H. E. Logan and L. T. Wang, JHEP **0601**, 099 (2006) [arXiv:hep-ph/0506313].

[55] G. Azuelos *et al.*, Eur. Phys. J. C **39S2**, 13 (2005) [arXiv:hep-ph/0402037].

[56] S. Antusch, J. Kersten, M. Lindner and M. Ratz, Nucl. Phys. B **658**, 203 (2003) [arXiv:hep-ph/0211385].

[57] S. H. Lee, S. Sasaki, I. Vasserman, D. R. Walters and D. E. Kim, *In the Proceedings of 27th International Free Electron Laser Conference (FEL 2005), Stanford, California, 21-26 Aug 2005, pp TUOC003* [arXiv:/].

[58] T. Han, H. E. Logan, B. Mukhopadhyaya and R. Srikanth, Phys. Rev. D **72**, 053007 (2005) [arXiv:hep-ph/0505260].

[59] F. del Aguila, M. Masip and J. L. Padilla, Phys. Lett. B **627**, 131 (2005) [arXiv:hep-ph/0506063].

[60] S. R. Choudhury, N. Gaur and A. Goyal, Phys. Rev. D **72**, 097702 (2005) [arXiv:hep-ph/0508146].

[61] A. Abada, G. Bhattacharyya and M. Losada, Phys. Rev. D **73**, 033006 (2006) [arXiv:hep-ph/0511275].

[62] J. Schechter and J. W. F. Valle, Phys. Rev. D **22**, 2227 (1980).

[63] E. Ma and U. Sarkar, Phys. Rev. Lett. **80**, 5716 (1998) [arXiv:hep-ph/9802445].

[64] N. Arkani-Hamed, A. G. Cohen, E. Katz and A. E. Nelson, JHEP **0207**, 034 (2002) [arXiv:hep-ph/0206021].

[65] "ORCA", http://cmsdoc.cern.ch/orca

[66] "CMSSW", http://cmsdoc.cern.ch/cms/cpt/Software/html/General/

[67] [CMS Collaboration], "CMS: The computing project. Technical design report," CERN-LHCC-2005-023, (2005)

[68] V. Innocente, L. Silvestris and D. Stickland, Comput. Phys. Commun. **140**, 31 (2001).

[69] "CMSIM", http://cmsdoc.cern.ch/cmsim/cmsim.html

[70] "CMKIN" http://cmsdoc.cern.ch/cmsoo/projects/CMKIN/

[71] "OSCAR", http://cmsdoc.cern.ch/oscar

[72] "FAMOS" http://cmsdoc.cern.ch/FAMOS/

[73] T. Sjostrand, et al. "PYTHIA 6.2: Physics and manual", [hep-ph/0108264]

[74] "COMPHEP", http://comphep.sinp.msu.ru/

[75] G. Altarelli and G. Parisi, Nucl. Phys. B **126**, 298 (1977).

[76] V. N. Gribov and L. N. Lipatov, Sov. J. Nucl. Phys. **15**, 438 (1972) [Yad. Fiz. **15**, 781 (1972)].

[77] S. Agostinelli *et al.* [GEANT4 Collaboration], Nucl. Instrum. Meth. A **506**, 250 (2003).

[78] T. Sjostrand, L. Lonnblad, S. Mrenna and P. Skands, arXiv:hep-ph/0308153.

[79] M. Case, et al., "Detector Description Domain Architecture and Data Model", CMS. NOTE 2001-057 (2001).

[80] "CMS Software and Computing Group", "Object Oriented Reconstruction for CMS Analysis", cms-in1999-001, (1999)

[81] "IGUANA Web Site", http://iguana.web.cern.ch/iguana/

[82] "SCRAM", http://cmsdoc.cern.ch/Releases/SCRAM

[83] "CMS Remote Analysis Builder", http://cmsdoc.cern.ch/cms/ccs/wm/www/Crab

[84] R. Frühwirth, NIMPA **A262**, 2-3, 444-450, (1987)

[85] V. Innocente, M. Maire, E. Nagy, "GEANE: Average Tracking and Error Propagation Package", IT-ASD W5013-E", (1991)

[86] S. V. Chekanov, arXiv:hep-ph/0211298.

[87] G. C. Blazey *et al.*, arXiv:hep-ex/0005012.

[88] J. M. Butterworth, J. P. Couchman, B. E. Cox and B. M. Waugh, Comput. Phys. Commun. **153**, 85 (2003) [arXiv:hep-ph/0210022].

[89] S. D. Ellis and D. E. Soper, Phys. Rev. D **48**, 3160 (1993) [arXiv:hep-ph/9305266].

[90] G. Arnison *et al.* [UA1 Collaboration], Phys. Lett. B **122**, 103 (1983).

[91] "ROOT", http://root.cern.ch/".

[92] G. Bagliesi *et al.*, CERN-CMS-NOTE-2006-028, (2006)

[93] T. Sjostrand, P. Eden, C. Friberg, L. Lonnblad, G. Miu, S. Mrenna and E. Norrbin, Comput. Phys. Commun. **135**, 238 (2001) [arXiv:hep-ph/0010017].

[94] G. Barenboim, K. Huitu, J. Maalampi and M. Raidal, Phys. Lett. B **394**, 132 (1997) [arXiv:hep-ph/9611362].

[95] D. E. Acosta *et al.* [CDF Collaboration], Phys. Rev. Lett. **93**, 221802 (2004) [arXiv:hep-ex/0406073].

[96] V. M. Abazov *et al.* [D0 Collaboration], Phys. Rev. Lett. **93**, 141801 (2004) [arXiv:hep-ex/0404015].

[97] W. M. Yao *et al.* [Particle Data Group], J. Phys. G **33**, 1 (2006).

[98] E. Boos *et al.* [CompHEP Collaboration], Nucl. Instrum. Meth. A **534**, 250 (2004) [arXiv:hep-ph/0403113].

[99] A. S. Belyaev *et al.*, arXiv:hep-ph/0101232.

[100] A. L. Read, CERN-OPEN-2000-205, (2000)

[101] R. Barate *et al.* [LEP Working Group for Higgs boson searches and ALEPH Collaboration and and], Phys. Lett. B **565**, 61 (2003) [arXiv:hep-ex/0306033].

Acknowledgements

I would like to thank everybody who have given some direct or indirect contribution to this theses. Very special thanks to my colleagues in the National Institute of Chemical Physics and Biophyiscs: Andi Hektor, Mario Kadastik, Yuji Kajiyama, Ilja Livenson, Liis Rebane, Kristjan Kannike and of course my supervisor Martti Raidal.

Very warm thanks to my earlier (MSc) supervisor Ene Ergma, who guided me to particle physics.

My PhD work was financially supported by the Estonian Science Foundation (the grants hold by Martti Raidal), by the Estonian Government (the grant for the CMS experiment at CERN) and by the FP6 of the European Union (the BalticGrid project).

Publications

I

.

M. Raidal *et al.*,
"Flavour physics of leptons and dipole moments,"
EPJ. C **57** (2008) 715 [arXiv:0801.1826].

Flavour physics of leptons and dipole moments *

M. Raidal[1,2], *A. van der Schaaf*[1,3], *I. Bigi*[1,4], *M.L. Mangano*[1,5], *Y. Semertzidis*[1,6], *S. Abel*[7], *S. Albino*[8], *S. Antusch*[9], *E. Arganda*[10], *B. Bajc*[11], *S. Banerjee*[12], *C. Biggio*[9], *M. Blanke*[9,13], *W. Bonivento*[14], *G.C. Branco*[15,5], *D. Bryman*[16], *A.J. Buras*[13], *L. Calibbi*[17,18,19], *A. Ceccucci*[5], *P.H. Chankowski*[20], *S. Davidson*[21], *A. Deandrea*[21], *D.P. DeMille*[22], *F. Deppisch*[23], *M. Diaz*[24], *B. Duling*[13], *M. Felcini*[5], *W. Fetscher*[25], *D.K. Ghosh*[26], *M. Giffels*[27], *G. Giudice*[5], *E. Goudzovskij*[28], *T. Han*[29], *P.G. Harris*[30], *M.J. Herrero*[10], *J. Hisano*[31], *R.J. Holt*[32], *K. Huitu*[33], *A. Ibarra*[34], *O. Igonkina*[35,36], *A. Ilakovac*[37], *J. Imazato*[38], *G. Isidori*[28,39], *F.R. Joaquim*[10], *M. Kadastik*[2], *Y. Kajiyama*[2], *S.F. King*[40], *K. Kirch*[41], *M.G. Kozlov*[42], *M. Krawczyk*[20,5], *T. Kress*[27], *O. Lebedev*[5], *A. Lusiani*[43], *E. Ma*[44], *G. Marchiori*[43], *I. Masina*[5], *G. Moreau*[45], *T. Mori*[46], *M. Muntel*[2], *F. Nesti*[47], *C.J.G. Onderwater*[48], *P. Paradisi*[49], *S.T. Petcov*[17,50], *M. Picariello*[51], *V. Porretti*[18], *A. Poschenrieder*[13], *M. Pospelov*[52], *L. Rebane*[2], *M.N. Rebelo*[15,5], *A. Ritz*[52], *L. Roberts*[53], *A. Romanino*[17], *A. Rossi*[19], *R. Rückl*[54], *G. Senjanovic*[55], *N. Serra*[14], *T. Shindou*[34], *Y. Takanishi*[17], *C. Tarantino*[13], *A.M. Teixeira*[45], *E. Torrente-Lujan*[56], *K.J. Turzynski*[57,20], *T.E.J. Underwood*[7], *S.K. Vempati*[58], *O. Vives*[18]

[1] Convener
[2] National Institute for Chemical Physics and Biophysics, 10143 Tallinn, Estonia
[3] Physik-Intitut der Universität Zürich, CH-8057 Zürich, Switzerland
[4] Physics Dept., University of Notre Dame du Lac, Notre Dame, IN 46556, USA
[5] Physics Dept., CERN, CH-1211 Geneva, Switzerland
[6] Brookhaven National Laboratory, Upton, NY 11973-5000, USA
[7] Institute for Particle Physics Phenomenology, Durham University, Durham DH1 3LE, UK
[8] II. Institute for Theoretical Physics, University of Hamburg, D-22761 Hamburg, Germany
[9] Max-Planck-Institut für Physik, D-80805, München, Germany
[10] Departamento de Fisica Teorica and IFT/CSIC-UAM, Universidad Autonoma de Madrid, E-28049 Madrid, Spain
[11] J. Stefan Institute, 1000 Ljubljana, Slovenia
[12] Dept. of Physics, University of Victoria, Victoria, BC, V8W 3P6 , Canada
[13] Physics Dept., TU Munich , D-85748 Garching, Germany
[14] Università degli Studi di Cagliari and INFN Cagliari, I-09042 Monserrato, (CA), Italy
[15] Departamento de Física and Centro de Física Teórica de Partículas (CFTP), Instituto Superior Técnico (IST), 1049-001 Lisboa, Portugal
[16] Dept. of Physics and Astronomy, Univ. of British Columbia, TRIUMF, Vancouver, BC, V6T 2A3, Canada
[17] SISSA and INFN, Sezione di Trieste, I-34013 Trieste, Italy
[18] Departament de Física Teòrica, Universitat de València-CSIC, E-46100, Burjassot, Spain
[19] Dipartimento di Fisica 'G. Galilei' and INFN, I-35131 Padova, Italy
[20] Institute of Theoretical Physics, University of Warsaw, 00-681 Warsaw, Poland
[21] IPNL, CNRS, Université Lyon-1, F-69622 Villeurbanne Cedex, France
[22] Physics Dept., Yale University, New Haven, CO 06520, USA
[23] School of Physics and Astronomy, University of Manchester, Manchester, M13 9PL, UK
[24] Pontificia Univ. Catolica de Chile, Facultad de Fisica, Santiago 22, Chile
[25] Dept. of Physics, ETH Honggerberg, CH-8093 Zurich, Switzerland
[26] Theoretical Physics Division, Physical Research Lab., Navrangpura, Ahmedabad 380 009, India
[27] III. Physikalisches Institut B, RWTH Aachen, D-52056 Aachen, Germany
[28] Scuola Normale Superiore, I-56100 Pisa, Italy
[29] Univ. of Wisconsin, Dept. of Physics, High Energy Physics, Madison, WI 53706, USA

*Report of Working Group 3 of the CERN Workshop "Flavour in the era of the LHC", Geneva, Switzerland, November 2005 – March 2007.

[30] Dept. of Physics and Astronomy, University of Sussex, Falmer, Brighton BN1 9QH, UK
[31] ICRR, University of Tokyo, Japan
[32] Physics Division, Argonne National Laboratory, Argonne, IL 60439-4843, USA
[33] Dept. of Physics, Univ. of Helsinki, and Helsinki Institute of Physics, FIN-00014 Helsinki, Finland
[34] DESY, Theory group, D-22603 Hamburg, Germany
[35] Physics Dept., University of Oregon, Eugene, OR, USA
[36] NIKHEF, 1098 SJ Amsterdam, the Netherlands
[37] Dept. of Physics, University of Zagreb, HR-10002 Zagreb, Croatia
[38] IPNS, KEK, Ibaraki 305-0801, Japan
[39] INFN, Laboratori Nazionali di Frascati, I-00044 Frascati, Italy
[40] School of Physics and Astronomy, University of Southampton, SO17 1BJ Southampton, UK
[41] Paul Scherrer Institut, CH-5232 Villigen, Switzerland
[42] Petersburg Nuclear Physics Institute, Gatchina 188300, Russia
[43] INFN and Dipartimento di Fisica, Universita di Pisa, I-56127 Pisa, Italy
[44] Dept. of Physics and Astronomy, University of California, Riverside, California 92521, USA
[45] Laboratoire de Physique Théorique, UMR 8627 Université de Paris-Sud XI, F-91405 Orsay Cedex, France
[46] ICEPP, University of Tokyo, Tokyo, 113-0033, Japan
[47] Università dell'Aquila and INFN LNGS, I-67010, L'Aquila, Italy
[48] Kernfysisch Versneller Instituut (KVI), NL 9747 AA Groningen, the Netherlands
[49] University of Rome "Tor Vergata" and INFN sez. RomaII, I-00133 Roma, Italy
[50] Institute of Nuclear Research and Nuclear Energy, Bulgarian Academy of Sciences, 1784 Sofia, Bulgaria
[51] INFN and Dipartimento di Fisica, Università del Salento, I-73100 Lecce, Italy
[52] Dept. of Physics and Astronomy, Univ. of Victoria, Victoria, BC, V8P 5C2, Canada
[53] Dept. of Physics, Boston University, Boston, MA 02215, USA
[54] Inst. for Theoretical Physics and Astrophysics, Univ. of Würzburg, D-97074 Würzburg, Germany
[55] International Centre for Theoretical Physics, Trieste, Italy
[56] Dept. of Physics, Univ. of Murcia, E-30100 Murcia, Spain
[57] Physics Dept., University of Michigan, Ann Arbor, MI 48109, USA
[58] Centre for High Energy Physics, Indian Institute of Science, Bangalore, 560012, India

Abstract

This chapter of the report of the "Flavour in the era of the LHC" Workshop discusses the theoretical, phenomenological and experimental issues related to flavour phenomena in the charged lepton sector and in flavour-conserving CP-violating processes. We review the current experimental limits and the main theoretical models for the flavour structure of fundamental particles. We analyze the phenomenological consequences of the available data, setting constraints on explicit models beyond the Standard Model, presenting benchmarks for the discovery potential of forthcoming measurements both at the LHC and at low energy, and exploring options for possible future experiments.

measurement of $\mu \to e\gamma$ with polarized muons. Measuring the angular distribution of the outgoing electrons, one can determine the size of left- and right-handed contributions separately [639]. In addition, detecting also the electron spin would yield information on the relative phase between these two contributions [640]. We recall that the LHT model is peculiar in this respect as it does not involve any right-handed contribution.

On the other hand, the contribution of mirror leptons to $(g-2)_\mu$, being a flavour conserving observable, is negligible [628, 631], so that the possible discrepancy between SM prediction and experimental data [641] can not be cured. This should also be contrasted with the MSSM with large $\tan\beta$ and not too heavy scalars, where those corrections could be significant, thus allowing to solve the possible discrepancy between SM prediction and experimental data.

5.1.3.3 Conclusions

We have seen that LFV decays open up an exciting playground for testing the LHT model. Indeed, they could offer a very clear distinction between this model and supersymmetry. Of particular interest are the ratios $B(\ell_i \to eee)/B(\ell_i \to e\gamma)$ that are $\mathcal{O}(1)$ in the LHT model but strongly suppressed in supersymmetric models even in the presence of significant Higgs contributions. Similarly, finding the $\mu - e$ conversion rate in nuclei at the same level as $B(\mu \to e\gamma)$ would point into the direction of LHT physics rather than supersymmetry.

5.1.4 Low scale triplet Higgs neutrino mass scenarios in Little Higgs models

An important open issue to address in the context of Little Higgs models is the origin of non-zero neutrino masses [642–646]. The neutrino mass mechanism which naturally occurs in these models is the triplet Higgs mechanism [234] which employs a scalar with the $SU(2)_L \times U(1)_Y$ quantum numbers $T \sim (3,2)$. The existence of such a multiplet in some versions of the Little Higgs models is a direct consequence of global symmetry breaking which makes the SM Higgs light. For example, in the minimal Littlest Higgs model [614], the triplet Higgs with non-zero hypercharge occurs from the breaking of global $SU(5)$ down to $SO(5)$ symmetry as one of the Goldstone bosons. Its mass $M_T \sim g_s f$, where $g_s < 4\pi$ is a model dependent coupling constant in the weak coupling regime [647], is therefore predicted to be below the cut-off scale Λ, and could be within the mass reach of LHC. The present lower bound for the invariant mass of T is set by Tevatron to $M_T \geq 136$ GeV [648, 649].

Although the triplet mass scale is of order $\mathcal{O}(1)$ TeV, the observed neutrino masses can be obtained naturally. Due to the specific quantum numbers the triplet Higgs boson couples only to the left-chiral lepton doublets $L_i \sim (2,-1)$, $i = e, \mu, \tau$, via the Yukawa interactions of Eq. (3.61) and to the SM Higgs bosons via Eq. (3.62). Those interactions induce lepton flavour violating decays of charged leptons which have not been observed. The most stringent constraint on the Yukawa couplings comes from the upper limit on the tree-level decay $\mu \to eee$ and is[16] $Y_T^{ee} Y_T^{e\mu} < 3 \cdot 10^{-5} (M/TeV)^2$ [650, 651]. Experimental bounds on the tau Yukawa couplings are much less stringent. The hierarchical light neutrino masses imply $Y_T^{ee}, Y_T^{e\mu} \ll Y_T^{\tau\tau}$ consistently with the direct experimental bounds.

Non-zero neutrino masses and mixing is presently the only experimentally verified signal of new physics beyond the SM. In the triplet neutrino mass mechanism [234] presented in Section 3.2.3.2 the neutrino masses are given by

$$(m_\nu)^{ij} = Y_T^{ij} v_T, \tag{5.26}$$

where v_T is the induced triplet VEV of Eq. (3.63). It is natural that the smallness of neutrino masses is explained by the smallness of v_T. In the little Higgs models this can be achieved by requiring the Higgs mixing parameter $\mu \ll M_T$, which can be explained, for example, via shining of explicit lepton number violation from extra dimensions as shown in Ref. [652, 653], or if the triplet is related to the Dark Energy

[16] In Little Higgs models with T-parity there exist additional sources of flavour violation from the mirror fermion sector [628, 631] discussed in the previous subsection.

of the Universe [654, 655]. Models with additional (approximate) T-parity [615] make the smallness of v_T technically natural (if the T-parity is exact, v_T must vanish). In that case $Y_T v_T \sim \mathcal{O}(0.1)$ eV while the Yukawa couplings Y can be of order charged lepton Yukawa couplings of the SM. As a result, the branching ratio of the decay $T \to WW$ is negligible. We also remind that v_T contributes to the SM oblique corrections, and the precision data fit $\hat{T} < 2 \cdot 10^{-4}$ [656] sets an upper bound $v_T \leq 1.2$ GeV on that parameter.

Notice the particularly simple connection between the flavour structure of light neutrinos and the Yukawa couplings of the triplet via Eq. (5.26). Therefore, independently of the overall size of the Yukawa couplings, one can predict the leptonic branching ratios of the triplet from neutrino oscillations. For the normally hierarchical light neutrino masses neutrino data implies negligible T branching fractions to electrons and $B(T^{++} \to \mu^+\mu^+) \approx B(T^{++} \to \tau^+\tau^+) \approx B(T^{++} \to \mu^+\tau^+) \approx 1/3$. Those are the final state signatures predicted by the triplet neutrino mass mechanism for collider experiments.

At LHC T^{++} can be produced singly and in pairs. The cross section of the single T^{++} production via the WW fusion process [650] $qq \to q'q'T^{++}$ scales as $\sim v_T^2$. In the context of the littlest Higgs model this process, followed by the decays $T^{++} \to W^+W^+$, was studied in Refs. [657–659]. The detailed ATLAS simulation of this channel shows [659] that in order to observe an 1 TeV T^{++}, one must have $v_T > 29$ GeV. This is in conflict with the precision physics bound $v_T \leq 1.2$ GeV as well as with the neutrino data. Therefore the WW fusion channel is not experimentally promising for the discovery of doubly charged Higgs.

On the other hand, the Drell-Yan pair production process [650, 660–666]

$$pp \to T^{++}T^{--}$$

is not suppressed by any small coupling and its cross section is known up to next to leading order [662] (possible additional contributions from new physics such as Z_H are strongly suppressed and we neglect those effects here). Followed by the lepton number violating decays $T^{\pm\pm} \to \ell^\pm\ell^\pm$, this process allows to reconstruct $T^{\pm\pm}$ invariant mass from the same charged leptons rendering the SM background to be very small in the signal region. If one also assumes that neutrino masses come from the triplet Higgs interactions, one fixes the $T^{\pm\pm}$ leptonic branching ratios. This allows to test the triplet neutrino mass model at LHC. The pure Monte Carlo study of this scenario shows [665] that T^{++} up to the mass 300 GeV is reachable in the first year of LHC ($L = 1$ fb^{-1}) and T^{++} up to the mass 800 GeV is reachable for the luminosity $L = 30$ fb^{-1}. Including the Gaussian measurement errors to the Monte Carlo the corresponding mass reaches become [665] 250 GeV and 700 GeV, respectively. The errors of those estimates of the required luminosity for discovery depend strongly on the size of statistical Monte Carlo sample of the background processes.

5.2 Flavour and CP-violation in SUSY extensions of the SM

Supersymmetric models provide the richest spectrum of lepton flavour and CP-violating observables among all models. They are also among the best studied scenarios of new physics beyond the Standard Model. In this Section we review phenomenologically most interesting aspects of some of the supersymmetric scenarios.

5.2.1 Mass insertion approximation and phenomenology

In the low energy supersymmetric extensions of the SM the flavour and CP-violating interactions would originate from the misalignment between fermion and sfermion mass eigenstates. Understanding why all these processes are strongly suppressed is one of the major problems of low energy supersymmetry, the *supersymmetric flavour and CP problem*. The absence of deviations from the SM predictions in LFV and CPV (and other flavour changing processes in the quark sector) experiments suggests the presence

II

.

G. L. Bayatian *et al.* [CMS Collaboration]
"CMS technical design report, volume II: Physics performance"
J. Phys. G **34** (2007) 995.
(based on an internal CMS Analysis Note CMS AN 2006/081)

Available on CMS information server

CMS AN 2006/081

CMS Analysis Note

18 April 2006

Study of doubly charged Higgs boson pair production with $\mu\mu$, $\mu\tau$ and $\tau\tau$ in the final state

M. Kadastik, A. Hektor, K. Kannike, M. Müntel, M. Raidal

National Institute of Chemical Physics and Biophysics, Tallinn, Estonia

Abstract

In this analysis note we discuss the search methods for doubly charged Higgs bosons pair-produced by the Drell-Yan process ($pp \rightarrow \Delta^{++}\Delta^{--}$). We investigate the decays involving both muons and taus. The search is carried out over the mass range of 200 - 600 GeV with 100 GeV steps. Branching ratios are assumed to be equal among the final states with $\mu\mu$, $\mu\tau$ and $\tau\tau$. The integrated luminosity used in this study is 10 fb^{-1} based on the amount of background datasets available. As no background is expected we can measure the cross section directly and estimate the systematic and statistical uncertainties. We are able to discover the doubly charged Higgs boson up to the mass of 210 GeV and can set the 95% CL exclusion limit at the mass of 480 GeV.

1 Introduction

The main motivation of the Large Hadron Collider (LHC) experiments is to reveal the secrets of electroweak symmetry breaking. If the standard model (SM) Higgs boson will be discovered, the question arises what stabilizes its mass against the Planck scale quadratically divergent radiative corrections. The canonical answer to this question is supersymmetry which implies very rich phenomenology of predicted sparticles in the future collider experiments.

More recently another possibility of formulating the physics of electroweak symmetry breaking, called the little Higgs, was proposed [2, 6, 3]. In those models the SM Higgs boson is a pseudo Goldstone mode of a broken global symmetry and remains light, much lighter than the other new modes of the model which have masses of order the symmetry breaking scale $\mathcal{O}(1)$ TeV. In order to cancel one-loop quadratic divergences to the SM Higgs mass a new set of heavy gauge bosons W', Z' with the SM quantum numbers identical to W Z, and a vectorlike heavy quark pair T, $\bar{T}$ with charge 2/3 must be introduced. Notice that those fields are put in by hand in order to construct a model with the required properties. However, the minimal model based on the $SU(5)/SO(5)$ global symmetry, the so-called littlest Higgs model [1], has a firm prediction from the symmetry breaking pattern alone: the existence of another $\mathcal{O}(1)$ TeV pseudo Goldstone boson Δ with the $SU(2)_L \times U(1)_Y$ quantum numbers $\Delta \sim (3, 2)$.

Interestingly, the existence of triplet Higgs Δ might also be required to generate Majorana masses to the left-handed neutrinos [18]. Non-zero neutrino masses and mixing is presently the only experimentally verified signal of new physics beyond the SM. In the triplet neutrino mass mechanism [14] the neutrino mass matrix is generated via

$$(m_\nu)_{ij} = (Y_\Delta)_{ij} v_\Delta, \tag{1}$$

where $(Y_\Delta)_{ij}$ are the Majorana Yukawa couplings of the triplet to the lepton generations $i, j = e, \mu, \tau$ which are described by the Lagrangian

$$L = i\bar{\ell}^c_{Li} \tau_2 Y^{ij}_\Delta (\tau \cdot \Delta) \ell_{Lj} + h.c., \tag{2}$$

and v_Δ is the effective vacuum expectation value of the neutral component of the triplet induced via the explicit coupling of Δ to the SM Higgs doublet H as $\mu \Delta^0 H^0 H^0$. Here μ has a dimension of mass. In the concept of seesaw $\mu \sim M_\Delta$, and the smallness of neutrino masses is attributed to the very high scale of triplet mass M_Δ via the smallness of $v_\Delta = \mu v^2 / M^2_\Delta$, where $v = 174$ GeV.

However, in the littlest Higgs model the triplet mass scale is $\mathcal{O}(1)$ TeV which alone cannot suppress v_Δ. Therefore in this model $\mu \ll M_\Delta$, which can be achieved, for example, via shining from extra dimensions as shown in ref. [12, 13] or if the triplet is related to the Dark Energy of the Universe [15]. In that case $v_\Delta \sim \mathcal{O}(0.1)$ eV while the Yukawa couplings Y_Δ can be large. For the normally hierarchical light neutrino masses neutrino data implies very small Δ decay branching fractions to electrons and $BR(\Delta^{++} \to \mu^+\mu^+) \approx BR(\Delta^{++} \to \tau^+\tau^+) \approx BR(\Delta^{++} \to \mu^+\tau^+) \approx 1/3$. We remind also that v_Δ contributes to the SM oblique corrections, and the precision data fit $\hat{T} < 2 \cdot 10^{-4}$ [16] sets an upper bound $v_\Delta \leq 1.2$ GeV on that parameter.

At LHC Δ^{++} can be produced singly and in pairs. The cross section of the single Δ^{++} production via the WW fusion process [11] $qq \to q'q'\Delta^{++}$ scales as $\sim v^2_\Delta$. In the context of the littlest Higgs model this process, followed by the decays $\Delta^{++} \to W^+W^+$, was studied in ref. [9, 10, 4]. The detailed ATLAS simulation of this channel shows [4] that in order to observe 1 TeV Δ^{++}, one must have $v_\Delta > 29$ GeV. This is in conflict with the precision physics bound $v_\Delta \leq 1.2$ GeV as well as with the neutrino data. Therefore the WW fusion channel is not experimentally promising for the discovery of very heavy doubly charged Higgs.

On the other hand, the Drell-Yan pair production process [8, 11] $pp \to \Delta^{++}\Delta^{--}$ is not suppressed by any small coupling and its cross section is known up to next to leading order [17] (possible additional contributions from new physics such as Z' are strongly suppressed for any practical purposes). Followed by the lepton number violating decays $\Delta^{\pm\pm} \to \ell^\pm\ell^\pm$, this process allows to reconstruct $\Delta^{\pm\pm}$ invariant mass from the same charged leptons rendering the SM background to be very small in the signal region. If one also assumes that neutrino masses come from the triplet Higgs interactions, one fixes the $\Delta^{\pm\pm}$ leptonic branching ratios. This allows to test neutrino mass models at LHC.

2 Event Generation

Signal samples are generated using PYTHIA. Only pair-production through Drell-Yan is assumed (no single production through WW fusion). Datasets are produced from 200 GeV to 600 GeV Higgs mass with 100 GeV increments. In the events produced, the taus can decay both leptonically and hadronically while in analysis we only consider hadronic decays.

Both signal datasets and ZZ datasets have been generated with the aid of CMKIN 5.1.1. Full detector simulation has been performed using OSCAR 3.6.5 in winter mode followed by digitization with ORCA 8.7.4. The full analysis is performed in ORCA 8.9.4. Pileup is not used as it has no effect on muons and tau identification is not affected by presence of low luminosity pile up as shown in [7]. Table 1 shows the amount of events generated for the different signal datasets. Table 2 shows the amount of events analyzed for background datasets. NLO cross sections used for the background samples can be seen in Table 3.

Table 1: Number of events generated for signal datasets

m($\Delta^{\pm\pm}$) in GeV	200	300	400	500	600
Number of events	2762	700	700	900	900

Table 2: Number of events analyzed for background datasets.

background	tt→4l	Zbb	ZZ	ttZ
Number of events	1 170 600	666 000	8489	119542

Table 3: Background processes cross sections used (in fb)

background	tt→4l	Zbb	ZZ	ttZ
Cross section times BR	$88.4 \cdot 10^3$	$26.2 \cdot 10^3$	212	650

3 Background processes

The important backgrounds which have to be considered for this analysis are as follows:

- $t\bar{t}\rightarrow W^+W^-b\bar{b}$ for this dataset we have used generated samples with PYTHIA, CompHep, AlpGen, TopRex and MadGraph. The W bosons have been forced to decay leptonically. The total integrated luminosity available by these datasets is $22 fb^{-1}$. Official datasets used: hg03_wbwb_2l_alpgen, hg03_wbwb_2l_comph, hg03_wbwb_2l_madgr, eg03_tt_2l_pyth and eg03_tt_2l_topr.
- $t\bar{t}Z\rightarrow\ W^+W^-Z^0b\bar{b}$ the W and Z bosons are allowed to decay arbitrarily. For this dataset we have used generated samples with CompHep with total integrated luminosity of $184 fb^{-1}$. Official dataset used: bt03_ttZ_ttH
- $Zb\bar{b}$ where the Z decays to muons or taus. The total integrated luminosity of this dataset is limited to $8 fb^{-1}$ due to low statistics available for the dataset hg03_mumubb_60_100. Official datasets used: hg03_mumubb_60_100, hg03_mumubb_100, hg05_2tau2b_60_100_compHEP and hg05_2tau2b_gt_100_compHEP.
- ZZ/$\gamma^\star$ where the Z-s are forced to decay leptonically (e, μ, τ). The total integrated luminosity for this dataset is $127 fb^{-1}$. This dataset was generated in parallel with the signal dataset using the official CMKIN datacard for ZZ production.

Considering the amount of total available background we use the assumption of total integrated luminosity of $10 fb^{-1}$.

4 Event selection

The events must be triggered in HLT (High Level Trigger) with at least one isolated muon present. We do not use L1 trigger explicitly as HLT is only triggered when L1 trigger for a single muon is passed.

In addition to HLT trigger the event will only be used if it is possible to reconstruct the event primary vertex. The vertex is reconstructed using the highest $p_\perp$ tracks. If the primary vertex fails to be reconstructed the event is rejected.

The event selection efficiency is dependant on the doubly charged Higgs mass as can be seen in Table 4 which in turn is dependent on lepton selection efficiency shown in Table 5. Background efficiencies are shown in Table 6.

5 Offline reconstruction and selection cuts

The muons are reconstructed using IsolatedGlobalMuonReconstructor. The tau leptons are reconstructed using tau jet candidates and missing transverse energy after selection cuts. The doubly charged Higgs boson invariant mass

is reconstructed from the same charge lepton pairs after all selection cuts.

The selection cuts used on muons:

- the transverse momentum must be higher than 50 GeV. For background events 80% of muons have $p_\perp$ less than 50 GeV. For 200 GeV signal it is 27% and for higher signal masses it reduces to around 10%. The distribution can be seen on Figure 1.
- the distance to primary vertex in z-direction must not exceed 0.03 cm. This does not cut away any muons but limits analysis to leptons coming from the same primary vertex. At low luminosity it does not cut anything and is just a quality cut for the future use when a single event can have multiple collisions.

The selection cuts used on tau jets:

- for tau jets we consider tau decays which involve 1 or 3 charged tracks. We use ConcreteTauJetWithTracks reconstruction object which implements the tau jet filtering algorithms described in Physics TDR volume 1. Two scenarios are considered. Either 1 or 3 charged tracks in signal cone and no charged tracks in isolation cone or 2 tracks in signal cone and exactly one charged track in the isolation cone.
- the maximum distance to primary vertex in z-direction of any charged track in the tau jet must not exceed 0.2 cm. At low luminosity it does not cut anything and is just a quality cut for the future use when a single event can have multiple collisions.
- the hottest tau jet HCAL tower transverse energy must be higher than 2 GeV. This eliminates high energy electrons which pass through ECAL and confuse the algorithm into considering the electron as a tau jet. This cut eliminates 86% of all electrons considered as tau candidates and only removes 7.5% of real tau jets. The distribution can be seen on Figure 2.
- the transverse energy of the tau jet candidate must exceed 50 GeV. It has been chosen to be the same as the cut used on muons.
- no muon track should be in a cone with $\Delta R = 0.3$ constructed around the tau jet candidate. If there is then the candidate is dropped. This eliminates false tau jet candidates which are generated when a charged muon track passes the same region as photons or hadrons. With this cut only a few real tau jets are discarded however most of the false tau jets coming from this misidentification are discarded.

Missing transverse energy ($E_\perp^{miss}$) is reconstructed in three steps. As a first step the raw $E_\perp^{miss}$ is reconstructed from the calorimeters. As step two Type 1 corrections (using the difference of raw reconstructed jets and calibrated jets) are added to the $E_\perp^{miss}$. As a final step the muon transverse components are subtracted to get the real missing transverse energy.

Only events with at least four muons or tau jets total are accepted. If the event is accepted a decision is made wether it can be reconstructed. The possible final states are:

- $\Delta^{++}\Delta^{--} \rightarrow 4\mu$ - this channel is investigated in previous subsection.
- $\Delta^{++}\Delta^{--} \rightarrow 3\mu 1\tau$ - this channel is easily reconstructible as there is only one neutrino and it goes the direction of the tau jet.
- $\Delta^{++}\Delta^{--} \rightarrow 2\mu 2\tau$ - this channel can also be reconstructed using the assumption that the neutrinos go the same direction as the tau jets.
- $\Delta^{++}\Delta^{--} \rightarrow 1\mu 3\tau$ - this channel can be reconstructed only with very good $E_\perp^{miss}$ resolution as it requires an additional assumption that the masses of the two reconstructed Higgs bosons are the same. However the reconstruction is very sensitive to $E_\perp^{miss}$ accuracy and often the event has to be dropped due to absurd τ-lepton energies. These events are dropped with the invariant mass cut described below.
- $\Delta^{++}\Delta^{--} \rightarrow 4\tau$ - this channel can not be reconstructed and in many cases will not trigger as no muons are found in the event. This also contributes to a lower efficiency at HLT as these events do not pass the single muon HLT trigger.

Once the event leptons are reconstructed, some additional tasks are performed:

- Z^0 boson reconstruction - if the odd sign pairing gives an invariant mass of 91 ± 5 GeV then these leptons are removed from further use.
- Same charge lepton pairs are reconstructed and only those reconstructed Higgs candidate pairs whose invariant mass difference is within 20% of each other are considered. The difference in background distribution and signal distribution can be seen on Figure 2.

6 Efficiencies

Assuming the above mentioned branching ratios the expected theoretical limits on the different final state discovery channels can be investigated. The branching ratio of tau leptons to tau jets is 65%, this gives:

- $\Delta^{++}\Delta^{--} \rightarrow 3\mu 1\tau = 2/9 events * 0.65 = 14.4\%$.
- $\Delta^{++}\Delta^{--} \rightarrow 2\mu 2\tau = 3/9 events * 0.65^2 = 14.1\%$.
- $\Delta^{++}\Delta^{--} \rightarrow 1\mu 3\tau = 2/9 events * 0.65^3 = 6.1\%$.

So the total theoretical limit of discovery when searching with at least one tau jet in the final state gives 34.6% efficiency. Using datasets which have been generated with the above mentioned branching ratios taken into account the efficiencies of the different cuts at different doubly charged Higgs boson masses can be seen in Table 4. Taking into account the signal cross section depending on the Higgs boson mass the total number of observable candidates at an integrated luminosity of $10 fb^{-1}$ is given in Table 7.

Table 4: Trigger and cut efficiencies for signal as a function of the $\Delta^{\pm\pm}$ mass. Total efficiency is the product of the single efficiencies.

$m_{\Delta}^{\pm\pm}$ (GeV)	200	300	400	500	600
HLT trigger	83.4%	86.0%	86.7%	85.8%	88.3%
Primary Vertex	96.7%	98.5%	97.0%	97.5%	98.0%
4 leptons in final state	9.9%	17.2 %	23.6%	24.7%	26.7%
two pairs and at least one τ	41.1%	46.1%	41.7%	53.2%	52.9%
Mass difference	71.9%	77.2%	80.4%	74.3%	63.6%
Total signal efficiency	2.3%	5.1%	6.6%	8.1%	7.7%

Table 5: Single muon and tau selection efficiencies and purity.

$m_{\Delta}^{\pm\pm}$ (GeV)	200	300	400	500	600
Single μ selection efficiency	70.7%	82.0%	86.1%	87.2%	89.2%
1 - purity of accepted muons:	0.1%	0.4%	0.8%	0.7%	1.0%
Single τ selection efficiency	36.6%	42.3%	50.6%	53.3%	53.3%
1 - purity of accepted tau jets:	2.2%	2.2%	4.2%	3.6%	3.2%

Table 6: Trigger and cut efficiencies for background. Total efficiency is the product of the single efficiencies.

Process	$t\bar{t}$	$t\bar{t}Z$	ZZ	Zbb
HLT trigger	40.7%	20.3%	40.0%	42.1%
Primary Vertex	99.3%	99.8%	96.7%	98.2%
4 leptons in final state	0.0015%	0.04 %	3.0%	0.0005%
two pairs and at least one τ	-	0.1%	-	-
Mass difference	-	100%	-	-
Total signal efficiency	-	0.0008%	-	-

7 Systematic errors

At the integrated luminosity of $10 fb^{-1}$ the cuts implemented above result in almost background free signal. For datasets with integrated luminosity above $10 fb^{-1}$ giving zero events ($t\bar{t}$, ZZ^*) we assume the background to be zero events for the purpose of this study. For $t\bar{t}Z$ where we have one event passing all cuts in the dataset we get 0.05 events when scaled with cross section and luminosity. For Zbb where we have background statistics for $8 fb^{-1}$ with zero events passing the cuts. We have run the same analysis with $p_{\perp}$ cuts 40 GeV, 30 GeV and 20 GeV with also zero events passing the cuts which confirms our assumption that leptons coming from Zbb are too soft to produce a background for our process. Considering the smallness of the background we assume no background at $10 fb^{-1}$ for the following analysis.

The systematic errors used for signal is as follows:

- muon misidentification ($\Delta\mu$) - 1% per muon.
- muon isolation ($\Delta\mu_{isol}$)- 2% per event.
- tau jets ($\Delta\tau$)- 9% per tau jet.
- luminosity ($\Delta\mathcal{L}$) - 5%.
- PDF and scale ($\Delta\sigma$)- 10% (theoretical, not used when we have no background and go to cross section measurement).

As the events are a mixture of different decay modes the total selection efficiency error ($\Delta\varepsilon_S$) is calculated per decay channel and then added together using different weights to account for the non-uniform distribution within the dataset

$$\Delta 3\mu 1\tau = \sqrt{3\Delta\mu^2 + \Delta\tau^2} = 8.2\%,$$

$$\Delta 2\mu 2\tau = \sqrt{2\Delta\mu^2 + 2\Delta\tau^2} = 11.4\%,$$

$$\Delta 1\mu 3\tau = \sqrt{\Delta\mu^2 + 3\Delta\tau^2} = 13.9\%,$$

giving

$$\Delta\varepsilon_S = \frac{144\Delta 3\mu 1\tau + 141\Delta 2\mu 2\tau + 61\Delta 1\mu 3\tau}{346} = 10.5\%$$

The total systematic error for cross section measurement is then

$$\frac{\Delta\sigma}{\sigma} = \sqrt{{\Delta\mu_{isol}}^2 + \Delta\mathcal{L}^2 + {\Delta\varepsilon_S}^2} = 13\%.$$

The statistical errors were evaluated constructing the shortest Bayesian confidence interval for the confidence level of 67%[5].

8 Results

The expected number of events and the NLO cross section with expected measurement errors (both statistical and systematic) are given in Table 7.

Table 7: Expected number of events, NLO cross section and expected measurement errors

$m_{\Delta}^{\pm\pm}$ (GeV)	200	300	400	500	600
Expected nr of events at $10fb^{-1}$	26	10	4	2	1
NLO cross section and expected measurement errors (in fb)	$93.9^{+19.3}_{-17.5} \pm 12.2$	$19.6^{+6.6}_{-5.6} \pm 2.5$	$5.9^{+3.4}_{-2.5} \pm 0.8$	$2.2^{+1.9}_{-1.3} \pm 0.3$	$0.9^{+1.3}_{-0.7} \pm 0.1$
Statistical significance	5.37	3.50	2.36	1.69	1.28

The invariant mass plots for 200, 300, 400, 500 GeV doubly charged Higgs boson searches are shown on Figures 3 and 4.

The statistical significance and cross section distributions can be seen on Figure 5. As no events of background are expected at $10fb^{-1}$ we can detect the doubly charged Higgs boson with a mass of up to ≈ 210 GeV. Reasonable evidence at 3σ level can be seen up to 340 GeV and 95% CL exclusion limit is at 480 GeV.

9 Acknowledgments

We would like to thank A. Nikitenko, T. Rommerskirchen and S. Lehti for their useful comments and recommendations.

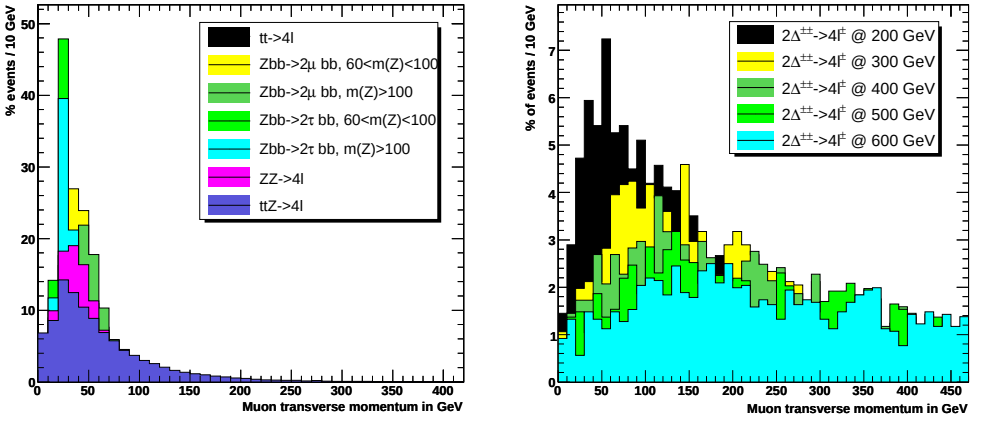

Figure 1: Distribution of μ transverse momentum for background (left) and signal (right).

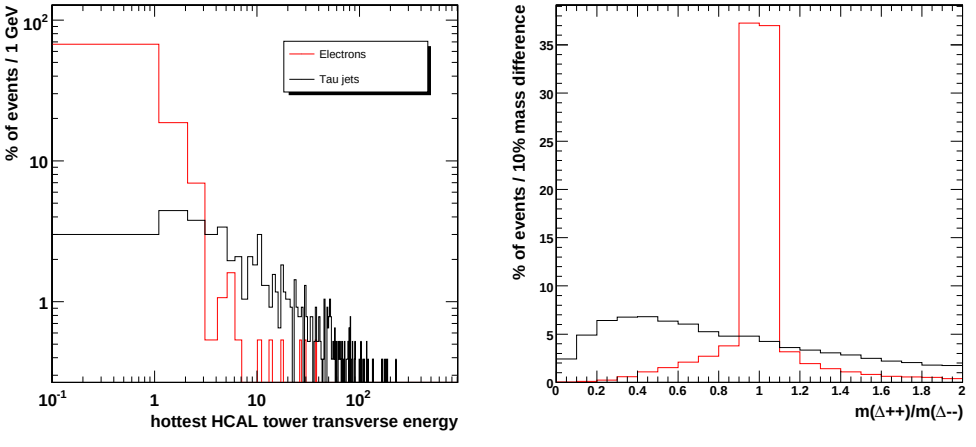

Figure 2: Left: Distribution of hottest HCAL tower $p_\perp$ for τ-jet candidates and electrons. Right: Distribution of m(Δ_1)/m(Δ_2) for background and signal.

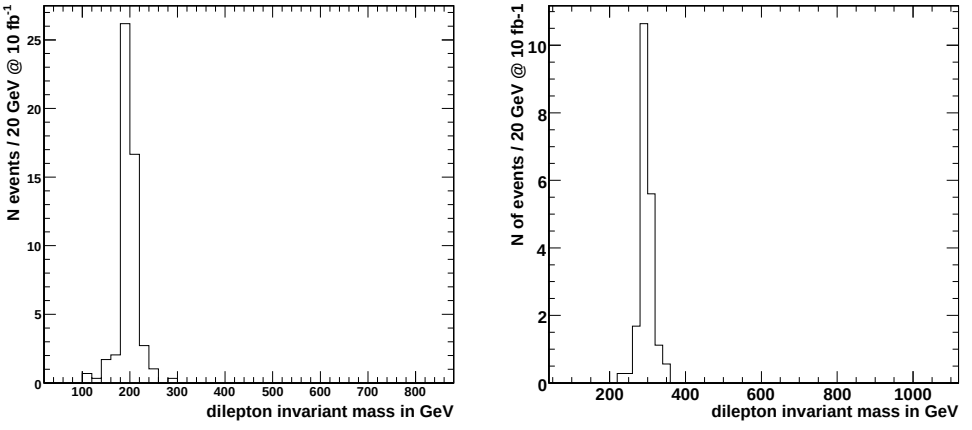

Figure 3: Invariant mass plots for M($\Delta^{\pm\pm}$)=200 GeV and 300 GeV.

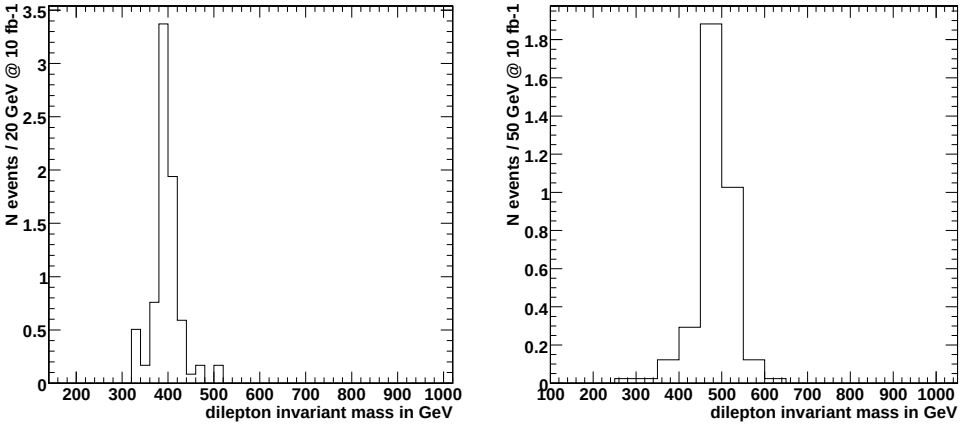

Figure 4: Invariant mass plots for M($\Delta^{\pm\pm}$)=400 GeV and 500 GeV.

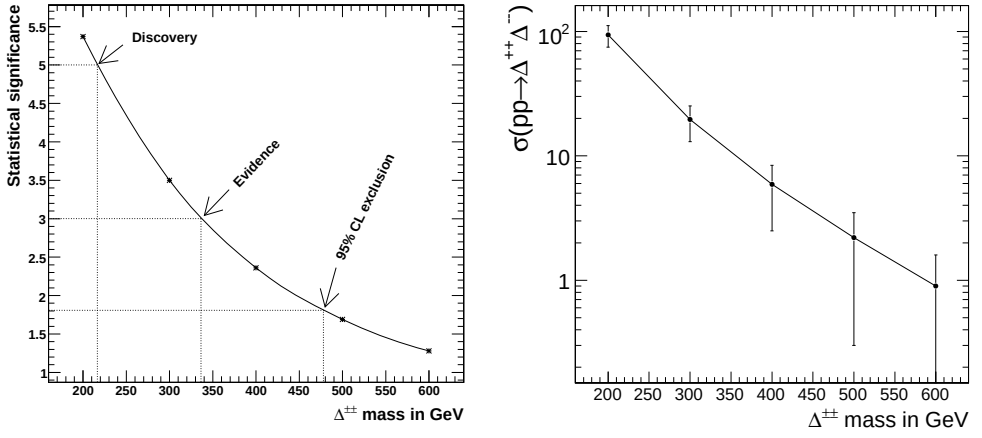

Figure 5: Left: statistical significance. Right: cross section with statistical errors

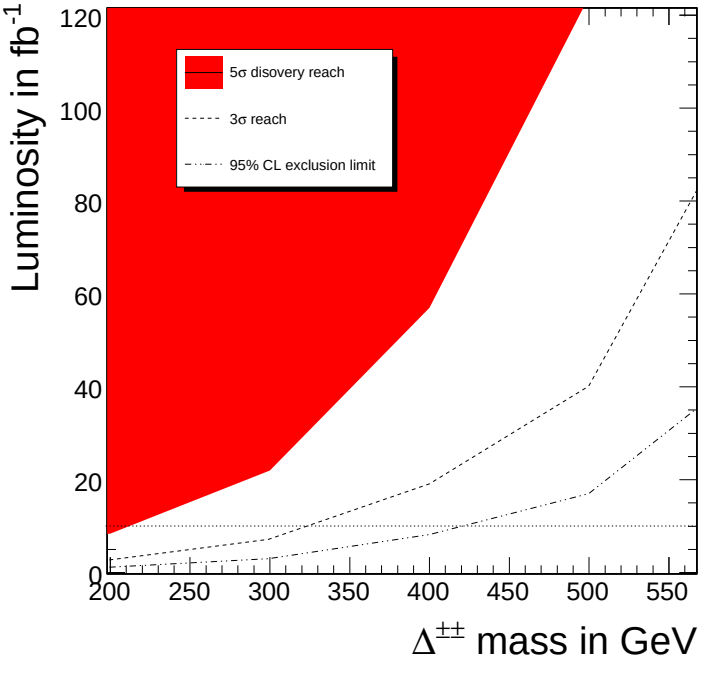

Figure 6: Mass reach in dependance to luminosity. 5σ, 3σ levels for discovery are given as well as 95% CL for exclusion if nothing is found by that time.

References

[1] N. Arkani-Hamed, A. G. Cohen, E. Katz, and A. E. Nelson. The littlest higgs. *JHEP*, 07:034, 2002.

[2] Nima Arkani-Hamed, Andrew G. Cohen, and Howard Georgi. (de)constructing dimensions. *Phys. Rev. Lett.*, 86:4757–4761, 2001.

[3] Nima Arkani-Hamed, Andrew G. Cohen, and Howard Georgi. Electroweak symmetry breaking from dimensional deconstruction. *Phys. Lett.*, B513:232–240, 2001.

[4] G. Azuelos et al. Exploring little higgs models with atlas at the lhc. *Eur. Phys. J.*, C39S2:13–24, 2005.

[5] S. I. Bityukov, N. V. Krasnikov, and V. A. Taperechkina. Confidence intervals for poisson distribution parameter. 2001.

[6] Hsin-Chia Cheng, Christopher T. Hill, Stefan Pokorski, and Jing Wang. The standard model in the latticized bulk. *Phys. Rev.*, D64:065007, 2001.

[7] S. Gennai A. Kalinowski M. Konecki D. Kotlinski F. Moortgat A. Nikitenko L. Wendland G. Bagliesi, S. Dutta and S. Wakefield. Tau jet reconstruction and tagging at high level trigger and off-line. *CMS NOTE - 2006/028*.

[8] J. F. Gunion, J. Grifols, A. Mendez, B. Kayser, and Fredrick I. Olness. Higgs bosons in left-right symmetric models. *Phys. Rev.*, D40:1546, 1989.

[9] Tao Han, Heather E. Logan, Bob McElrath, and Lian-Tao Wang. Phenomenology of the little higgs model. *Phys. Rev.*, D67:095004, 2003.

[10] Tao Han, Heather E. Logan, and Lian-Tao Wang. Smoking-gun signatures of little higgs models. 2005.

[11] K. Huitu, J. Maalampi, A. Pietila, and M. Raidal. Doubly charged higgs at lhc. *Nucl. Phys.*, B487:27–42, 1997.

[12] Ernest Ma, Martti Raidal, and Utpal Sarkar. Verifiable model of neutrino masses from large extra dimensions. *Phys. Rev. Lett.*, 85:3769–3772, 2000.

[13] Ernest Ma, Martti Raidal, and Utpal Sarkar. Phenomenology of the neutrino-mass-giving higgs triplet and the low-energy seesaw violation of lepton number. *Nucl. Phys.*, B615:313–330, 2001.

[14] Ernest Ma and Utpal Sarkar. Neutrino masses and leptogenesis with heavy higgs triplets. *Phys. Rev. Lett.*, 80:5716–5719, 1998.

[15] Ernest Ma and Utpal Sarkar. Connecting dark energy to neutrinos with an observable higgs triplet. 2006.

[16] Guido Marandella, Christian Schappacher, and Alessandro Strumia. Little-higgs corrections to precision data after lep2. *Phys. Rev.*, D72:035014, 2005.

[17] Margarete Muhlleitner and Michael Spira. A note on doubly-charged higgs pair production at hadron colliders. *Phys. Rev.*, D68:117701, 2003.

[18] J. Schechter and J. W. F. Valle. Neutrino masses in su(2) x u(1) theories. *Phys. Rev.*, D22:2227, 1980.

IOP PUBLISHING JOURNAL OF PHYSICS G: NUCLEAR AND PARTICLE PHYSICS

J. Phys. G: Nucl. Part. Phys. **34** (2007) 995–1579 doi:10.1088/0954-3899/34/6/S01

CMS Physics Technical Design Report, Volume II: Physics Performance

The CMS Collaboration

Received 3 January 2007
Published 20 April 2007
Online at stacks.iop.org/JPhysG/34/995

Abstract

CMS is a general purpose experiment, designed to study the physics of pp collisions at 14 TeV at the Large Hadron Collider (LHC). It currently involves more than 2000 physicists from more than 150 institutes and 37 countries. The LHC will provide extraordinary opportunities for particle physics based on its unprecedented collision energy and luminosity when it begins operation in 2007.

The principal aim of this report is to present the strategy of CMS to explore the rich physics programme offered by the LHC. This volume demonstrates the physics capability of the CMS experiment. The prime goals of CMS are to explore physics at the TeV scale and to study the mechanism of electroweak symmetry breaking—through the discovery of the Higgs particle or otherwise. To carry out this task, CMS must be prepared to search for new particles, such as the Higgs boson or supersymmetric partners of the Standard Model particles, from the start-up of the LHC since new physics at the TeV scale may manifest itself with modest data samples of the order of a few fb^{-1} or less.

The analysis tools that have been developed are applied to study in great detail and with all the methodology of performing an analysis on CMS data specific benchmark processes upon which to gauge the performance of CMS. These processes cover several Higgs boson decay channels, the production and decay of new particles such as Z' and supersymmetric particles, B_s production and processes in heavy ion collisions. The simulation of these benchmark processes includes subtle effects such as possible detector miscalibration and misalignment. Besides these benchmark processes, the physics reach of CMS is studied for a large number of signatures arising in the Standard Model and also in theories beyond the Standard Model for integrated luminosities ranging from $1\,\mathrm{fb}^{-1}$ to $30\,\mathrm{fb}^{-1}$. The Standard Model processes include QCD, B-physics, diffraction, detailed studies of the top quark properties, and electroweak physics topics such as the W and Z^0 boson properties. The production and decay of the Higgs particle is studied for many observable decays, and the precision with which the Higgs boson properties can be derived is determined. About ten different supersymmetry benchmark points are analysed using full simulation. The CMS discovery reach is evaluated in the SUSY parameter space covering a large variety of decay signatures.

Furthermore, the discovery reach for a plethora of alternative models for new physics is explored, notably extra dimensions, new vector boson high mass states, little Higgs models, technicolour and others. Methods to discriminate between models have been investigated.

This report is organized as follows. Chapter 1, the Introduction, describes the context of this document. Chapters 2–6 describe examples of full analyses, with photons, electrons, muons, jets, missing E_{T}, B-mesons and τ's, and for quarkonia in heavy ion collisions. Chapters 7–15 describe the physics reach for Standard Model processes, Higgs discovery and searches for new physics beyond the Standard Model.

Acknowledgments

This report is the result of several years of work on the preparation for physics analysis at the LHC with CMS. Subprojects in all areas were involved (Detector, PRS, Software, and Computing) in order to produce the large Monte Carlo simulation samples needed, to develop the software to analyse those samples, to perform the studies reported in this Report, and to write and review our findings.

We wish to thank, for the many useful discussions, our theory and phenomenology colleagues, in particular J Campbell, D Dominici, A Djouadi, S Heinemeyer, W Hollik, V Khoze, T Plehn, M Raidal, M Spira and G Weiglein for their contributions to this Report.

For their constructive comments and guidance, we would like to thank the CPT internal reviewers: J Alexander, J Branson, Y Karyotakis, M Kasemann and R Tenchini.

We would like to thank L Malgeri and R Tenchini for their efficient organisation of the CMS Notes.

For their patience in meeting sometimes impossible demands, we wish to thank the CMS Secretariat: K Aspola, M Azeglio, N Bogolioubova, D Denise, D Hudson, G Martin, and M C Pelloux.

We also would like to thank G Alverson and L Taylor for their invaluable technical assistance in the preparation of this manuscript.

Finally, we wish to thank the CMS management for their strong support and encouragement.

The CMS Collaboration

Table 12.3. The NLO background processes cross sections used (in fb).

background	$t\bar{t} \to 4l$	Z $b\bar{b}$	ZZ	$t\bar{t}$ Z
Cross section times BR	$88.4 \cdot 10^3$	$52.4 \cdot 10^3$	229.5	650

section is 1% to 6%. The uncertainty on signal cross section is 10% to 15%. The uncertainty on the luminosity $\mathcal{L}$ is $\sim 5\%$ for an integrated luminosity of $10\,\text{fb}^{-1}$.

Using a background cross section uncertainty of 6%, a signal cross section uncertainty of 10% and a luminosity uncertainty of 5% the approximated uncertainties on the exclusion mass limit and on the discovery mass limit are:

$$\text{Exclusion Limit} = (760\ ^{+0.5}_{-2}(\text{bkg}) \pm 10(\text{signal}) \pm 4(\text{lumi}))\,\text{GeV/c}^2 \quad (12.3)$$

$$\text{Discovery Limit} = (650\ ^{+0.4}_{-0.3}(\text{bkg})\ ^{+3}_{-0.4}(\text{signal}) \pm 0.2(\text{lumi}))\,\text{GeV/c}^2. \quad (12.4)$$

12.2.2. Search for the final states with τ leptons

12.2.2.1. Introduction. In this section, we discuss the doubly charged Higgs boson pair-production via a Drell–Yan process and investigate decays which involve taus and muons. The branching ratios are assumed to be 1/3 for the following three channels: $\Delta^{\pm\pm} \to 2\mu^{\pm}$, $\Delta^{\pm\pm} \to \mu^{\pm}\tau^{\pm}$ and $\Delta^{\pm\pm} \to 2\tau^{\pm}$. The reasoning comes from recent neutrino mixing measurements. As the neutrino mixing matrix and doubly charged Higgs boson decays are directly related then the appropriate branchings can be determined.

12.2.2.2. Event generation. The doubly charged Higgs boson pair-production via Drell–Yan process is generated using PYTHIA. Datasets are produced with Higgs boson mass from $200\,\text{GeV/c}^2$ to $600\,\text{GeV/c}^2$. The taus from Higgs boson decays can decay both leptonically and hadronically while in analysis we only consider hadronic decays.

The backgrounds which were considered for this analysis are as follows:

- $t\bar{t} \to \text{W}^+\text{W}\, b\bar{b}$ generated by PYTHIA, COMPHEP, ALPGEN, TOPREX and MADGRAPH with W boson decay $\text{W} \to \ell\nu$ ($\ell = \text{e}, \mu, \tau$) forced.
- $t\bar{t}\,\text{Z} \to W^+W^-Z\, b\bar{b}$ generated with COMPHEP. The W and Z bosons are allowed to decay arbitrarily.
- Z$b\bar{b}$ where the Z boson decays to muons and τ leptons, generated with COMPHEP.
- ZZ generated with PYTHIA, where the Z bosons are forced to decay leptonically (e, μ, τ). The contribution of γ^* is included with $\text{m}_{\gamma^*} > 12\,\text{GeV/c}^2$.

The next-to-leading order (NLO) cross sections times branching ratios used for the backgrounds can be found in Table 12.3. The Monte Carlo statistics of the generated background exceed $30\,\text{fb}^{-1}$ except Z$b\bar{b}$ background, where it is $8\,\text{fb}^{-1}$. Therefore the results will be presented for an integrated luminosity of $10\,\text{fb}^{-1}$.

12.2.2.3. Event selection and reconstruction. The events are triggered by the single muon trigger at Level 1 and HLT. After HLT the event is only used if it is possible to reconstruct the event primary vertex. If the primary vertex fails to be reconstructed the event is rejected.

The muons are reconstructed using Global Muon Reconstructor. The τ leptons are reconstructed using τ-jet candidates and missing transverse energy after selection cuts. The doubly charged Higgs boson invariant mass is reconstructed from the same charge lepton pairs after all selection cuts.

The selection cuts used on muons are:

- The transverse momentum must be higher than 50 GeV/c. For background events 80% of muons have p_T less than 50 GeV/c while for the signal with Higgs boson mass 200 GeV/c^2 it is 27% and for higher masses it reduces to around 10%.
- The distance to primary vertex in z-direction must not exceed 0.03 cm. It does not cut away any muons from the signal events but limits analysis to leptons coming from the same primary vertex.

The selection cuts used on τ jets are:

- For τ jets we consider τ decays which involve 1 or 3 charged tracks. We use τ-jet candidates which passed the τ-jet filtering algorithms described in [280]. Two isolation criteria are used. Either one or three charged tracks in the signal cone and no charged tracks in the isolation cone or two tracks in signal cone and exactly one charged track in the isolation cone.
- The maximal distance to the primary vertex in the z-direction of any charged track in the τ jet must not exceed 0.2 cm.
- The transverse energy of the hottest HCAL tower of the τ jet must be higher than 2 GeV. This cut eliminates 86% of all electrons taken as τ candidates and only removes 7.5% of real τ jets.
- The transverse energy of the τ jet candidate must exceed 50 GeV. It has been chosen to be the same as the cut used on muons.
- No muon track should be in a cone with $\Delta R = 0.3$ constructed around the τ-jet candidate. If there is, then the candidate is dropped. This eliminates false τ-jet candidates which are generated when a charged muon track passes the same region as photons or hadrons. With this cut only a few real τ jets are discarded however most of the false τ jets coming from this misidentification are rejected.

Missing transverse energy (E_T^{miss}) is reconstructed using calorimeter Type 1 E_T^{miss} (E_T^{miss} with the jet energy corrections) and p_T of muons.

Only events with at least four objects, muons or τ jets, are accepted. The possible final states are:

- $\Delta^{++}\Delta^{--} \to 4\mu$: this channel is investigated in the previous subsection.
- $\Delta^{++}\Delta^{--} \to 3\mu 1\tau$: this channel is easily reconstructible as there is only one neutrino and it goes the direction of the τ jet.
- $\Delta^{++}\Delta^{--} \to 2\mu 2\tau$: this channel can also be reconstructed using the assumption that the neutrinos go in the same directions as the τ jets.
- $\Delta^{++}\Delta^{--} \to 1\mu 3\tau$: this channel can be reconstructed only with very good E_T^{miss} resolution as it requires an additional assumption that the masses of the two reconstructed Higgs bosons are the same. However the reconstruction is very sensitive to E_T^{miss} accuracy and often the event has to be dropped due to negative τ-lepton energies.
- $\Delta^{++}\Delta^{--} \to 4\tau$: this channel can not be reconstructed (and triggered by the single muon trigger).

Once the event leptons are reconstructed, some additional selections are performed:

- Z boson veto: if the odd sign pairing gives an invariant mass of 91 ± 5 GeV/c^2 then these leptons are removed from further use.
- Same charge lepton pairs are reconstructed and only those reconstructed Higgs candidate pairs whose invariant mass difference is within 20% of each other are considered.

The reconstructed mass of doubly charged Higgs boson is shown on Figure 12.7 for the Higgs boson masses 200 and 500 GeV/c^2.

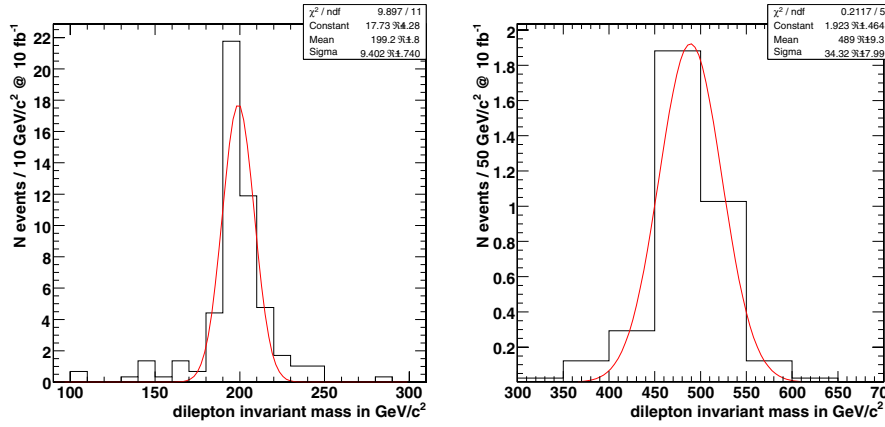

Figure 12.7. The reconstructed invariant mass for $M(\Delta^{\pm\pm}) = 200\,\mathrm{GeV/c^2}$ and $500\,\mathrm{GeV/c^2}$.

Table 12.4. The signal selection efficiencies for different $\Delta^{\pm\pm}$ masses. Total efficiency is the product of the single efficiencies.

$m_{\Delta}^{\pm\pm}$ ($\mathrm{GeV/c^2}$)	200	300	400	500	600
Level 1 and HLT	83.7%	86.0%	86.7%	85.8%	88.3%
Primary vertex	96.9%	98.5%	97.0%	97.5%	98.0%
4 leptons in final state	10.1%	17.2 %	23.6%	24.7%	26.7%
two pairs and at least one τ	44.9%	46.1%	41.7%	53.2%	52.9%
Mass difference	62.5%	77.2%	80.4%	74.3%	63.6%
Total signal efficiency	2.3%	5.1%	6.6%	8.1%	7.7%

12.2.2.4. Selection efficiencies. The upper limit of the signal selection efficiency is given by the fraction of events with $3\mu 1\tau$, $2\mu 2\tau$, $1\mu 3\tau$ ($\tau \rightarrow$ hadrons) topology relative to all possible final states with muons and τ leptons from decays of two Higgs bosons. Assuming the above mentioned branching ratios the upper limit is $\simeq 35\%$. The fraction of every selected topology is given below:

- $\Delta^{++}\Delta^{--} \rightarrow 3\mu 1\tau = 2/9$ events $\times\, 0.65 = 14.4\%$
- $\Delta^{++}\Delta^{--} \rightarrow 2\mu 2\tau = 3/9$ events $\times\, 0.65^2 = 14.1\%$
- $\Delta^{++}\Delta^{--} \rightarrow 1\mu 3\tau = 2/9$ events $\times\, 0.65^3 = 6.1\%$.

where 0.65 is the branching ratio of $\tau \rightarrow$ hadrons decays. Table 12.4 summarises the efficiencies of each selection (relative to the previous one) for the signal of different $\Delta^{\pm\pm}$ masses. The lepton selection efficiency and purity is shown in Table 12.5. Background efficiencies are shown in Table 12.6.

12.2.2.5. Systematic errors. At the integrated luminosity of $10\,\mathrm{fb^{-1}}$ the cuts implemented above result in an almost background free signal. For datasets with Monte Carlo statistics above $30\,\mathrm{fb^{-1}}$ giving zero Monte Carlo events after all selections ($t\bar{t}$, ZZ^*) we assume the background to be zero. For $t\bar{t}Z$ background where is one Monte Carlo event passing all cuts, which corresponds to 0.05 expected events when scaled with cross section and luminosity.

Table 12.5. Single muon and τ selection efficiencies and purity.

$m_{\Delta}^{\pm\pm}$ (GeV/c^2)	200	300	400	500	600
Single μ selection efficiency	70.7%	82.0%	86.1%	87.2%	89.2%
1 - purity of accepted muons:	0.1%	0.4%	0.8%	0.7%	1.0%
Single τ selection efficiency	36.6%	42.3%	50.6%	53.3%	53.3%
1 - purity of accepted τ jets:	2.2%	2.2%	4.2%	3.6%	3.2%

Table 12.6. Selection efficiencies for background. Total efficiency is the product of the single efficiencies.

Process	$t\bar{t}$	$t\bar{t}$ Z	ZZ	Zbb
Level 1 and HLT trigger	40.7%	20.3%	40.0%	42.1%
Primary vertex	99.3%	99.8%	96.7%	98.2%
4 leptons in final state	0.0015%	0.04 %	3.0%	0.0005%
two pairs and at least one τ	–	0.1%	–	–
Mass difference	–	100%	–	–
Total signal efficiency	–	0.0008%	–	–

For Z $b\bar{b}$ background where the Monte Carlo statistics corresponds to 8 fb^{-1} no events passed all cuts. The analysis was repeated with p_{T} cut on muon (τ jet) of 40 GeV/c, 30 GeV/c and 20 GeV/c, again with no events passing the cuts, which confirms the assumption that leptons coming from Z $b\bar{b}$ are too soft to produce a background. Considering the smallness of all backgrounds we assume no background at 10 fb^{-1} for the following analysis.

The systematic uncertainties used for the signal are the following:

- muon misidentification ($\Delta\mu$): 1% per muon;
- muon isolation ($\Delta\mu_{isol}$): 2% per event;
- τ jets identification ($\Delta\tau$): 9% per τ jet;
- luminosity ($\Delta\mathcal{L}$): 5%;
- PDF and scale ($\Delta\sigma$) 10% (theoretical uncertainty, it is not used for the signal cross section measurement with no background).

As the events are a mixture of different decay modes the total selection efficiency uncertainty ($\Delta\varepsilon_S$) is calculated per decay channel and then added together with the corresponding weights:

$$\Delta 3\mu 1\tau = \sqrt{3\Delta\mu^2 + \Delta\tau^2} = 8.2\%,$$

$$\Delta 2\mu 2\tau = \sqrt{2\Delta\mu^2 + 2\Delta\tau^2} = 11.4\%,$$

$$\Delta 1\mu 3\tau = \sqrt{\Delta\mu^2 + 3\Delta\tau^2} = 13.9\%,$$

giving

$$\Delta\varepsilon_S = \frac{144\Delta 3\mu 1\tau + 141\Delta 2\mu 2\tau + 61\Delta 1\mu 3\tau}{346} = 10.5\%.$$

The total systematic error for cross section measurement is then

$$\frac{\Delta\sigma}{\sigma} = \sqrt{\Delta\mu_{isol}{}^2 + \Delta\mathcal{L}^2 + \Delta\varepsilon_S{}^2} = 13\%.$$

Table12.7. Expected number of events, NLO cross section with expected statistical and systematic uncertainty of the cross section measurement at $10\,\text{fb}^{-1}$, and integrated luminosity needed for exclusion at 95% CL.

$m_{\Delta}^{\pm\pm}$ (GeV)	200	300	400	500
N_{ev} expected at $10\,\text{fb}^{-1}$	26	10	4	2
$\sigma_{NLO} \pm \text{stat} \pm \text{syst}$ (fb)	$93.9^{+19.3}_{-17.5} \pm 12.2$	$19.6^{+6.6}_{-5.6} \pm 2.5$	$5.9^{+3.4}_{-2.5} \pm 0.8$	$2.2^{+1.9}_{-1.3} \pm 0.3$
Luminosity for 95% CL exclusion, fb^{-1}	1.3	3.0	7.7	16.8

The statistical errors were evaluated constructing the shortest Bayesian confidence interval for the confidence level of 67% [669].

12.2.2.6. Results. The expected number of events at $10\,\text{fb}^{-1}$ and the NLO cross section with expected statistical and systematic uncertainty of the cross section measurement are given in Table 12.7. Table 12.7 shows also the integrated luminosity needed for exclusion at 95% CL.

III

.

A. Hektor, M. Kadastik, M. Müntel, M. Raidal, and L. Rebane.
"Testing neutrino masses in little Higgs models via discovery of doubly charged Higgs at LHC."
Nucl. Phys. B **787** (2007) 198 [arXiv:0705.1495].

Available online at www.sciencedirect.com
ScienceDirect
Nuclear Physics B 787 (2007) 198–210
NUCLEAR PHYSICS B

Testing neutrino masses in little Higgs models via discovery of doubly charged Higgs at LHC

A. Hektor, M. Kadastik, M. Müntel, M. Raidal, L. Rebane *

National Institute of Chemical Physics and Biophysics, Ravala 10, Tallinn 10143, Estonia

Received 7 June 2007; accepted 18 July 2007

Available online 27 July 2007

Abstract

We have investigated the possibility of direct tests of little Higgs models incorporating triplet Higgs neutrino mass mechanism at LHC experiments. We have performed Monte Carlo studies of Drell–Yan pair production of doubly charged Higgs boson Φ^{++} followed by its leptonic decays whose branching ratios are fixed from the neutrino oscillation data. We propose appropriate selection rules for the four-lepton signal, including reconstructed taus, which are optimized for the discovery of Φ^{++} with the lowest LHC luminosity. As the Standard Model background can be effectively eliminated, an important aspect of our study is the correct statistical treatment of the LHC discovery potential. Adding detection efficiencies and measurement errors to the Monte Carlo analyses, Φ^{++} can be discovered up to the mass 250 GeV in the first year of LHC, and 700 GeV mass is reachable for the integrated luminosity $L = 30$ fb^{-1}.

1. Introduction

The main motivation of the Large Hadron Collider (LHC) experiment is to reveal the secrets of electroweak symmetry breaking. If the light Standard Model (SM) Higgs boson H will be discovered, the question arises what stabilizes its mass against the Planck scale quadratically divergent radiative corrections. The canonical answer to this question is supersymmetry, predicting a very rich phenomenology of sparticles in the future collider experiments.

Alternatively, the light SM Higgs boson may signal some strong dynamics at high scale $\Lambda \sim 4\pi f$, where f is the decay constant of the new strongly interacting theory [1]. The most

* Corresponding author.
E-mail address: liis.rebane@cern.ch (L. Rebane).

0550-3213/$ – see front matter
doi:10.1016/j.nuclphysb.2007.07.014

interesting class of models in such a scheme are the little Higgs models [2–4]. In those models the SM Higgs boson is a pseudo Goldstone mode of a broken global symmetry and remains much lighter than the other modes of the model, thus solving the little hierarchy problem and postponing the solution to the fundamental hierarchy problem to the scale Λ. Those models are also very interesting from collider physics point of view since they predict the existence of new particles, such as a new set of heavy gauge bosons W_H, Z_H, a vectorlike heavy quark pair T, $\bar{T}$ with charge $2/3$, and triplet Higgs bosons Φ. If the new particle masses are $\mathcal{O}(1)$ TeV, direct tests of the models are possible at LHC [5–7].

An important open issue to address in the context of little Higgs models is the origin of non-zero neutrino masses [8–12]. The neutrino mass mechanism which naturally occurs in those models is the triplet Higgs mechanism [13,14] (sometimes called type II seesaw) which employs a scalar with the $SU(2)_L \times U(1)_Y$ quantum numbers $\Phi \sim (3, 2)$. The existence of such a multiplet in some versions of the little Higgs models is a direct consequence of global symmetry breaking which makes the SM Higgs light. For example, in the minimal littlest Higgs model [15], the triplet Higgs with non-zero hypercharge arises from the breaking of global $SU(5)$ down to $SO(5)$ symmetry as one of the Goldstone bosons. Its mass $M_\Phi \sim g_s f$, where $g_s < 4\pi$ is a model dependent coupling constant in the weak coupling regime [1], is therefore predicted to be below the cut-off scale Λ, and could be within the mass reach of LHC. Although the triplet mass scale is $\mathcal{O}(1)$ TeV, the observed neutrino masses can be obtained naturally. Firstly, non-observation of rare decays $\mu \to eee$, $\mu \to e\gamma$, $\tau \to \ell\ell\ell$, where $\ell = e, \mu$, implies that the triplet Higgs boson Yukawa couplings Y_{ij} must be small, thus suppressing also the neutrino masses. Secondly, the vaccuum expectation value (vev) of the neutral component of triplet v_Φ contributes at tree level to the SM oblique corrections, and is therefore severely constrained by precision data. There exist additional mechanisms which can explain the smallness of v_Φ in little Higgs models. Since the smallness of v_Φ is the most natural explanation of the smallness of neutrino masses in the little Higgs models, we assume this to be the case in this work.

The aim of this paper is to study the possibility of direct tests of little Higgs models *and* neutrino mass mechanisms at LHC experiments via pair productions and subsequent decays of triplet Higgs boson. We study the Drell–Yan pair production of doubly charged component of the triplet [16–21]

$$pp \to \Phi^{++}\Phi^{--}, \tag{1}$$

followed by the leptonic decays. Notice that (i) the production cross section does not depend on any unknown model parameter but the mass of Φ^{++}; (ii) smallness of v_Φ in this scenario, following from the smallness of neutrino masses, implies that the decays $\Phi^{++} \to W^+W^+$ are negligible, and we neglect this channel in the following analyses; (iii) the Φ^{++} leptonic decay branching fractions do not depend on the size of the Yukawa couplings but only on their ratios which are known from neutrino oscillation experiments. In the triplet model the normally hierarchical light neutrino masses predict $\mathrm{BR}(\Phi^{++} \to \mu^+\mu^+) \approx \mathrm{BR}(\Phi^{++} \to \tau^+\tau^+) \approx \mathrm{BR}(\Phi^{++} \to \mu^+\tau^+) \approx 1/3$. Therefore this scenario is predictive and testable at LHC experiments.

The production process (1) has been studied before in various theory papers. In this work we first carry out a pure Monte Carlo study of the signal and background processes in the environment of LHC detectors. After that we improve our analyses by adding particle reconstruction efficiencies and Gaussian distortion functions for particle momentas and E_T^{miss}. Those mimic the detector inefficiency effects at the Monte Carlo level. We believe that those effects help us to estimate the realistic mass reach of the LHC detectors to the process under study.

In our study the new results are the following. For the signal reconstruction we use new criteria, such as equality of invariant masses of positively and negatively charged leptons together with total Σp_T cut for all leptons, which allows us to achieve better reconstructions efficiencies compared to the standard cuts. We also reconstruct tau lepton final states with more than one τ, which has not done before in this context. As all the SM background can be eliminated in the case of this process, correct statistical analyses of the results in the limit of no background is an important aspect of our study. For the discovery criteria we have used the Log-Likelihood Ratio (LLR) statistical method to demand 5σ discovery potential to be bigger than 95% ($1 - \mathrm{CL}_{s+b} > 0.95$). Our results are optimized for the discovery of process (1) with the lowest possible LHC luminosity. The pure Monte Carlo study shows that Φ^{++} up to the mass 300 GeV is reachable in the first year of LHC ($L = 1$ fb^{-1}) and Φ^{++} up to the mass 800 GeV is reachable for the luminosity $L = 30$ fb^{-1}. Including the Gaussian measurement errors in the Monte Carlo the corresponding mass reaches become 250 GeV and 700 GeV, respectively. The errors of our estimates of the required luminosity for discovery depend strongly on the size of statistical Monte Carlo sample of the background processes.

The paper is organized as follows. In Section 2 we present the collider phenomenology of triplet Higgs boson and relate collider observables to neutrino mass measurements. In Section 3 we discuss the Monte Carlo produced signal and background processes. In Section 4 we present the details of reconstruction and analysis procedure and results. Detector effects are discussed in Section 5. Finally we conclude in Section 6.

2. Neutrino masses and collider phenomenology

In this work we consider little Higgs scenarios in which, due to the breaking of global symmetry protecting the SM Higgs boson mass, the spectrum of the model contains also a pseudo Goldstone boson with the $SU(2)_L \times U(1)_Y$ quantum numbers $\Phi \sim (3, 2)$ [15,22]. Although Φ is predicted to be heavier than the SM Higgs boson, the little Higgs philosophy implies that its mass could be $\mathcal{O}(1)$ TeV [1]. Due to the specific quantum numbers the triplet Higgs boson couples only to the left-chiral lepton doublets $L_i \sim (2, -1)$, $i = e, \mu, \tau$, via the Yukawa interactions given by

$$L = i\bar{L}_i^c \tau_2 Y^{ij} (\tau \cdot \Phi) L_j + \text{h.c.}, \tag{2}$$

where Y_{ij} are the Majorana Yukawa couplings. The interactions (2) induce lepton flavour violating decays of charged leptons which have not been observed. The most stringent constraint on the Yukawa couplings comes from the upper limit on the tree-level decay $\mu \to eee$ and is[1] $Y_{ee} Y_{e\mu} < 3 \times 10^{-5}$ (M/TeV)^2 [18,23]. Experimental bounds on the tau Yukawa couplings are much less stringent. In our collider studies we take $Y_{\tau\tau} = 0.01$ and rescale other Yukawa couplings accordingly. In particular, hierarchical light neutrino masses imply $Y_{ee}, Y_{e\mu} \ll Y_{\tau\tau}$ consistently with the direct experimental bounds.

According to Eq. (2), the neutral component of the triplet Higgs boson Φ^0 couples to the left-handed neutrinos with the same strength as Φ^{++} couples to the charged leptons. If Φ^0 acquires a vev v_Φ, non-zero Majorana masses are generated for the left-handed neutrinos [13,14]. Non-zero neutrino masses and mixing is presently the only experimentally verified signal of new physics

[1] In little Higgs models with T-parity there exist additional sources of flavour violation from the mirror fermion sector [24,25].

beyond the SM. In the triplet neutrino mass mechanism the neutrino masses are given by

$$(m_\nu)_{ij} = Y_{ij} v_\Phi. \tag{3}$$

We assume that the smallness of neutrino masses is explained by the smallness of v_Φ. In a realistic scenario massless Majoron, the Goldstone boson of broken lepton number, must be avoided. This is achieved by an explicit coupling of Φ to the SM Higgs doublet H via $\mu \Phi^0 H^0 H^0$ [14], where μ has a dimension of mass. If $\mu \sim M_\Phi$, in the concept of seesaw [26] the smallness of neutrino masses is attributed to the very high scale of triplet mass M_Φ because $v_\Phi = \mu v^2 / M_\Phi^2$, where $v = 174$ GeV. However, in the little Higgs models the triplet mass scale $\mathcal{O}(1)$ TeV alone cannot suppress v_Φ. Therefore in this model $\mu \ll M_\Phi$, which can be achieved, for example, via shining of explicit lepton number violation from extra dimensions as shown in Refs. [27,28], or if the triplet is related to the Dark Energy of the Universe [29,30]. Models with additional (approximate) T-parity [22] make the smallness of v_Φ technically natural. However, if the T-parity is exact, v_Φ must vanish. In this work we do not consider the naturalness criteria and assume that the above described neutrino mass scenario is realized in nature. In that case $Y v_\Phi \sim \mathcal{O}(0.1)$ eV while the Yukawa couplings Y can be on the order of charged lepton Yukawa couplings of the SM. As a result, the branching ratio of the decay $\Phi \to WW$ is negligible. We also remind that v_Φ contributes to the SM oblique corrections, and the precision data fit $\hat{T} < 2 \times 10^{-4}$ [31] sets an upper bound $v_\Phi \leqslant 1.2$ GeV on that parameter.

Notice the particularly simple connection between the flavour structure of light neutrinos and the Yukawa couplings of the triplet via Eq. (3). Therefore, independently of the overall size of the Yukawa couplings, one can predict the leptonic branching ratios of the triplet from neutrino oscillations. For the normally hierarchical light neutrino masses neutrino data implies negligible Φ branching fractions to electrons and $\mathrm{BR}(\Phi^{++} \to \mu^+\mu^+) \approx \mathrm{BR}(\Phi^{++} \to \tau^+\tau^+) \approx \mathrm{BR}(\Phi^{++} \to \mu^+\tau^+) \approx 1/3$. Those are the final state signatures predicted by the triplet neutrino mass mechanism for collider experiments.

At LHC Φ^{++} can be produced singly and in pairs. The cross section of the single Φ^{++} production via the WW fusion process [18] $qq \to q'q'\Phi^{++}$ scales as $\sim v_\Phi^2$. In the context of the littlest Higgs model this process, followed by the decays $\Phi^{++} \to W^+W^+$, was studied in Refs. [5,7,32]. The detailed ATLAS simulation of this channel shows [32] that in order to observe an 1 TeV Φ^{++}, one must have $v_\Phi > 29$ GeV. This is in conflict with the precision physics bound $v_\Phi \leqslant 1.2$ GeV as well as with the neutrino data. Therefore the WW fusion channel is not experimentally promising for the discovery of doubly charged Higgs.

On the other hand, the Drell–Yan pair production process $pp \to \Phi^{++}\Phi^{--}$ is not suppressed by any small coupling and its cross section is known up to next to leading order [19] (possible additional contributions from new physics such as Z_H are strongly suppressed and we neglect those effects here). Followed by the lepton number violating decays $\Phi^{\pm\pm} \to \ell^\pm\ell^\pm$, this process allows to reconstruct $\Phi^{\pm\pm}$ invariant mass from the same charged leptons rendering the SM background to be very small in the signal region. If one also assumes, as we do in this work, that neutrino masses come from the triplet Higgs interactions, one fixes the $\Phi^{\pm\pm}$ leptonic branching ratios. This allows to test the triplet neutrino mass model at LHC.

3. Monte Carlo simulation of the signal and backgrounds

The production of the doubly-charged Higgs is implemented in the PYTHIA Monte Carlo generator [33]. The final and initial state interactions and hadronization have been taken into account. We have used the CTEQ5L parton distribution functions.

Table 1
Cross-sections, numbers of Monte Carlo generated events and the corresponding integrated luminosities of the generated events. For the signal events we have taken the branching ratios $\mathrm{BR}(\Phi^{\pm\pm} \to \mu^{\pm}\mu^{\pm}) = \mathrm{BR}(\Phi^{\pm\pm} \to \mu^{\pm}\tau^{\pm}) = \mathrm{BR}(\Phi^{\pm\pm} \to \tau^{\pm}\tau^{\pm}) = 1/3$

Process	Total σ (fb)	N of events generated	Corresponding luminosity (fb^{-1})
Signal			
$M_{\Phi} = 200$ GeV	7.78E+01	1.00E+05	1.28E+03
$M_{\Phi} = 500$ GeV	1.99E+00	1.00E+05	5.03E+04
$M_{\Phi} = 1000$ GeV	5.58E−02	1.00E+05	1.79E+06
Background			
$pp \to t\bar{t} \to 4\ell$	8.84E+04	2.55E+07	2.88E+02
$pp \to t\bar{t}\,Z$	6.50E+02	1.50E+05	2.3E+02
$pp \to ZZ$	2.12E+02	1.00E+05	4.72E+02

In the following analysis the normal hierarchy of neutrino masses and a very small value of the lowest neutrino mass is assumed. Such a model predicts that Higgs decay into electrons can be neglected and that there are three dominant decay channels for Φ^{++} with approximately equal branching ratios:

- $\Phi^{\pm\pm} \to \mu^{\pm}\mu^{\pm}$,
- $\Phi^{\pm\pm} \to \mu^{\pm}\tau^{\pm}$,
- $\Phi^{\pm\pm} \to \tau^{\pm}\tau^{\pm}$.

We have studied only pair production of doubly charged Higgs due to the reasons pointed out above. $\Phi^{\pm\pm}$ pair decay products can combine to five different τ and μ combinations: 4μ, $3\mu1\tau$, $2\mu2\tau$, $1\mu3\tau$ and 4τ. Before reaching the detector, τ decays into an e, μ or a hadronic jet (marked as j below) with branching ratios of 0.18, 0.17 and 0.65, respectively [34]. τ hadronic jets and μ's are well visible and reconstructible in detector. The reconstruction of an energetic τ from electron decay is sensitive to detector effects, involving sophisticated background processes [35]. In the current analyses we will neglect this channel, which will cause 31% loss of the total signal. Such loss is still sufficiently low and can be considered acceptable. Table 1 gives the cross sections and the Monte Carlo generated event numbers in our study.

The signatures of Φ decay are very clean due to (i) high transfer momentum of the decay products, (ii) lepton number violation and (iii) pair production of Φ. The Standard Model particles are lighter than Φ, so the background μ's and τ's must have smaller transverse energy and they do not produce an invariant mass peak in $\mu^{+}\mu^{+}$, $\mu^{+}\tau^{+}$, $\tau^{+}\tau^{+}$, final states. The present lower bound for the invariant mass of Φ is set by Tevatron to $M_{\Phi} \geqslant 136$ GeV [36,37]. In our study, four-lepton background processes with reasonable cross sections and high p_T leptons arise from three Standard Model processes

- $pp \to t\bar{t}$,
- $pp \to t\bar{t}Z$,
- $pp \to ZZ$.

PYTHIA was used to generate $t\bar{t}$ and ZZ background ($t\bar{t}$ is forced to decay to $WWb\bar{b}$ and W leptonically). The CTEQ5L parton distribution functions were used. CompHEP was used to

generate the $Zt\bar{t}$ background via its PYTHIA interface [38,39]. All the datasets were generated in Baltic Grid. In addition to background processes shown in Table 1, some other four-lepton background processes exist involving b-quarks in the final state (for example, $pp \to b\bar{b}$). As such processes are very soft, it is possible to use the effective tagging methods [40] and totally eliminate this soft background [41]. Also, we do not consider possible background processes from the physics beyond the Standard Model.

4. Reconstruction and analysis of the Monte Carlo data

To study the feasibility of detecting the signal over background, we have to work with five possible reconstruction channels according to the following final states.

- $\Phi^{++}\Phi^{--} \to 4\mu$: The cleanest and most simple channel.
- $\Phi^{++}\Phi^{--} \to 3\mu 1\tau$: The channel is easily reconstructable using an assumption that the neutrino originating from the τ decay is collinear with τ-jet and gives majority to the missing transverse energy (E_T^{miss}).
- $\Phi^{++}\Phi^{--} \to 2\mu 2\tau$: The signature can be reconstructed using the same assumptions for both τ-neutrinos. The whole E_T^{miss} vector has to be used here, while in the previous channel only one component was needed.
- $\Phi^{++}\Phi^{--} \to 1\mu 3\tau$: The channel can be reconstructed theoretically relying on an additional requirement that the two Higgs bosons have equal invariant masses. However, the reconstruction is very sensitive to the experimental accuracy of E_T^{miss} determination.
- $\Phi^{++}\Phi^{--} \to 4\tau$: The channel cannot be reconstructed (and triggered by the single muon trigger).

First, we apply general detector related cut-offs for the Monte Carlo generated data. Generated particles were reconstructed within the pseudorapidity region $|\eta| < 2.4$ and with transverse momentum higher than 5 GeV. These are the natural restrictions of the CMS and ATLAS detectors at the LHC. Only the pseudorapidity region $|\eta| < 2.4$ is reachable for the detector and only the events with $p_T > 5$ GeV are typically triggered. These restrictions suppress mainly the soft Standard Model background. The efficiency of lepton reconstruction and charge identification rate are very high, we use the values 0.9 and 0.95, respectively [42].

The invariant mass of two like-sign μ's and/or τ's are calculated using equation:

$$\left(m_I^{\pm\pm}\right)^2 = \left(p_1^{\pm} + p_2^{\pm}\right)^2, \tag{4}$$

where $p_{1,2}$ is the μ or τ 4-momentum. Since the like-sign signal of μ's or τ's originate from a doubly charged Higgs boson, the invariant mass peak measures the mass of doubly charged Higgs, $m_I = M_\Phi$. 4-μ final state allows to obtain invariant masses directly from Eq. (4). In channels involving one or several τ's, which are registered as τ-jets or secondary μ's (marked as μ' below), the momenta of jets has to be corrected according to the equation system:

$$\mathbf{p}_\tau^i = k^i \mathbf{p}_{\text{jet}}^i, \tag{5}$$

$$\mathbf{p}_{T\text{miss}} = \sum_i \mathbf{p}_{T\nu}^i, \tag{6}$$

$$M_{\Phi^{++}} = M_{\Phi^{--}}, \tag{7}$$

Table 2
Probabilities of all possible decay chains for Φ pairs in our scenario. "x" in the table marks τ or, after τ decay, τ-jet. The reconstructed signatures are marked in bold, the remaining signatures were not reconstructed. After omitting the channels that include $\tau \to e$ decay, 69% of the total signal is left. In total 64% of the signal has been reconstructed

Decay channel	After Higgs decay ($x = \tau$)	After τ decay ($x = \text{jet}_\tau$)				
		0 ($\tau \to \mu'$)	1 ($\tau \to \mu'$)	2 ($\tau \to \mu'$)	3 ($\tau \to \mu'$)	4 ($\tau \to \mu'$)
$2\Phi \to 4\mu$	0.1111	**0.1111**	**0.0377**	**0.0107**	0.0012	0.0001
$2\Phi \to 3\mu 1x$	0.2222	**0.1443**	**0.0736**	**0.0125**	0.0014	
$2\Phi \to 2\mu 2x$	0.3333	**0.1407**	**0.0478**	0.0054		
$2\Phi \to 1\mu 3x$	0.2222	**0.0610**	0.0207			
$2\Phi \to 4x$	0.1111	0.0198				
Sum	1.0	**0.64** + 0.05				

where i counts τ's, $\mathbf{p}$ marks 3-momentum, $\mathbf{p}_{T\nu}$ is the vector of transverse momentum of the produced neutrinos, $\mathbf{p}_{T\text{miss}}$ is the vector of missing transverse momentum (measured by the detector) and $k_i > 1$ are positive constants. Eq. (5) describes the standard approximation that the decay products of a heavily boosted τ are collinear [42]. Eq. (6) assumes missing transverse energy only to be comprised of neutrinos from τ decays. In general, it is not a high-handed simplification, because the other neutrinos in the event are much less energetic and the detector error of E_T^{miss} is order of magnitude smaller [43]. Using the first two formulas, it is possible to reconstruct up to two τ's per event. Additional requirement of Eq. (7) allows to reconstruct the third τ per pair event, although very low measurement errors are needed.

A significant fraction of τ's (0.18) decay into μ''s that cannot be distinguished from primary μ's in the detector. Still, if reconstructed invariant masses of Φ^{++} and Φ^{--} are considerably different, we can suspect that one or several μ's originate form τ decays. In such case we can again use Eqs. (5)–(7) to correct the 4-momenta of decay products. When only one secondary muon is present, E_T^{miss} points into the same direction as its p_T. Otherwise E_T^{miss} is a superposition of neutrino transverse momenta. Such correction tightens the invariant mass peak of the signal and does not produce any artificial background.

The occurrence probability of different reconstruction channels are presented in Table 2. The second column shows probabilities of Higgs decay to N μ's and M τ's. Next columns describe the final state after τ decay to μ''s and/or jets. Different columns mark the number of secondary μ's and the rows designate τ-jets in the detector recordings. The events having at least one $\tau \to e$ in a final state are omitted in our analysis, as well as events with $M > 3$ or $N(\mu') > 2$. The proportions of reconstructible signatures are marked in a bold-face. The table shows that 0–3 jet channels together with μ correction are almost equally important and overall reconstructible channels comprise 64% of total events.

A clear signal extraction from the Standard Model background can be achieved using a set of selection rules imposed on a reconstructed event in the following order.

- S1: events with at least 2 positive and 2 negative muons or jets which have $|\eta| < 2.4$ and $p_T > 5$ GeV are selected.
- S2: $\sum p_T$ (scalar) sum of 2 most energetic positive and negative μ's or τ-jets has to be bigger than a certain value (depending on Higgs mass).
- S3: Z-tagging—if invariant mass of the pair of opposite charged μ's or τ-jets is nearly equal to Z mass (85–95 GeV), then the particles are eliminated from the analysis.

- S4: as Φ's are produced in pairs, the reconstructed invariant masses (in one event) have to be equal. We have used the condition

$$0.8 < m_I^{++}/m_I^{--} < 1.2. \tag{8}$$

If the invariant masses satisfy the condition then we include them to the histogram, otherwise we suspect that some μ's may originate from τ decay, and make an attempt to find corrections to their momenta according to the method described above.

The rule S1 is an elementary detector trigger. S2, performing scalar sum of p_T, is an untraditional cut. The advantage compared to the widely used p_T cut for a single particle is clearly visible from Fig. 1. The left panel shows that the maximum of Higgs line reaches clearly out of the background while on the right panel the maximum is deeply inside the background.

Z-tagging in S3 suppresses $pp \to ZZ$ and $pp \to t\bar{t}Z$ background. S4 is based on the equality of the invariant masses of like-signed μ's or τ's. Fig. 2 gives a clear picture of the behavior of signal and background for the S4 selection rule. Naturally, some freedom is needed due to the Φ

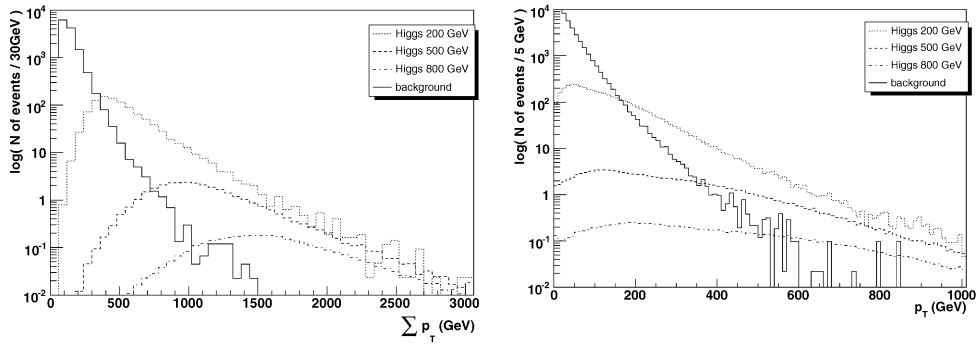

Fig. 1. The left panel shows the distribution of events according to scalar sum of 2 most energetic (highest p_T) positively and 2 most energetic negatively charged muons or jets ($\sum p_T$). The right panel shows the distribution of events considering traditional p_T cut for single particles. Both figures correspond to luminosity $L = 30\ \text{fb}^{-1}$.

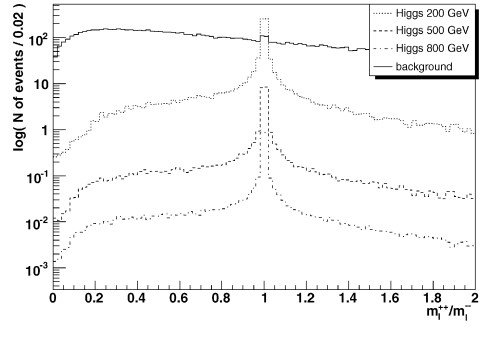

Fig. 2. Distribution of events according to the ratio of reconstructed invariant masses ($m_{\Phi^{++}}/m_{\Phi^{--}}$) (no other cuts are applied). The figure corresponds to luminosity $L = 30\ \text{fb}^{-1}$.

Table 3
Optimal $\sum p_T$ cut for different Higgs masses and the corresponding minimal discovery luminosities: the lower ($L_{\min}$) corresponds to the generated background in our analyses and the higher ($L_{\max}$) corresponds to 95% upper limit of the background error

Mass of Φ (GeV)	200	300	400	500	600	700	800	900	1000
Optimal $\sum p_T$ for S2 (GeV)	300	400	600	700	860	860	860	860	860
MC $L_{\min}$ (fb^{-1})	0.25	0.93	2.0	3.6	8	17	34	62	120
MC $L_{\max}$ (fb^{-1})	0.26	1.03	3.1	7.0	17	38	77	160	320

decay width and experimental errors of the detector. We require that the ratio m_I^{++}/m_I^{--} has to be in the region from 0.8 to 1.2.

While the selection rules S1, S3 and S4 are independent of the Higgs mass, the selection rule S2 ($\sum p_T$ cut) has to be optimized for a certain Higgs mass value. The cut may be set to a very high value which eliminates all background events, but inevitable loss in signal may postpone the discovery of new physics at LHC. Thus it is natural to take the minimal discovery luminosity ($L_{\min}$) as the optimization criteria. Looking for a cut value that enables to make a discovery with the lowest luminosity, we are dealing with small signal and background expectations by definition. Simple significance estimators cannot be exploited here. We have used the log-likelihood ratio (LLR) statistical method [44,45] to demand 5σ discovery potential to be bigger than 95% ($1 - \mathrm{CL}_{s+b} > 0.95$) as for a discovery criteria. This is a rather strong requirement, because it allows to make a discovery (meaning the fluctuation of background may mimic the outcome of an experiment with probability less than 2.9×10^{-7} (5σ)) during the specified luminosity with a probability of 95% (if $s + b$ hypothesis is correct). The widely used convention, that significance should exceed five, gives only 50% discovery potential in Gaussian limit and diminishes to very small values when background approaches zero.

The best value for S2 cut does depend on M_Φ but is not too sensitive to it. Typically the $\sum p_T$ can be assigned a value with a precision of 100 GeV while affecting the minimum luminosity by only a couple of percent. In the Table 3 the approximated middle point of this value is given. As the best S2 cut is very strong, it suppresses almost entirely the generated background (being combined with the other selection rules). For Higgs masses above 500 GeV the background is totally suppressed and the discovery potential criteria meets the requirement for 3 signal events (6 invariant masses). Nevertheless we cannot infer that the background is really zero in nature. To estimate the statistical error due to final number of generated background events we have found 95% upper limit of background according to Poisson statistics (Table 4, in brackets). Using this limit in LLR analysis we get much higher luminosities for discovery. Even a very small background expectancy ($b = 0.01$) gives some possibility to have one (9.9×10^{-3}) or two (4.9×10^{-5}) background events in the experiment and these outcomes cannot be interpreted as discovery anymore. This phenomenon shifts the minimal required luminosity to much higher values denoted as $L_{\max}$ in Table 3.

An example of invariant mass distribution after applying selection rules are shown in Fig. 3 for $M_\Phi = 500$ GeV. A tabulated example is given for $M_\Phi = 200, 500, 800$ GeV in Table 4 corresponding to the luminosity $L = 30$ fb^{-1}. The strength of S2 cut is clearly visible: almost no decrease in signal while the number of the background events descends close to final minimum value. A peculiar behavior of S4—reducing the background, while also increasing the signal in its peak—is the effect of applying the $\tau \to \mu'$ correction method described above.

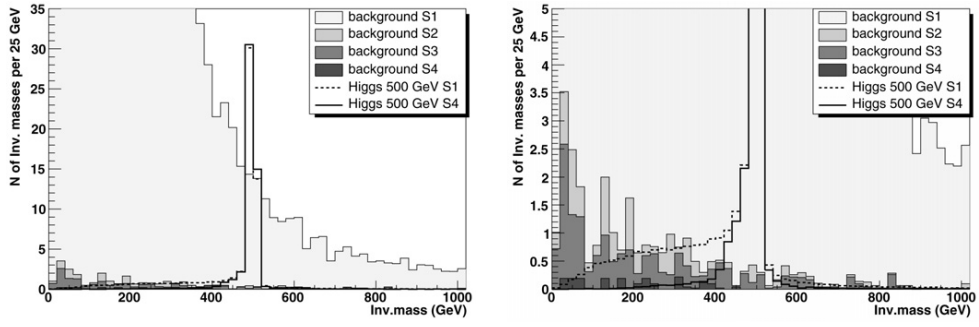

Fig. 3. Distribution of invariant masses after applying selection rules (S1–S4) for Higgs $M_\Phi = 500$ GeV and the Standard Model background ($L = 30$ fb^{-1}). The histogram in the right panel is a zoom of the left histogram to illustrate the effects of the selection rules S2–S4.

Table 4
Effectiveness of the selection rules for the background and signal. All event numbers in the table are normalized for $L = 30$ fb^{-1}. The numbers in brackets mark errors at 95% confidence level for Poisson statistics. The signal increases after S4 due to the reconstructed $\tau \to \mu'$ decays

Process	N of invariant masses				
	N of Φ	S1	S2	S3	S4
Energy range 150–250 GeV					
$M_\Phi = 200$ GeV	4670	1534	1488	1465	1539
$t\bar{t} \to 4\ell$	–	1222 (168)	172 (8.5)	134 (6.9)	17.6 (3.7)
$t\bar{t}Z$	–	21.3 (4.0)	15.5 (1.0)	6.3 (1.2)	2.2 (1.1)
ZZ	–	95.0 (12.0)	22.5 (0.7)	9.8 (0.5)	1.7 (0.2)
Energy range 375–625 GeV					
$M_\Phi = 500$ GeV	119.2	48.4	47.5	46.8	49.5
$t\bar{t} \to 4\ell$	–	178 (28)	2.1 (0.9)	1.65 (0.87)	0.10 (0.35)
$t\bar{t}Z$	–	6.6 (1.7)	2.3 (1.0)	1.0 (1.0)	0.00 (0.1)
ZZ	–	9.4 (2.9)	1.4 (0.2)	0.68 (0.19)	0.08 (0.09)
Energy range 600–1000 GeV					
$M_\Phi = 800$ GeV	11.67	5.05	5.00	4.92	5.21
$t\bar{t} \to 4\ell$	–	77 (12)	0.00 (0.22)	0.00 (0.22)	0.00 (0.07)
$t\bar{t}Z$	–	2.6 (1.2)	0.39 (0.4)	0.39 (0.4)	0.00 (0.1)
ZZ	–	2.5 (0.8)	0.34 (0.16)	0.17 (0.09)	0.00 (0.02)

5. Including measurement errors to Monte Carlo

In this section we make an attempt to estimate simplified detector effects at the level of Monte Carlo analyses. In order to do that we have added overall detection efficiencies for the Monte Carlo generated μ's and τ-jets—0.98 and 0.6, respectively. Additionally, we applied Gaussian distortion functions to Monte Carlo produced data for μ's, τ-jets and E_T^{miss} which were used to alter randomly those quantities in the analysis. Although the precision of μ detection is sensitive to p_T of μ and $|\eta|$ we use the mean values for a rough estimation. We make the following assumptions based on [41–43].

Table 5
Optimal $\sum p_T$ cuts and minimal discovery luminosities for different Higgs masses when the estimates of detector measurement errors are taken into account. Two boundaries for the minimal luminosity are given: the lower ($L_{\min}$) corresponds to the generated background and the higher ($L_{\max}$) corresponds to 95% upper limit of the background error

Mass of Φ (GeV)	200	300	400	500	600	700	800	900	1000
Optimal $\sum p_T$ for S2 (GeV)	300	400	600	700	860	860	860	860	860
Det Eff $L_{\min}$ (fb^{-1})	0.526	1.20	3.0	6.6	15	30	60	111	200
Det Eff $L_{\max}$ (fb^{-1})	0.546	2.19	6.5	16.6	39	86	190	420	900

Table 6
The importance of reconstruction channels at Monte Carlo level and considering detector efficiency effects

	Percentage of the channel after reconstruction				
Decay channel	4μ	$3\mu 1j$	$2\mu 2j$	$1\mu 3j$	$\tau \to \mu$ correction
Monte Carlo	21	28	26	9	16
MC + efficiencies	38	25	12	1	24

The direction of muon (τ-jet) is altered with the Gaussian distribution: mean $\mu = 0.0005$ (0.031) and variance $\sigma^2 = 0.003$ (0.017). The transverse momentum is altered according to the $p_{T,\text{rec}}/p_{T,\text{Monte Carlo}}$ Gaussian distribution: mean $\mu = 1.$ (0.897) and variance $\sigma^2 = 0.03$ (0.089). Both components of missing transverse energy are altered independently according to the Gaussian distribution (mean $\mu = 0$ GeV and variance $\sigma^2 = 25$ GeV) by adding the piece to its Monte Carlo value.

The result of such a distortion is a decrease in both signal and background approximately by factor two (Table 5). As the background and the signal decrease proportionally, the luminosity needed for discovery roughly doubles. Remarkably the optimized S2 cut value does not change significantly. The proportion of the reconstruction channels in the total analysis has changed remarkably as shown in Table 6. The reason is clearly the small detection efficiency of τ-jets. The $1\mu 3j$ channel comprises only 1% of the total signal if the detector effects are considered, while in the pure Monte Carlo analysis it forms 9%. The additional possible detector effects make the $\tau \to \mu$ correction even more relevant.

6. Conclusions and outlook

We have studied possible direct test of little Higgs scenarios which light particle spectrum includes a triplet scalar multiplet at LHC experiments. We have investigated the Drell–Yan pair production of the doubly charged Higgs boson and its subsequent leptonic decays. In addition to solving the little hierarchy problem, this scenario can also explain the origin of non-zero neutrino masses and mixing via the triplet Higgs neutrino mass mechanism. Simple connection between the observed neutrino mixing and triplet Yukawa couplings allows us to predict the leptonic branching ratios of the triplet. Thus the experimental signatures of the model do not depend on the size of the triplet Yukawa couplings allowing direct tests of this scenario at LHC.

In our analyses we have considered four μ and/or τ final states including up to 3 tau leptons. We propose four selection rules to achieve the optimized signal and background ratio. As the Φ^{++} decays are lepton number violating, we have shown that the background can be practically eliminated. In such an unusual situation we have used the LLR statistical method to demand 5σ discovery potential to be bigger than 95% ($1 - \text{CL}_{s+b} > 0.95$) as the discovery criterion.

The results of optimized cut values are presented in Table 3. Considering the pure Monte Carlo study, Φ^{++} up to the mass 300 GeV can be discovered in the first year of LHC ($L = 1$ fb^{-1}) and Φ^{++} up to the mass 800 GeV can be discovered for the integrated luminosity $L = 30$ fb^{-1}. Including particle reconstruction efficiencies as well as Gaussian distortion functions for the particle momentas and missing energy which mimic detector inefficiencies at Monte Carlo level, our results show that Φ^{++} can be discovered up to the mass 250 GeV in the first year of LHC and 700 GeV mass is reachable for the integrated luminosity $L = 30$ fb^{-1}.

For further studies of this scenario at LHC progress can be made both physics-wise as well as technically. Full simulations of the detector effects are needed which also include the electron, muon and tau final states. For better determination of statistical errors coming from the background studies bigger SM background datasets must be produced. This requires huge computing resources. If these goals can be achieved, the proposed phenomenology opens a new window to study the neutrino properties at colliders. In addition to the considerations in this paper, one can determine at LHC experiments the hierarchy (normal or inverse) of light neutrino mass spectrum, and to estimate the two Majorana phases which are not measurable in neutrino oscillation experiments [46].

Acknowledgements

We thank the Estonian Science Foundation for the Grant No. 6140. The work described in this paper was also supported by the European Union through the FP6-2004-Infrastructures-6-contract No. 026715 project “BalticGrid”.

References

[1] G.F. Giudice, C. Grojean, A. Pomarol, R. Rattazzi, hep-ph/0703164.
[2] N. Arkani-Hamed, A.G. Cohen, H. Georgi, Phys. Rev. Lett. 86 (2001) 4757, hep-th/0104005.
[3] H.C. Cheng, C.T. Hill, S. Pokorski, J. Wang, Phys. Rev. D 64 (2001) 065007, hep-th/0104179.
[4] N. Arkani-Hamed, A.G. Cohen, H. Georgi, Phys. Lett. B 513 (2001) 232, hep-ph/0105239.
[5] T. Han, H.E. Logan, B. McElrath, L.T. Wang, Phys. Rev. D 67 (2003) 095004, hep-ph/0301040.
[6] W. Kilian, J. Reuter, Phys. Rev. D 70 (2004) 015004, hep-ph/0311095.
[7] T. Han, H.E. Logan, L.T. Wang, JHEP 0601 (2006) 099, hep-ph/0506313.
[8] J. Lee, hep-ph/0504136.
[9] T. Han, H. Logan, B. Mukhopadhyaya, R. Srikanth, Phys. Rev. D 72 (2005) 053007, hep-ph/0505260.
[10] F. del Aguila, M. Masip, J.L. Padilla, Phys. Lett. B 627 (2005) 131, hep-ph/0506063.
[11] S.R. Choudhury, N. Gaur, A. Goyal, Phys. Rev. D 72 (2005) 097702, hep-ph/0508146.
[12] A. Abada, G. Bhattacharyya, M. Losada, Phys. Rev. D 73 (2006) 033006, hep-ph/0511275.
[13] J. Schechter, J.W.F. Valle, Phys. Rev. D 22 (1980) 2227.
[14] E. Ma, U. Sarkar, Phys. Rev. Lett. 80 (1998) 5716, hep-ph/9802445.
[15] N. Arkani-Hamed, A.G. Cohen, E. Katz, A.E. Nelson, JHEP 0207 (2002) 034, hep-ph/0206021.
[16] J.F. Gunion, C. Loomis, K.T. Pitts, in: the Proceedings of 1996 DPF/DPB Summer Study on New Directions for High-Energy Physics (Snowmass 96), Snowmass, Colorado, 25 June–12 July 1996, pp. LTH096, hep-ph/9610237.
[17] J.F. Gunion, J. Grifols, A. Mendez, B. Kayser, F.I. Olness, Phys. Rev. D 40 (1989) 1546.
[18] K. Huitu, J. Maalampi, A. Pietila, M. Raidal, Nucl. Phys. B 487 (1997) 27, hep-ph/9606311.
[19] M. Muhlleitner, M. Spira, Phys. Rev. D 68 (2003) 117701, hep-ph/0305288.
[20] A.G. Akeroyd, M. Aoki, Phys. Rev. D 72 (2005) 035011, hep-ph/0506176.
[21] T. Rommerskirchen, T. Hebbeker, J. Phys. G 33 (2007) N47.
[22] S. Chang, JHEP 0312 (2003) 057, hep-ph/0306034.
[23] C.X. Yue, S. Zhao, hep-ph/0701017.
[24] S.R. Choudhury, A.S. Cornell, A. Deandrea, N. Gaur, A. Goyal, Phys. Rev. D 75 (2007) 055011, hep-ph/0612327.
[25] M. Blanke, A.J. Buras, B. Duling, A. Poschenrieder, C. Tarantino, hep-ph/0702136.

[26] P. Minkowski, Phys. Lett. B 67 (1977) 421;
M. Gell-Mann, P. Ramond, R. Slansky, in: P. Van Nieuwenhuizen, D. Freedman (Eds.), Proceedings of the Supergravity Stony Brook Workshop, New York, 1979, North-Holland, Amsterdam;
T. Yanagida, in: A. Sawada, A. Sugamoto (Eds.), Proceedings of the Workshop on Unified Theories and Baryon Number in the Universe, Tsukuba, Japan 1979, KEK Report No. 79-18, Tsukuba;
R. Mohapatra, G. Senjanovic, Phys. Rev. Lett. 44 (1980) 912.
[27] E. Ma, M. Raidal, U. Sarkar, Phys. Rev. Lett. 85 (2000) 3769, hep-ph/0006046.
[28] E. Ma, M. Raidal, U. Sarkar, Nucl. Phys. B 615 (2001) 313, hep-ph/0012101.
[29] E. Ma, U. Sarkar, Phys. Lett. B 638 (2006) 356, hep-ph/0602116.
[30] N. Sahu, U. Sarkar, hep-ph/0701062.
[31] G. Marandella, C. Schappacher, A. Strumia, Phys. Rev. D 72 (2005) 035014, hep-ph/0502096.
[32] G. Azuelos, et al., Eur. Phys. J. C 39S2 (2005) 13, hep-ph/0402037.
[33] T. Sjostrand, P. Eden, C. Friberg, L. Lonnblad, G. Miu, S. Mrenna, E. Norrbin, Comput. Phys. Commun. 135 (2001) 238, hep-ph/0010017.
[34] W.M. Yao, et al., Particle Data Group, J. Phys. G 33 (2006) 1.
[35] D. Acosta, et al., CMS Collaboration, The CMS Physics Technical Design Report, vol. 1, Section 10.4: Electron reconstruction and selection, CERN/LHCC vols. 2006–001, 2006. CMS TDR 8.1.
[36] D. Acosta, et al., CDF Collaboration, Phys. Rev. Lett. 93 (2004) 221802, hep-ex/0406073.
[37] V.M. Abazov, et al., D0 Collaboration, Phys. Rev. Lett. 93 (2004) 141801, hep-ex/0404015.
[38] E. Boos, et al., CompHEP Collaboration, Nucl. Instrum. Methods A 534 (2004) 250, hep-ph/0403113.
[39] A.S. Belyaev, et al., hep-ph/0101232.
[40] D. Acosta, et al., CMS Collaboration, The CMS Physics Technical Design Report, vol. 1, Section 12.2: b-tagging tools, CERN/LHCC 2006–001, 2006. CMS TDR 8.1.
[41] D. Acosta, et al., CMS Collaboration, The CMS Physics Technical Design Report, vol. 2, Physics Performance, J. Phys. G: Nucl. Part. Phys. 34 (2007) 995–1579.
[42] CMS Collaboration, The Compact Muon Solenoid. Muon Technical Design Report, CERN-LHCC-97-32.
[43] D. Acosta, et al., CMS Collaboration, The CMS Physics Technical Design Report, vol. 1, Section 11.5: Missing transverse energy, CERN/LHCC vols. 2006–001, 2006, CMS TDR 8.1.
[44] A.L. Read, Modified frequentist analysis of search results (The CL(s) method), CERN-OPEN-2000-205.
[45] R. Barate, et al., LEP Working Group for Higgs boson searches, Phys. Lett. B 565 (2003) 61, hep-ex/0306033.
[46] M. Kadastik, M. Raidal, L. Rebane, in preparation.

IV

.

B. C. Allanach *et al.*
"Les Houches 'physics at TeV colliders 2005' beyond the standard model working group: Summary report."
(2006) [arXiv:hep-ph/0602198].

LES HOUCHES "PHYSICS AT TEV COLLIDERS 2005" BEYOND THE STANDARD MODEL WORKING GROUP: SUMMARY REPORT

B.C. Allanach[1], **C. Grojean**[2,3], **P. Skands**[4], *E. Accomando*[5], *G. Azuelos*[6,7], *H. Baer*[8], *C. Balázs*[9], *G. Bélanger*[10], *K. Benakli*[11], *F. Boudjema*[10], *B. Brelier*[6], *V. Bunichev*[12], *G. Cacciapaglia*[13], *M. Carena*[4], *D. Choudhury*[14], *P.-A. Delsart*[6], *U. De Sanctis*[15], *K. Desch*[16], *B.A. Dobrescu*[4], *L. Dudko*[12], *M. El Kacimi*[17], *U. Ellwanger*[18], *S. Ferrag*[19], *A. Finch*[20], *F. Franke*[21], *H. Fraas*[21], *A. Freitas*[22], *P. Gambino*[5], *N. Ghodbane*[3], *R.M. Godbole*[23], *D. Goujdami*[17], *Ph. Gris*[24], *J. Guasch*[25], *M. Guchait* [26], *T. Hahn*[27], *S. Heinemeyer*[28], *A. Hektor*[29], *S. Hesselbach*[30], *W. Hollik*[27], *C. Hugonie*[31], *T. Hurth*[3,32], *J. Idárraga*[6], *O. Jinnouchi*[33], *J. Kalinowski*[34], *J.-L. Kneur*[31], *S. Kraml*[3], *M. Kadastik*[29], *K. Kannike*[29], *R. Lafaye*[3,35], *G. Landsberg*[36], *T. Lari*[15], *J. S. Lee*[37], *J. Lykken*[4], *F. Mahmoudi*[38], *M. Mangano*[3], *A. Menon*[9,39], *D.J. Miller*[40], *T. Millet* [41], *C. Milstène*[4], *S. Montesano*[15], *F. Moortgat*[3], *G. Moortgat-Pick*[3], *S. Moretti*[42,43], *D.E. Morrissey*[44], *S. Muanza*[4,41,45], *M.M. Muhlleitner*[3,10], *M. Müntel*[29], *H. Nowak*[46], *T. Ohl*[21], *S. Peñaranda*[3], *M. Perelstein*[13], *E. Perez*[46,47], *S. Perries*[41], *M. Peskin*[31], *J. Petzoldt*[20], *A. Pilaftsis*[48], *T. Plehn*[27,49], *G. Polesello*[50], *A. Pompoš*[51], *W. Porod*[52], *H. Przysiezniak*[35], *A. Pukhov*[53], *M. Raidal*[29], *D. Rainwater*[54], *A.R. Raklev*[55], *J. Rathsman*[30], *J. Reuter*[56], *P. Richardson*[57], *S.D. Rindani*[58], *K. Rolbiecki*[34], *H. Rzehak*[59], *M. Schumacher*[60], *S. Schumann*[61], *A. Semenov*[62], *L. Serin*[45], *G. Servant*[2,3], *C.H. Shepherd-Themistocleous*[42], *S. Sherstnev*[53], *L. Silvestrini*[63], *R.K. Singh*[23], *P. Slavich*[10], *M. Spira*[59], *A. Sopczak*[20], *K. Sridhar*[26] *L. Tompkins*[45,64], *C. Troncon*[15], *S. Tsuno*[65], *K. Wagh*[23], *C.E.M. Wagner*[9,39], *G. Weiglein*[57], *P. Wienemann*[16], *D. Zerwas*[45], *V. Zhukov*[66,67].

Editors of proceedings in bold
convenor of *Beyond the Standard Model* working group
[1] DAMTP, CMS, Wilberforce Road, Cambridge, CB3 0WA, UK
[2] SPhT, CEA-Saclay, Orme des Merisiers, F-91191 Gif-sur-Yvette Cedex, France
[3] Physics Department, CERN, CH-1211 Geneva 23, Switzerland
[4] Fermilab (FNAL), PO Box 500, Batavia, IL 60510, USA
[5] INFN, Sezione di Torino and Università di Torino, Dipartimento di Fisica Teorica, Italy
[6] Université de Montréal, Canada
[7] TRIUMF, Vancouver, Canada
[8] Department of Physics, Florida State University, Tallahassee, FL 32306, USA
[9] HEP Division, Argonne National Laboratory, 9700 Cass Ave., Argonne, IL 60449, USA
[10] LAPTH, 9 Chemin de Bellevue, B.P. 110, Annecy-le-Vieux 74941, France
[11] LPTHE, Universités de Paris VI et VII, France
[12] Moscow State University, Russia
[13] Institute for High Energy Phenomenology, Cornell University, Ithaca, NY 14853, USA
[14] Department of Physics and Astrophysics, University of Delhi, Delhi 110 007, India
[15] Università di Milano - Dipartimento di Fisica and Istituto Nazionale di Fisica Nucleare - Sezione di Milano, Via Celoria 16, I-20133 Milan, Italy
[16] Albert-Ludwigs Universität Freiburg, Physikalisches Institut, Hermann-Herder Str. 3, D-79104 Freiburg, Germany
[17] Université Cadi Ayyad, Faculté des Sciences Semlalia, B.P. 2390, Marrakech, Maroc

[18] LPT, Université de Paris XI, Bât. 210, F-91405 Orsay Cedex, France
[19] Department of Physics, University of Oslo,Oslo, Norway
[20] Lancaster University, Lancaster LA1 4YB, UK
[21] Institut für Theoretische Physik und Astrophysik, Universität Würzburg, Germany
[22] Institute for Theoretical Physics, Univ. of Zurich, CH-8050 Zurich, Switzerland
[23] Indian Institute of Science, IISc, Bangalore, 560012, India
[24] LPC Clermont-Ferrand, Université Blaise Pascal, France
[25] Departament d'Estructura i Constituents de la Matèria, Facultat de Física, Universitat de Barcelona, Diagonal 647, E-08028 Barcelona, Catalonia, Spain
[26] Tata Institute of Fundamental Research, Homi Bhabha Road, Mumbai 400005, India
[27] MPI für Physik, Werner-Heisenberg-Institut, D–80805 München, Germany
[28] Depto. de Física Teórica, Universidad de Zaragoza, 50009 Zaragoza, Spain
[29] National Institute of Chemical Physics and Biophysics, Ravala 10, Tallinn 10144, Estonia
[30] High Energy Physics, Uppsala University, Box 535, S-751 21 Uppsala, Sweden
[31] LPTA, UMR5207-CNRS, Université Montpellier II, F-34095 Montpellier Cedex 5, France
[32] SLAC, Stanford University, Stanford, California 94409 USA
[33] Physics Div. 2, Institute of Particle and Nuclear Studies, KEK, Tsukuba Japan
[34] Instytut Fizyki Teoretycznej, Uniwersytet Warszawski, PL-00681 Warsaw, Poland
[35] LAPP, 9 Chemin de Bellevue, B.P. 110, Annecy-le-Vieux 74941, France
[36] Brown University, Providence, Rhode Island, USA
[37] CTP, School of Physics, Seoul National University, Seoul 151-747, Korea
[38] Physics Department, Mount Allison University, Sackville NB, E4L 1E6 Canada
[39] Enrico Fermi Institute, University of Chicago, 5640 S. Ellis Ave., Chicago, IL 60637, USA
[40] Department of Physics and Astronomy, University of Glasgow, Glasgow G12 8QQ, UK
[41] IPN Lyon, 69622 Villeurbanne, France
[42] School of Physics and Astronomy, University of Southampton, SO17 1BJ, UK
[43] Particle Physics Division, Rutherford Appleton Laboratory, Oxon OX11 0QX, UK
[44] Department of Physics, University of Michigan, Ann Arbor, MI 48109, USA
[45] LAL, Université de Paris-Sud, Orsay Cedex, France
[46] Deutsches Elektronen-Synchrotron DESY, D–15738 Zeuthen, Germany
[47] SPP, DAPNIA, CEA-Saclay, F-91191 Gif-sur-Yvette Cedex, France
[48] School of Physics and Astronomy, University of Manchester, Manchester M13 9PL, UK
[49] University of Edinburgh, GB
[50] INFN, Sezione di Pavia, Via Bassi 6, I-27100 Pavia, Italy
[51] University of Oklahoma, USA
[52] Instituto de Física Corpuscular, C.S.I.C., València, Spain
[53] Skobeltsyn Inst. of Nuclear Physics, Moscow State Univ., Moscow 119992, Russia
[54] Dept. of Physics and Astronomy, University of Rochester, NY, USA
[55] Dept. of Physics and Technology, University of Bergen, N-5007 Bergen, Norway
[56] DESY Theory Group, Notkestr. 85, D-22603 Hamburg, Germany
[57] IPPP, University of Durham, Durham DH1 3LE, UK
[58] Physical Research Laboratory, Ahmedabad, India
[59] Paul Scherrer Institut, CH–5232 Villigen PSI, Switzerland
[60] Zweites Physikalisches Institut der Universität, D-37077 Göttingen, Germany
[61] Institute for Theoretical Physics, TU Dresden, 01062, Germany
[62] Joint Institute for Nuclear Research (JINR), 143980, Dubna, Russia
[63] INFN, Sezione di Roma and Università di Roma "La Sapienza", I-00185 Rome, Italy

[64] University of California, Berkeley, USA
[65] Department of Physics, Okayama University, Okayama, 700-8530, Japan
[66] IEKP, Universität Karlsruhe (TH), P.O. Box 6980, 76128 Karlsruhe, Germany
[67] SINP, Lomonosov Moscow State University, 119992 Moscow , Russia

Abstract
The work contained herein constitutes a report of the "Beyond the Standard Model" working group for the Workshop "Physics at TeV Colliders", Les Houches, France, 2–20 May, 2005. We present reviews of current topics as well as original research carried out for the workshop. Supersymmetric and non-supersymmetric models are studied, as well as computational tools designed in order to facilitate their phenomenology.

Acknowledgements

We would like to heartily thank the funding bodies, organisers, staff and other participants of the Les Houches workshop for providing a stimulating and lively environment in which to work.

Part 28

Testing the Littlest Higgs model in Φ^{++} pair production at LHC

A. Hektor, M. Kadastik, K. Kannike, M. Müntel and M. Raidal

Abstract

Motivated by predictions of the littlest Higgs model, we carry out a Monte Carlo study of doubly charged Higgs pair production in a typical LHC experiment. We assume additionally that triplet Higgs also generates the observed neutrino masses which fixes the Φ^{++} leptonic branching ratios. This allows to test neutrino mass models at LHC. We have generated and analyzed the signal as well as the background processes for both four muon and two muon final states. Studying the invariant mass distribution of the like-sign muon pairs allows to discover the doubly charged Higgs with the mass $M_\Phi = 1050$ GeV. Relaxing the neutrino mass assumption, and taking $BR(\Phi^{++} \to \mu^+\mu^+) = 1$, the LHC discovery reach increases to $M_\Phi = 1.2$ TeV

1. INTRODUCTION

The main motivation of the Large Hadron Collider (LHC) experiments is to reveal the secrets of electroweak symmetry breaking. If the standard model (SM) Higgs boson will be discovered, the question arises what stabilizes its mass against the Planck scale quadratically divergent radiative corrections. The canonical answer to this question is supersymmetry which implies very rich phenomenology of predicted sparticles in the future collider experiments.

More recently another possibility of formulating the physics of electroweak symmetry breaking, called the little Higgs, was proposed [458, 488, 522]. In those models the SM Higgs boson is a pseudo Goldstone mode of a broken global symmetry and remains light, much lighter than the other new modes of the model which have masses of order the symmetry breaking scale $\mathcal{O}(1)$ TeV. In order to cancel one-loop quadratic divergences to the SM Higgs mass a new set of heavy gauge bosons W', Z' with the SM quantum numbers identical to W Z, and a vectorlike heavy quark pair T, $\bar{T}$ with charge 2/3 must be introduced. Notice that those fields are put in by hand in order to construct a model with the required properties. However, the minimal model based on the $SU(5)/SO(5)$ global symmetry, the so-called littlest Higgs model [459], has a firm prediction from the symmetry breaking pattern alone: the existence of another $\mathcal{O}(1)$ TeV pseudo Goldstone boson Φ with the $SU(2)_L \times U(1)_Y$ quantum numbers $\Phi \sim (3, 2)$.

Interestingly, the existence of triplet Higgs Φ might also be required to generate Majorana masses to the left-handed neutrinos [523]. Non-zero neutrino masses and mixing is presently the only experimentally verified signal of new physics beyond the SM. In the triplet neutrino mass mechanism [524], which we assume in this work, the neutrino mass matrix is generated via

$$(m_\nu)_{ij} = (Y_\Phi)_{ij} v_\Phi, \tag{1}$$

where $(Y_\Phi)_{ij}$ are the Majorana Yukawa couplings of the triplet to the lepton generations $i, j = e, \mu, \tau$ which are described by the Lagrangian

$$L = i\bar{\ell}^c_{Li}\tau_2 Y^{ij}_\Phi(\tau\cdot\Phi)\ell_{Lj} + h.c., \tag{2}$$

and v_Φ is the effective vacuum expectation value of the neutral component of the triplet induced via the explicit coupling of Φ to the SM Higgs doublet H as $\mu\Phi^0 H^0 H^0$. Here μ has a dimension of mass. In the concept of seesaw $\mu \sim M_\Phi$, and the smallness of neutrino masses is attributed to the very high scale of triplet mass M_Φ via the smallness of $v_\Phi = \mu v^2/M^2_\Phi$, where $v = 174$ GeV. However, in the littlest Higgs model the triplet mass scale is $\mathcal{O}(1)$ TeV which alone cannot suppress v_Φ. Therefore in this model $\mu \ll M_\Phi$, which can be achieved, for example, via shining as shown in ref. [525, 526]. In that case $v_\Phi \sim \mathcal{O}(0.1)$ eV. We remind also that v_Φ contributes to the SM oblique corrections, and the precision data fit $\hat{T} < 2\cdot 10^{-4}$ [494] sets an upper bound $v_\Phi \leq 1.2$ GeV on that parameter.

The cross section of the single Φ^{++} production via the WW fusion process [527] $qq \to q'q'\Phi^{++}$ scales as $\sim v^2_\Phi$. In the context of the littlest Higgs model this process, followed by the decays $\Phi^{++} \to W^+W^+$, was studied in ref. [498, 500, 501]. The detailed ATLAS simulation of this channel shows [500] that in order to observe 1 TeV Φ^{++}, one must have $v_\Phi > 29$ GeV. This is in conflict with the precision physics bound $v_\Phi \leq 1.2$ GeV as well as with the neutrino data. Therefore the WW fusion channel is not experimentally promising for the discovery of the doubly charged Higgs.

In this work we perform a Monte Carlo analyses of the Drell-Yan pair production [527, 528] $pp \to \Phi^{++}\Phi^{--}$ of the doubly charged Higgs boson followed by the leptonic decays $\Phi^{\pm\pm} \to 2\ell^\pm$ in a typical LHC experiment. We assume that neutrino masses come from the coupling to the triplet Higgs which fixes the Φ^{++} leptonic branching ratios. Due to the smallness of v_Φ we can neglect the decays to WW. The advantages of this process are the following.

1. The production cross section is known, it does not depend on the unknown model parameters.
2. The decay $\Phi^{++} \to \ell^+\ell^+$ is lepton number violating and allows to reconstruct Φ^{++} invariant mass from the same charged leptons rendering the SM background very small in the signal region.
3. The known neutrino mixing Eq.(1) predicts the branching ratios as $BR(\Phi^{++} \to \mu^+\mu^+) = BR(\Phi^{++} \to \tau^+\tau^+) = BR(\Phi^{++} \to \mu^+\tau^+) = 1/3$. We assume that neutrinos have a normal hierarchy which implies negligible decay rates to the electron final states.

We consider only the muon final states which are the easiest to observe at the LHC environment. We have generated the production process and the leptonic decays of $\Phi^{\pm\pm}$ as well as the relevant background processes using PYTHIA Monte Carlo generator [17], and analyzed both the $2\mu^+2\mu^-$ and $2\mu^\pm$ final states. We have used the default set of PYTHIA parameters (parton structure functions, gauge couplings etc.) except that we fix the Φ^{++} branching ratios via $Y^{\mu\mu}_\Phi = \sqrt{2}Y^{\mu\tau}_\Phi = Y^{\tau\tau}_\Phi = 1$. Rescaling of those couplings to satisfy data from the searches for lepton flavour violating processes [527, 529] does not affect our results. We also comment on the results of our analyses if this assumption is relaxed and $BR(\Phi^{++} \to \mu^+\mu^+) = 1$.

Process	N of expected events	$S1$ $p_T > 75\ (50)$ GeV	$S2$ $\eta < 2.5$	$S3$ $2\mu^+2\mu^-$
background				
$ZZ \to 2\mu^+2\mu^-$	177	12 (42)	9.5 (30)	0.7 (3.0)
$t\bar{t} \to 2\mu^+2\mu^-$	$1.3 \cdot 10^8$	$1.1 \cdot 10^4$ $(6 \cdot 10^4)$	$1 \cdot 10^4$ $(5.8 \cdot 10^4)$	0 (4.5)
$b\bar{b} \to 2\mu^+2\mu^-$	$2.8 \cdot 10^{10}$	$1.1 \cdot 10^4$ $(1.1 \cdot 10^5)$	$7.1 \cdot 10^3$ $(8.5 \cdot 10^4)$	0 (0)
signal				
$M_\Phi = 200$ GeV	$2 \cdot 10^4$	5849 (9182)	5340 (8129)	818 (1723)
$M_\Phi = 500$ GeV	512	298 (330)	287 (314)	81 (97)
$M_\Phi = 1000$ GeV	15	9.7 (10.1)	9.5 (9.8)	3.1 (3.3)

Table 1: The number of expected background and signal events for the integrated luminosity $300\ fb^{-1}$, and the number of $\Phi^{\pm\pm}$ candidates from the $2\mu^+2\mu^-$ final states passing each cut. For the signal events we have taken $BR(\Phi^{++} \to \mu^+\mu^+) = 1/3$.

2. FOUR MUON FINAL STATES

Considering the four muon final states $2\mu^+2\mu^-$ as the experimental signature for the process $pp \to \Phi^{++}\Phi^{--}$ we have reconstructed the invariant mass of two like-sign muons,

$$m_I^2 = (p_1^\pm + p_2^\pm)^2, \tag{3}$$

with the four-momentas $p_{1,2}$. Since the like-sign signal muons originate from the same doubly charged Higgs boson, the invariant mass peak will measure the Higgs mass, $m_I = M_\Phi$. The four muon signature is the cleanest and the most robust one. The background arises mostly from the Z^0Z^0, $b\bar{b}$, and $t\bar{t}$ production and their muonic decay. Because those particles are lighter than Φ (the present bound from Tevatron is $M_\Phi \geq 136$ GeV [530, 531]) the background muons must be softer and should not give an invariant mass peak. To enhance the signal over background we have applied three selection rules as follows. S1: all muons with transverse momentum smaller than 75 GeV (50 GeV) are neglected. The larger (smaller) p_T cut is appropriate for the heavier (lighter) Higgs boson. S2: only the muons with pseudorapidity $\eta < 2.5$ are detectable at CMS or ATLAS and only those are selected. S3: only the events with 2 positive and 2 negative muons are selected.

We have generated with PYTHIA Monte Carlo the datasets of $2.8 \cdot 10^7$ $b\bar{b}$, $t\bar{t}$ and 10^6 ZZ events for the background, and the datasets of $5 \cdot 10^5$ signal events with $M_\Phi = 200,\ 500,\ 1000$ GeV. We have applied the selection rules described above and rescaled the results taking into account the cross section of the particular process. In Table 1 we present the expected number of background and signal events as well as the numbers of $\Phi^{\pm\pm}$ candidates passing each selection rule. We assume the total integrated luminosity to be $300 fb^{-1}$. The most effective cut is the p_T cut and therefore applied first. As one can see, the background is almost eliminated, especially for the cut $p_T > 75$ GeV. In Fig. 1 we plot the histogram for the invariant mass distribution of the like-sign muons passing all the cuts for $M_\Phi = 200$ GeV and $M_\Phi = 500$ GeV. The SM background is represented by black dashed line and the signal by red solid line. For those values of M_Φ the significance $S/\sqrt{B}$ is huge.

For the mass $M_\Phi = 1$ TeV one expects only ~ 3 signal candidates although the total number of produced $\Phi^{\pm\pm}$ is 30. Strong signal suppression occurs is because the probability

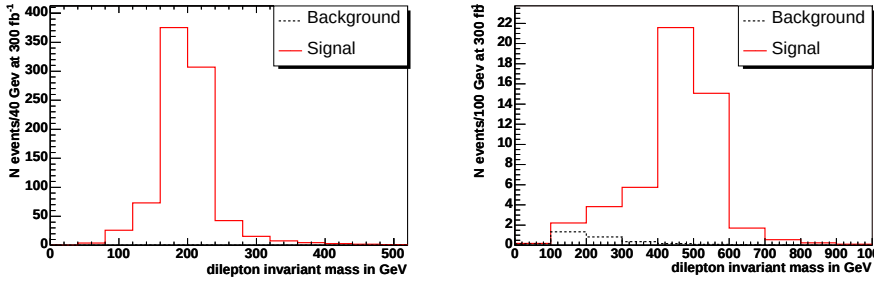

Figure 1: Distribution of the invariant mass of two like-sign muons after all cuts for the $2\mu^+2\mu^-$ final state in the case of $M_\Phi = 200$ GeV (left panel) and $M_\Phi = 500$ GeV (right panel) for $p_T > 75$ GeV. The background is almost invisible.

for both $\Phi^{\pm\pm}$ to decay to two muons is 1/9. The expected background is 0.7 (7.5) fake Higgs candidates depending on the p_T cut, but the background occurs at low invariant mass. Three Poisson distributed signal events with zero background at very high invariant mass constitutes the discovery of Φ^{++} at 95% C.L. However, if $BR(\Phi^{++} \to \mu^+\mu^+) = 1$ we expect to get 25.9 Higgs candidates for $M_\Phi = 1$ TeV. In this case the LHC mass reach extends up to 1.2 TeV.

3. TWO MUON FINAL STATES

In order to increase the LHC mass reach for $\Phi^{\pm\pm}$ discovery we also study the two like-sign muon final states. Although in this case one can identify more signal event candidates, also the background is larger. The dominant background processes giving $2\mu^\pm$ final states are listed in Table 2. Because the Monte Carlo generated data sets contain also additional muons from secondary processes we must also include the processes like $Z^0 \to \mu^+\mu^-$ to the background. Combining one of the Z decay products with the secondary muon we get the fake signal which has to be eliminated. The $t\bar{t}$, $b\bar{b}$, ZZ background and the signal datasets are the same as in the 4μ study, in addition we have generated new background datasets of 10^6 events.

To minimize the background we use the following selection rules. S1: event is counted only if it contains at least one like-sign muon pair. S2: event is rejected if it contains a quark with $p_T^{jet} > 20$ GeV. This corresponds to the jet veto and reduces the background from hadronic processes. S3: only muons with the pseudorapidity $\eta < 2.5$ are observable in CMS or ATLAS experiments. S4: we require an opening angle between the two like-sign muons to be $\phi < 2.5$. S5: only muons with $p_T > 50$ GeV are taken and the events with at least one like-sign muon pair are selected. The number of events passing each selection rule are given in Table 2. The total number of estimated background is 26 events which is larger than in the four muon case. But also the signal is more prominent.

To see the invariant mass distribution of the like-sign muons we plot in Fig. 2 the histograms for the signal (red solid) and background (dashed black) for $M_\Phi = 500$ GeV (left panel) and $M_\Phi = 1000$ GeV (right panel). As one can see, the invariant mass of background muons is smaller than the one of signal. Taking only the events with invariant mass $m_I > 300$ GeV one can get background free experimental signal of Φ^{++}. In this channel the doubly charged Higgs with the mass $M_\Phi = 1050$ GeV can be discovered. Again, if $BR(\Phi^{++} \to \mu^+\mu^+) = 1$

Process	N expected	$S1$ $2\mu^{\pm}$	$S2$ $p_T^{jet} > 20$ GeV	$S3$ $\eta < 2.5$	$S4$ $\phi < 2.5$	$S5$ $p_T > 50$ GeV
background						
$b\bar{b}$	$2.8 \cdot 10^{10}$	$9.4 \cdot 10^{8}$	$2.6 \cdot 10^{7}$	$2.5 \cdot 10^{6}$	$1.2 \cdot 10^{6}$	0
$t\bar{t}$	$1.3 \cdot 10^{8}$	$1.4 \cdot 10^{7}$	$3.6 \cdot 10^{5}$	$1.7 \cdot 10^{5}$	$1 \cdot 10^{5}$	4.4
WW	$2.7 \cdot 10^{4}$	1022	885	335	204	0
WZ	106	111	110	62	35	1.7
$Z \to 2\mu$	$1.5 \cdot 10^{7}$	$8.6 \cdot 10^{5}$	$6.6 \cdot 10^{5}$	$2.6 \cdot 10^{5}$	$1.5 \cdot 10^{5}$	12.8
$Z \to 2\tau$	$2.5 \cdot 10^{6}$	$1.4 \cdot 10^{5}$	$1.1 \cdot 10^{5}$	$4.5 \cdot 10^{4}$	$2.6 \cdot 10^{4}$	0
ZZ	177	369	363	207	115	7.5
total						26.4
signal						
$M_\Phi = 200$ GeV	$2 \cdot 10^{4}$	$1.6 \cdot 10^{4}$	$1.6 \cdot 10^{4}$	$1.3 \cdot 10^{4}$	8513	5832
$M_\Phi = 500$ GeV	512	401	389	356	225	199
$M_\Phi = 1000$ GeV	15	11	11	10	6	5.7

Table 2: The number of expected background and signal events for the integrated luminosity 300 fb^{-1}, and the number of $\Phi^{\pm\pm}$ candidates from the $2\mu^{\pm}$ final states passing each cut. For the signal events we have taken $BR(\Phi^{++} \to \mu^{+}\mu^{+}) = 1/3$.

we expect to get 15.9 Higgs candidates instead of 5.7, and LHC can reach 1.1 TeV Φ^{++}.

4. CONCLUSIONS

We have carried out Monte Carlo study of doubly charged Higgs pair production followed by the leptonic decays at the LHC experiments. Since the single Φ^{++} production is strongly suppressed, this is the only potentially observable channel at LHC. In addition, we have assumed that triplet Higgs also generates the observed neutrino masses which fixes the Φ^{++} leptonic decay branching ratios from neutrino data. We have generated the signal as well as the background processes for both four muon and two muon final states with PYTHIA Monte Carlo, and analyzed how to reduce maximally the SM background. Our results are plotted in Fig. 1 and Fig. 2 which show that the invariant mass distribution of the like-sign muon pairs allows to discover the doubly charged Higgs with the mass $M_\Phi = 1050$ GeV. Relaxing our assumption about branching ratios, and assuming $BR(\Phi^{++} \to \mu^{+}\mu^{+}) = 1$, the LHC discovery reach for Φ^{++} increases to $M_\Phi = 1.2$ TeV

Our results can be improved by including the tau-lepton reconstruction to the analyses. The background can further be reduced via vetoing the b-tagged events and by reconstructing Z and t, and neglecting leptons from their decays. Nevertheless, since the signal is so robust and clean, our results show that this is not necessary for $M_\Phi < 1$ TeV.

Acknowledgements

We thank S. Lehti, A. Nikitenko and A. Strumia for useful discussions and for the technical advice. This work is partially supported by ESF grant No 6140, by EC I3 contract No 026715 and by the Estonian Ministry of Education and Research. The calculations are performed in Estonian Grid [532] and Baltic Grid.

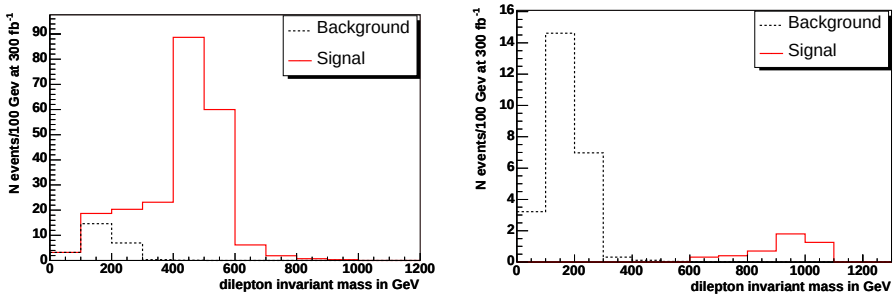

Figure 2: Distribution of the invariant mass of two like-sign muons passing all the cuts for the $2\mu^{\pm}$ final state in the case of $M_{\Phi} = 500$ GeV (left panel) and $M_{\Phi} = 1000$ GeV (right panel).

V

.

A. Hektor, M. Kadastik, K. Kannike, M. Müntel, M. Raidal
"Studying doubly charged Higgs pair production at the LHC."
Estonian Acad. Sci. Phys. Math. **55(2)** (2006) 128.

Proc. Estonian Acad. Sci. Phys. Math., 2006, **55**, 2, 128–136

Studying doubly charged Higgs pair production at the LHC

Andi Hektor, Mario Kadastik, Kristjan Kannike, Mait Müntel, and Martti Raidal

National Institute of Chemical Physics and Biophysics, Rävala 10, 10143 Tallinn, Estonia; andi.hektor@cern.ch

Received 21 February 2006

Abstract. The little Higgs models predict a rich phenomenology for the future collider experiments. Our attention is focused on the littlest Higgs model. We carry out a Monte Carlo study of the doubly charged Higgs pair production ($pp \to \Phi^{++}\Phi^{--}$) in a typical LHC experiment. The branching ratios are fixed using an assumption that, in addition, the observed masses of the neutrinos are generated by triplet Higgs: BR($\Phi^{\pm\pm} \to \mu^{\pm}\mu^{\pm}$) = BR($\Phi^{\pm\pm} \to \mu^{\pm}\tau^{\pm}$) = BR($\Phi^{\pm\pm} \to \tau^{\pm}\tau^{\pm}$) = $1/3$. We study the invariant mass distribution of same-charged muon pairs ($\Phi^{\pm\pm} \to 2\mu^{\pm\pm}$) together with the background processes from the standard model: $b\bar{b}$, $t\bar{t}$, and ZZ production. To suppress the background, we propose a new type of selection rule, suitable in the case of production of the pairs of equal mass particles ($\Phi^{\pm\pm}$). This selection rule ensures high significance of the signal over the background of the standard model and implies very small cut of the signal under study. At the Monte Carlo level the doubly charged Higgs can be visible at the LHC in the mass range up to approximate 1 TeV.

Key words: little Higgs models, triplet Higgs, neutrino physics, LHC physics.

1. INTRODUCTION

The main motivation for the Large Hadron Collider (LHC) experiment is to reveal the secrets of electroweak symmetry breaking. Still, after the possible discovery of the standard model (SM) Higgs boson, a question will arise: what stabilizes Higgs mass against the Planck scale quadratically divergent radiative corrections? An answer to that question could be supersymmetry, which implies a very rich phenomenology of predicted s-particles in the future collider experiments. However, recently another possibility of formulating the physics of electroweak symmetry breaking, so-called the little Higgs, was proposed [$^{1-3}$].

In the little Higgs models the SM Higgs boson is a pseudo Goldstone mode of a broken global symmetry and it remains light. It is much lighter than the other new modes of the model which have masses of order the symmetry breaking scale $\mathcal{O}(1)$ TeV. In order to cancel one-loop quadratic divergences to the SM Higgs mass, a new set of heavy gauge bosons W', Z' with the SM quantum numbers identical to W, Z, and a vector-like heavy quark pair T, $\bar{T}$ with charge 2/3 must be introduced. Notice that those fields are put in by hand in order to construct a model with the required properties. However, the minimal model, so-called littlest Higgs model based on the $SU(5)/SO(5)$ global symmetry, has a firm prediction from the symmetry breaking pattern alone: the existence of another $\mathcal{O}(1)$ TeV pseudo Goldstone boson Φ with the $SU(2)_L \times U(1)_Y$ quantum numbers $\Phi \sim (3, 2)$ [4].

Another important and yet open question in particle physics is the mechanism for providing the masses of neutrinos. The discussions lasted many decades and were finalized with the experimental improvement of the neutrino oscillations at the beginning of this millennium [5−7]. Interestingly, the existence of triplet Higgs Φ might also be required to generate Majorana masses to the left-handed neutrinos [8]. Nonzero neutrino masses and the mixing of neutrinos is the only experimentally well verified signal about the unknown physics beyond the SM. In the triplet neutrino mass mechanism [9], which we assume in this work, the neutrino mass matrix is generated via

$$(m_\nu)_{ij} = (Y_\Phi)_{ij} v_\Phi, \tag{1}$$

where $(Y_\Phi)_{ij}$ are the Majorana Yukawa couplings of the triplet to the lepton generations $i, j = e, \mu, \tau$, which are described by the Lagrangian

$$L = i\bar{\ell}^c_{Li}\tau_2 Y_\Phi^{ij}(\tau \cdot \Phi)\ell_{Lj} + h.c., \tag{2}$$

and v_Φ is the effective vacuum expectation value of the neutral component of the triplet induced via the explicit coupling of Φ to the SM Higgs doublet H as $\mu\Phi^0 H^0 H^0$. Here μ has dimension of mass.

In the concept of seesaw $\mu \sim M_\Phi$ and the smallness of neutrino masses is attributed to the very high scale of triplet mass M_Φ via the smallness of $v_\Phi = \mu v^2/M_\Phi^2$, where $v = 174$ GeV. However, in the littlest Higgs model the triplet mass scale is $\mathcal{O}(1)$ TeV, which alone cannot suppress v_Φ. Therefore in this model $\mu \ll M_\Phi$, which can be achieved, for example, via shining as shown by Ma et al. [10,11]. In that case $v_\Phi \sim \mathcal{O}(0.1)$ eV. We also remind that v_Φ contributes to the SM oblique corrections, and the precision data fit $\hat{T} < 2 \times 10^{-4}$ [12] sets an upper bound $v_\Phi \leq 1.2$ GeV on that parameter.

The cross section of the single $\Phi^{\pm\pm}$ production via the WW fusion process [13] $qq \rightarrow q'q'\Phi^{\pm\pm}$ scales as $\sim v_\Phi^2$. In the context of the littlest Higgs model this process, followed by the decays $\Phi^{\pm\pm} \rightarrow W^\pm W^\pm$, was studied in the papers [14−16]. The detailed ATLAS simulation of this channel shows [16] that in order to observe 1 TeV $\Phi^{\pm\pm}$, one must have $v_\Phi > 29$ GeV. This is in conflict

with the precision physics bound $v_\Phi \leq 1.2$ GeV as well as with the neutrino data. Therefore the WW fusion channel is not experimentally promising for the discovery of the doubly charged Higgs.

In this work we perform a Monte Carlo analysis of the Drell-Yan pair production [13,17] $pp \to \Phi^{++}\Phi^{--}$ of the doubly charged Higgs boson followed by the leptonic decays $\Phi^{\pm\pm} \to 2\ell^\pm$ in a typical LHC experiment. We assume that neutrino masses come from the coupling to the triplet Higgs, which fixes the $\Phi^{\pm\pm}$ leptonic branching ratios. Due to the smallness of v_Φ, we can neglect the decays to WW. The advantages of this process are the following:

1. For all practical purposes the production cross section is well predicted; its independence on the model-dependent unknown parameters can be neglected.
2. The decay $\Phi^{\pm\pm} \to \ell^\pm\ell^\pm$ is lepton number violating and allows reconstruction of $\Phi^{\pm\pm}$ invariant mass from the same charged leptons rendering the SM background very small in the signal region. Therefore it should provide a very clean detectable signature for the LHC detectors.
3. The known neutrino mixing Eq. (1) predicts the branching ratios as $\mathrm{BR}(\Phi^{\pm\pm} \to \mu^\pm\mu^\pm) = \mathrm{BR}(\Phi^{\pm\pm} \to \tau^\pm\tau^\pm) = \mathrm{BR}(\Phi^{\pm\pm} \to \mu^\pm\tau^\pm) = 1/3$. Here we assume that neutrinos have a normal hierarchy, which implies negligible decay rates to the electron final states.

In the current study we consider only the muon final states, which are the easiest to observe at the LHC environment. For example, the Compact Muon Solenoid (CMS) is optimized for muon signals and the discovery rate of energetic muons ($p_T > 2$ GeV and $|\eta| < 2.4$, where p_T is transfer momentum) is close to 95% [18].

We have generated the production process and the leptonic decays of $\Phi^{\pm\pm}$ as well as the relevant background processes using the PYTHIA Monte Carlo generator [19]. We focus our study on the $2\mu^+2\mu^-$ final states as it is a very characteristic signature compared to the SM signatures. We use the default set of parameters (parton structure functions, gauge couplings, etc.) from CMS CMKIN [18], except that we fix the $\Phi^{\pm\pm}$ branching ratios via $Y_\Phi^{\mu\mu} = \sqrt{2}Y_\Phi^{\mu\tau} = Y_\Phi^{\tau\tau} = 0.01$. Rescaling those couplings to satisfy data from the searches for lepton flavour violating processes [13,20] does not affect our results. We also comment on the results of our analyses if this assumption is relaxed and $\mathrm{BR}(\Phi^{\pm\pm} \to \mu^\pm\mu^\pm) = 1$.

2. SELECTION CRITERIA FOR THE $2\mu^+2\mu^-$ SIGNATURE

Considering the four muon final states $2\mu^+2\mu^-$ as the experimental signature for the process $pp \to \Phi^{++}\Phi^{--}$, we have reconstructed the invariant mass of two like-sign muons,

$$(m_I^{\pm\pm})^2 = (p_1^\pm + p_2^\pm)^2, \tag{3}$$

with the four-momentas $p_{1,2}$ of muons. Since the like-sign signal muons originate from the same doubly charged Higgs boson, the invariant mass peak will measure the Higgs mass, $m_I = M_\Phi$. The four-muon signature is the cleanest and the most

robust one. In addition, as the doubly charged Higgs is produced in pairs, we can use some unique selection techniques described below.

The background arises mostly from the ZZ, $b\bar{b}$, and $t\bar{t}$ production and their muonic decay. Because those particles are lighter than Φ (the present bound from Tevatron is $M_\Phi \geq 136$ GeV [21,22]), the background muons must have smaller p_T and it should not give an invariant mass peak. In addition, a self-generated low background process exists: if the branching ratio allows $\Phi^{\pm\pm} \to \tau^\pm\tau^\pm$ decay, then we get some soft energy muons from the τ decay (the branching ratio $\tau \to \mu$ is approximately 20%).

We have applied four selection rules for our Monte Carlo generated particle data:

S1: Only the muons with pseudorapidity $|\eta| < 2.4$ are detectable in the typical LHC detector, for example CMS [18]. Therefore, only the particles with $|\eta| < 2.4$ are selected from our Monte Carlo generation.

S2: All muons with transfer momentum $p_T < 25$ GeV are neglected.

S3: Only the events with at least two positive and two negative muons, so-called $2\mu^+2\mu^-$ events, are selected. The charge misidentification rate is very low for the LHC detectors as mentioned above.

S4: We require that both invariant masses in the pair production event be approximately equal. For this selection rule we have considered two different values of the cuts: (1) a wider one, $0.5 < m_I^{++}/m_I^{--} < 1.5$ and (2) a more restrictive one, $0.9 < m_I^{++}/m_I^{--} < 1.1$, where $m_I^{\pm\pm}$ is the invariant mass of the same charged muons.

The selection rule S1 is applied first as it is a natural restriction of the real detectors at the LHC. The restriction of the detectors suppresses mainly the soft energy background as it is more boosted. The S2 filter rules out all soft background particles and saves computational resources for the next steps of the analyses. The S3 rule is natural if we are looking for two doubly charged Higgs bosons with the opposite charges and we have a high charge identification rate (0.95). The final rule, S4, is based on the fact that the invariant masses of the same charged muon pairs have to be equal in the case of pair production of doubly charged Higgs boson. Naturally, some freedom is needed in the last condition due to decay width and experimental error of the detector. Therefore, we applied the two versions of the rule S4, marked below as $\mathrm{S4}_1$ and $\mathrm{S4}_2$.

3. MONTE CARLO ANALYSES

We have generated with PYTHIA Monte Carlo the data-sets of 2.8×10^7 $b\bar{b}, t\bar{t}$ and 10^6 ZZ events for the background, and the data-sets of 5×10^5 signal events with $M_\Phi = 200, 500, 1000$ GeV. We have applied the selection rules described above and rescaled the results taking into account the cross section of the particular process. The cross sections have been taken from the paper [19]. In Table 1 we present the expected number of background and signal events, as well

as the numbers of $\Phi^{\pm\pm}$ candidates ($2\mu^+2\mu^-$ events) in total and in the detector ($|\eta| < 2.4$). We assume the total integrated luminosity of the LHC to be $300 fb^{-1}$.

Table 2 describes the effect of the different selection rules. As one can see, after the last selection S4 the background is almost eliminated around the invariant mass peaks. In Table 3 we present the final significances of the Higgs signal and

Table 1. The number of expected background and signal events for the integral luminosity of 300 fb^{-1}. In case of Higgs events a self-generated background with $2\mu^+2\mu^-$ final state exists, which originates from secondary tau decay to muons. So, the primary $2\mu^+2\mu^-$ events are given in brackets. For the signal events we have taken the following branching ratios: BR($\Phi^{\pm\pm} \to \mu^\pm\mu^\pm$) = BR($\Phi^{\pm\pm} \to \mu^\pm\tau^\pm$) = BR($\Phi^{\pm\pm} \to \tau^\pm\tau^\pm$) = $1/3$

Process	N of 4ℓ events	N of $2\mu^+2\mu^-$ events	N of $2\mu^+2\mu^-$ events in detector (S1: $\|\eta\| < 2.4$)
Background			
$t\bar{t}$	2.6×10^7	4.6×10^5	3.0×10^5
$b\bar{b}$	2.8×10^{10}	2.5×10^7	9.7×10^6
ZZ	2.1×10^4	5.8×10^3	2.3×10^3
Signal			
M_Φ = 200 GeV	23354	4045 (2593)	2416 (1797)
M_Φ = 500 GeV	596.4	102 (66.0)	75.6 (55.8)
M_Φ = 1000 GeV	16.75	2.9 (1.87)	2.26 (1.68)

Table 2. The number of $\Phi^{\pm\pm}$ candidates form $2\mu^+2\mu^-$ final states passing all the selection rules. The primary $2\mu^+2\mu^-$ events are given in brackets. For the signal the branching ratios are BR($\Phi^{\pm\pm} \to \mu^\pm\mu^\pm$) = BR($\Phi^{\pm\pm} \to \mu^\pm\tau^\pm$) = BR($\Phi^{\pm\pm} \to \tau^\pm\tau^\pm$) = $1/3$

Process	Number of invariant masses			
	No cut	$p_T > 25$	$S4_1$	$S4_2$
Energy range 100−300 GeV				
$t\bar{t} \to 2\mu^+2\mu^-$	17192	875	381	86
$b\bar{b} \to 2\mu^+2\mu^-$	20196	1009	0	0
$ZZ \to 2\mu^+2\mu^-$	1313	655	345	67
M_Φ = 200 GeV	4831 (3593)	3909 (3212)	3664 (3178)	3182 (2863)
Energy range 250−750 GeV				
$t\bar{t} \to 2\mu^+2\mu^-$	754	76.6	13.6	0
$b\bar{b} \to 2\mu^+2\mu^-$	0	0	0	0
$ZZ \to 2\mu^+2\mu^-$	172	81.5	26.6	3.0
M_Φ = 500 GeV	151 (112)	143 (111)	129 (109)	98 (96)
Energy range 500−1500 GeV				
$t\bar{t} \to 2\mu^+2\mu^-$	18.4	1.9	0	0
$b\bar{b} \to 2\mu^+2\mu^-$	0	0	0	0
$ZZ \to 2\mu^+2\mu^-$	21.7	10.6	1.7	0
M_Φ = 1000 GeV	4.52 (3.37)	4.37 (3.36)	3.87 (3.30)	2.91 (2.88)

Table 3. The significance and the percentage of invariant masses left after the selection process. The primary $2\mu^+2\mu^-$ events are given in brackets. For the signal the branching ratios are BR($\Phi^{\pm\pm} \to \mu^\pm\mu^\pm$) = BR($\Phi^{\pm\pm} \to \mu^\pm\tau^\pm$) = BR($\Phi^{\pm\pm} \to \tau^\pm\tau^\pm$) = $1/3$. N/A – not available

Process	Significance			Signal left after the selection, %		
	$p_T > 25$	S4$_1$	S4$_2$	$p_T > 25$	S4$_1$	S4$_2$
Total background	N/A			0.036	0.011	0.002
$M_\Phi = 200$ GeV	77.5	135.9	257.0	80.9 (89.3)	75.8 (88.4)	65.8 (79.6)
$M_\Phi = 500$ GeV	11.3	20.4	57.0	94.4 (98.9)	85.5 (97.2)	64.8 (85.9)
$M_\Phi = 1000$ GeV	1.2	2.9	∞	96.6 (99.7)	85.6 (97.8)	64.3 (85.4)

the final lefts of the background and Higgs signal after all the selection filters. The significance is defined as $S/\sqrt{B}$, where S and B are the numbers of the signal and background events. Figure 1 plots the histogram for the invariant mass distribution of the like-sign muons for $M_\Phi = 500$ GeV and $M_\Phi = 1000$ GeV. The darkest histogram marks the signal left after the full selection and the lightest histogram marks the signal in the detector ($|\eta| < 2.4$). For those values of M_Φ the significance is huge.

For the mass $M_\Phi = 1$ TeV one expects only $\sim$3 doubly charged Higgs candidates, although the total number of produced $\Phi^{\pm\pm}$ is $\sim$33. As BR($\Phi^{\pm\pm} \to \mu^\pm\mu^\pm$) = 1/3, the strong signal suppression occurs because the probability for both $\Phi^{\pm\pm}$ to decay to two muons is $(1/3)^2$ = 1/9. So, the probability to produce two or more Higgs pair events is about 40%. Thus, the LHC can reach the Φ mass close to 1 TeV. However, if BR($\Phi^{\pm\pm} \to \mu^\pm\mu^\pm$) = 1, we expect to get $\sim$26 Higgs candidates for $M_\Phi = 1$ TeV. In this case the LHC mass reach extends up to 1.2 TeV.

4. CONCLUSIONS

We have carried out Monte Carlo study of doubly charged Higgs boson pair production, followed by leptonic decays at the LHC experiments. Since the single $\Phi^{\pm\pm}$ production is strongly suppressed, this is the only potentially observable channel at the LHC. In addition, we have assumed that triplet Higgs also generates the observed neutrino masses, which fixes the $\Phi^{\pm\pm}$ leptonic decay branching ratios from neutrino data. We have generated the signal as well as the background processes for four muon final states with PYTHIA Monte Carlo, and analysed how to reduce maximally the SM background to reach maximum significance of the signal. Our results are plotted in Fig. 1, which show that the invariant mass distribution of the like-sign muon pairs allows discovery of the doubly charged Higgs with the mass close to $M_\Phi = 1$ TeV. Relaxing our assumption about branching ratios, and assuming BR($\Phi^{\pm\pm} \to \mu^\pm\mu^\pm$) = 1, the LHC discovery reach for $\Phi^{\pm\pm}$ increases to $M_\Phi = 1.2$ TeV

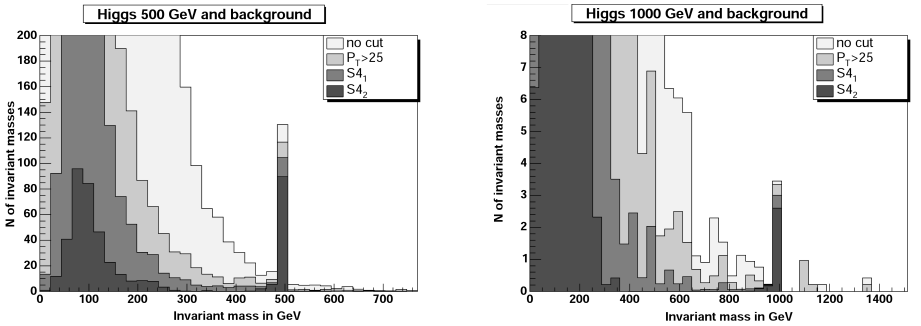

Fig. 1. Distribution of the invariant mass of two like-sign muons. The darkest histogram marks the signal after the full set of cuts for the $2\mu^+2\mu^-$ final state in the case of $M_\Phi = 500$ GeV and $M_\Phi = 1000$ GeV (the left and the right panel, respectively). The background is very low around the invariant mass peak of the Higgs signal. In addition to the standard model background, the small "tail" of the self-generated $\Phi \to \tau \to \mu$ background is visible at the smaller invariant mass region close to the Higgs mass peak. The lighter histograms mark the signal with less selections applied, as indicated in the figures.

Our results can be improved by including the tau-lepton reconstruction in the analyses. Alternatively, the background can further be reduced using some standard methods: vetoing the b-tagged events, by reconstructing Z and $t\bar{t}$, and neglecting leptons from their decays. In addition, the pair production gives some additional possibilities of constructing new selection rules. Nevertheless, since the signal is so robust and clean, our results show that this is not necessary for the region up to $M_\Phi < 1$ TeV.

ACKNOWLEDGEMENTS

We thank S. Lehti, A. Nikitenko, and A. Strumia for useful discussions and technical advice. This work is partially supported by grant No. 6140 of the Estonian Science Foundation, by EC I3 contract No. 026715, and by the Estonian Ministry of Education and Research. The calculations are performed in the Estonian Grid [23] and Baltic Grid.

REFERENCES

1. Arkani-Hamed, N., Cohen, A. G. and Georgi, H. (De)constructing dimensions. *Phys. Rev. Lett.*, 2001, **86**, 4757–4761.
2. Cheng, H.-C., Hill, C. T., Pokorski, S. and Wang, J. The standard model in the latticized bulk. *Phys. Rev.*, 2001, **D64**, 065007.
3. Arkani-Hamed, N., Cohen, A. G. and Georgi, H. Electroweak symmetry breaking from dimensional deconstruction. *Phys. Lett.*, 2001, **B513**, 232–240.

4. Arkani-Hamed, N., Cohen, A. G., Katz, E. and Nelson, A. E. The littlest Higgs. *JHEP*, 2002, **07**, 034.
5. Ashie, Y. et al. A measurement of atmospheric neutrino oscillation parameters by super-kamiokande i. *Phys. Rev.*, 2005, **D71**, 112005.
6. Aliu, E. et al. Evidence for muon neutrino oscillation in an accelerator-based experiment. *Phys. Rev. Lett.*, 2005, **94**, 081802.
7. Ahmed, S. N. et al. Measurement of the total active ^{8}B solar neutrino flux at the Sudbury Neutrino Observatory with enhanced neutral current sensitivity. *Phys. Rev. Lett.*, 2004, **92**, 181301.
8. Schechter, J. and Valle, J. W. F. Neutrino masses in $\mathrm{SU}(2) \times \mathrm{U}(1)$ theories. *Phys. Rev.*, 1980, **D22**, 2227–2235.
9. Ma, E. and Sarkar, U. Neutrino masses and leptogenesis with heavy Higgs triplets. *Phys. Rev. Lett.*, 1998, **80**, 5716–5719.
10. Ma, E., Raidal, M. and Sarkar, U. Verifiable model of neutrino masses from large extra dimensions. *Phys. Rev. Lett.*, 2000, **85**, 3769–3772.
11. Ma, E., Raidal, M. and Sarkar, U. Phenomenology of the neutrino-mass-giving Higgs triplet and the low-energy seesaw violation of lepton number. *Nucl. Phys.*, 2001, **B615**, 313–330.
12. Marandella, G., Schappacher, C. and Strumia, A. Little-Higgs corrections to precision data after CERN LEP2. *Phys. Rev.*, 2005, **D72**, 035014.
13. Huitu, K., Maalampi, J., Pietila, A. and Raidal, M. Doubly charged Higgs at LHC. *Nucl. Phys.*, 1997, **B487**, 27–42.
14. Han, T., Logan, H. E., McElrath, B. and Wang, L.-T. Phenomenology of the little Higgs model. *Phys. Rev.*, 2003, **D67**, 095004.
15. Han, T., Logan, H. E. and Wang, L.-T. 2005 Smoking-gun signatures of little Higgs models. http://arxiv.org/abs/hep-ph/0506313
16. Azuelos, G. et al. Exploring little Higgs models with atlas at the LHC. *Eur. Phys. J.*, 2005, **C39S2**, 13–24.
17. Gunion, J. F., Grifols, J., Mendez, A., Kayser, B. and Olness, F. I. Higgs bosons in left-right symmetric models. *Phys. Rev.*, 1989, **D40**, 1546.
18. Della Negra, M. et al. *CMS, the Muon Project: Technical Design Report*. CERN, 1997.
19. Sjostrand, T. et al. High-energy-physics event generation with PYTHIA 6.1. *Comput. Phys. Commun.*, 2001, **135**, 238–259.
20. Barenboim, G., Huitu, K., Maalampi, J. and Raidal, M. Constraints on doubly charged Higgs interactions at linear collider. *Phys. Lett.*, 1997, **B394**, 132–138.
21. Acosta, D. et al. Search for doubly-charged Higgs bosons decaying to dileptons in $p\bar{p}$ collisions at $\sqrt{s} = 1.96$ TeV. *Phys. Rev. Lett.*, 2004, **93**, 221802.
22. Abazov, V. M. et al. Search for doubly-charged Higgs boson pair production in the decay to $\mu^+\mu^+\mu^-\mu^-$ in $p\bar{p}$ collisions at $\sqrt{s} = 1.96$ TeV. *Phys. Rev. Lett.*, 2004, **93**, 141801.
23. Hektor, A., Anton, L., Kadastik, M., Skaburskas, K. and Teder, H. The first scientific results from the Estonian Grid. *Proc. Estonian Acad. Sci. Phys. Math.*, 2004, **54**, 111–127.

Topeltlaetud Higgsi bosoni paarissignaali uurimine LHC-eksperimendi juures

Andi Hektor, Mario Kadastik, Kristjan Kannike, Mait Müntel ja Martti Raidal

Nn väikesed Higgsi mudelid lubavad mitmekesist osakeste fenomenoloogiat tulevaste kiirendieksperimentide jaoks. Artiklis on uuritud võimalikke eksperi-

mentaalseid märke nn väikseima Higgsi mudeli poolt ennustatud nähtustest skaalal 0,2 kuni 1 TeV. Võimalike signatuuride uurimiseks on kasutatud meie poolt PYTHIA Monte Carlo generaatoriga toodetud andmeid, mis vastavad topeltlaetud Higgsi bosoni paaridele tüüpilise LHC-eksperimendi jaoks (prootonite kokkupõrge masskeskme energiaga ~ 14 TeV, integraalne luminositeet $300 fb^{-1}$). Selleks on fikseeritud topeltlaetud Higgsi erinevate lagunemiskanalite tõenäosused, kasutades meie poolt pakutud seost väikseima Higgsi mudeli ja neutriinode massimaatriksi vahel. Signatuure on hinnatud samamärgiliselt laetud müüonite paaride invariantsete masside põhjal ja seda koos standardmudelist pärit taustaprotsessidega. Kuna tegemist on topeltlaetud Higgsi paaride tekkimisega, siis saab taustaprotsesside mahasurumiseks rakendada mõningaid unikaalseid meetodeid. Tänu sellele võib signaali statistilist olulisust tunduvalt tõsta ja signatuuri on võimalik muuta nähtavaks kuni piirkonnani, kui Higgsi mass läheneb 1 TeV-ile.

CURRICULUM VITAE

Mait Müntel

Date and place of birth:	March 20, 1977, Tartu, Estonia
Citizenship:	Estonian
Maritial status:	Single
Address:	National Institute of Chemical Physics and Biophysics Akadeemia tee 23, 12618 Tallinn, Estonia
Phone:	(+372) 5554 2279
Fax:	(+372) 670 3662
E-mail:	maitm@cerh.ch

Education

1992-1995:	Miina Härma Gymnasium, Tartu, Estonia
2000:	BSc in physics (theoretical physics), University of Tartu
2002:	MSc in physics (theoretical physics), University of Tartu

Employement

1998-2000:	Teacher of physics, Secondary School of Rannu
2001-2003:	Teacher of physics, Lähte Ühisgümnaasium
2005-2006	Engineer, National Institute of Chemical Physics and Biophysic
2006-	Researcher, National Institute of Chemical Physics and Biophysic

Scientific work

Main fields of research: neutrino physics, new physics at LHC, leptogenesis

CURRICULUM VITAE in Estonian

Mait Müntel

Sünniaeg ja koht:	20. märts 1977, Tartu, Eesti
Kodakondsus:	Eesti
Perekonnaseis:	vallaline
Aadress:	Keemilise ja Bioloogilise Füüsika Instituut Akadeemia tee 23, 12618 Tallinn, Eesti
Telefon:	(+372) 5554 2279
Faks:	(+372) 670 3662
E-mail:	maitm@cern.ch

Haridus

1992-1995:	Miina Härma Gümnaasium
2000:	BSc füüsikas (teoreetiline füüsika), Tartu Ülikool
2002:	MSc füüsikas (teoreetiline füüsika), Tartu Ülikool

Teenistuskäik

1998-2000:	füüsika õpetaja, Rannu Keskkool
2001-2003:	füüsika õpetaja, Lähte Ühisgümnaasium
2005-2006	insener, Keemilise ja Bioloogilise Füüsika Instituut
2006-	teadur, Keemilise ja Bioloogilise Füüsika Instituut

Teadustegevus

Peamised töösuunad: neutriinofüüsika, standardmudeli järgne füüsika, CMS eksperiment (CERN LHC)

DISSERTATIONES PHYSICAE UNIVERSITATIS TARTUENSIS

1. **Andrus Ausmees.** XUV-induced electron emission and electron-phonon interaction in alkali halides. Tartu, 1991.
2. **Heiki Sõnajalg.** Shaping and recalling of light pulses by optical elements based on spectral hole burning. Tartu, 1991.
3. **Sergei Savihhin.** Ultrafast dynamics of F-centers and bound excitons from picosecond spectroscopy data. Tartu, 1991.
4. **Ergo Nõmmiste.** Leelishalogeniidide röntgenelektronemissioon kiiritamisel footonitega energiaga 70–140 eV. Tartu, 1991.
5. **Margus Rätsep.** Spectral gratings and their relaxation in some low-temperature impurity-doped glasses and chrystals. Tartu, 1991.
6. **Tõnu Pullerits.** Primary energy transfer in photosynthesis. Model calculations. Tartu, 1991.
7. **Olev Saks.** Attoampri diapasoonis voolude mõõtmise füüsikalised alused. Tartu, 1991.
8. **Andres Virro.** AlGaAsSb/GaSb heterostructure injection lasers. Tartu, 1991.
9. **Hans Korge.** Investigation of negative point discharge in pure nitrogen at atmospheric pressure. Tartu, 1992.
10. **Jüri Maksimov.** Nonlinear generation of laser VUV radiation for high-resolution spectroscopy. Tartu, 1992.
11. **Mark Aizengendler.** Photostimulated transformation of aggregate defects and spectral hole burning in a neutron-irradiated sapphire. Tartu, 1992.
12. **Hele Siimon.** Atomic layer molecular beam epitaxy of A^2B^6 compounds described on the basis of kinetic equations model. Tartu, 1992.
13. **Tõnu Reinot.** The kinetics of polariton luminescence, energy transfer and relaxation in anthracene. Tartu, 1992.
14. **Toomas Rõõm.** Paramagnetic H^{2-} and F^+ centers in CaO crystals: spectra, relaxation and recombination luminescence. Tallinn, 1993.
15. **Erko Jalviste.** Laser spectroscopy of some jet-cooled organic molecules. Tartu, 1993.
16. **Alvo Aabloo.** Studies of crystalline celluloses using potential energy calculations. Tartu, 1994.
17. **Peeter Paris.** Initiation of corona pulses. Tartu, 1994.
18. **Павел Рубин.** Локальные дефектные состояния в CuO_2 плоскостях высокотемпературных сверхпроводников. Тарту, 1994.
19. **Olavi Ollikainen.** Applications of persistent spectral hole burning in ultrafast optical neural networks, time-resolved spectroscopy and holographic interferometry. Tartu, 1996.
20. **Ülo Mets.** Methodological aspects of fluorescence correlation spectroscopy. Tartu, 1996.
21. **Mikhail Danilkin.** Interaction of intrinsic and impurity defects in CaS:Eu luminophors. Tartu, 1997.

22. **Ирина Кудрявцева.** Создание и стабилизация дефектов в кристаллах KBr, KCl, RbCl при облучении ВУФ-радиацией. Тарту, 1997.
23. **Andres Osvet.** Photochromic properties of radiation-induced defects in diamond. Tartu, 1998.
24. **Jüri Örd.** Classical and quantum aspects of geodesic multiplication. Tartu, 1998.
25. **Priit Sarv.** High resolution solid-state NMR studies of zeolites. Tartu, 1998.
26. **Сергей Долгов.** Электронные возбуждения и дефектообразование в некоторых оксидах металлов. Тарту, 1998.
27. **Kaupo Kukli.** Atomic layer deposition of artificially structured dielectric materials. Tartu, 1999.
28. **Ivo Heinmaa.** Nuclear resonance studies of local structure in $RBa_2Cu_3O_{6+x}$ compounds. Tartu, 1999.
29. **Aleksander Shelkan.** Hole states in CuO_2 planes of high temperature superconducting materials. Tartu, 1999.
30. **Dmitri Nevedrov.** Nonlinear effects in quantum lattices. Tartu, 1999.
31. **Rein Ruus.** Collapse of 3d (4f) orbitals in 2p (3d) excited configurations and its effect on the x-ray and electron spectra. Tartu, 1999.
32. **Valter Zazubovich.** Local relaxation in incommensurate and glassy solids studied by Spectral Hole Burning. Tartu, 1999.
33. **Indrek Reimand.** Picosecond dynamics of optical excitations in GaAs and other excitonic systems. Tartu, 2000.
34. **Vladimir Babin.** Spectroscopy of exciton states in some halide macro- and nanocrystals. Tartu, 2001.
35. **Toomas Plank.** Positive corona at combined DC and AC voltage. Tartu, 2001.
36. **Kristjan Leiger.** Pressure-induced effects in inhomogeneous spectra of doped solids. Tartu, 2002.
37. **Helle Kaasik.** Nonperturbative theory of multiphonon vibrational relaxation and nonradiative transitions. Tartu, 2002.
38. **Tõnu Laas.** Propagation of waves in curved spacetimes. Tartu, 2002.
39. **Rünno Lõhmus.** Application of novel hybrid methods in SPM studies of nanostructural materials. Tartu, 2002.
40. **Kaido Reivelt.** Optical implementation of propagation-invariant pulsed free-space wave fields. Tartu, 2003.
41. **Heiki Kasemägi.** The effect of nanoparticle additives on lithium-ion mobility in a polymer electrolyte. Tartu, 2003.
42. **Villu Repän.** Low current mode of negative corona. Tartu, 2004.
43. **Алексей Котлов.** Оксианионные диэлектрические кристаллы: зонная структура и электронные возбуждения. Tartu, 2004.
44. **Jaak Talts.** Continuous non-invasive blood pressure measurement: comparative and methodological studies of the differential servo-oscillometric method. Tartu, 2004.
45. **Margus Saal.** Studies of pre-big bang and braneworld cosmology. Tartu, 2004.

46. **Eduard Gerškevitš.** Dose to bone marrow and leukaemia risk in external beam radiotherapy of prostate cancer. Tartu, 2005.
47. **Sergey Shchemelyov.** Sum-frequency generation and multiphoton ionization in xenon under excitation by conical laser beams. Tartu, 2006.
48. **Valter Kiisk.** Optical investigation of metal-oxide thin films. Tartu, 2006.
49. **Jaan Aarik.** Atomic layer deposition of titanium, zirconium and hafnium dioxides: growth mechanisms and properties of thin films. Tartu, 2007.
50. **Astrid Rekker.** Colored-noise-controlled anomalous transport and phase transitions in complex systems. Tartu, 2007.
51. **Andres Punning.** Electromechanical characterization of ionic polymer-metal composite sensing actuators. Tartu, 2007.
52. **Indrek Jõgi.** Conduction mechanisms in thin atomic layer deposited films containing TiO_2. Tartu, 2007.
53. **Aleksei Krasnikov.** Luminescence and defects creation processes in lead tungstate crystals. Tartu, 2007.
54. **Küllike Rägo.** Superconducting properties of MgB_2 in a scenario with intra- and interband pairing channels. Tartu, 2008.
55. **Els Heinsalu.** Normal and anomalously slow diffusion under external fields. Tartu, 2008.
56. **Kuno Kooser.** Soft x-ray induced radiative and nonradiative core-hole decay processes in thin films and solids. Tartu, 2008.
57. **Vadim Boltrushko.** Theory of vibronic transitions with strong nonlinear vibronic interaction in solids. Tartu, 2008.
58. **Andi Hektor.** Neutrino Physics beyond the Standard Model. Tartu, 2008.
59. **Raavo Josepson.** Photoinduced field-assisted electron emission into gases. Tartu, 2008.
60. **Martti Pärs.** Study of spontaneous and photoinduced processes in molecular solids using high-resolution optical spectroscopy. Tartu, 2008.
61. **Kristjan Kannike.** Implications of neutrino masses. Tartu, 2008.
62. **Vigen Issahhanjan.** Hole and interstitial centres in radiation-resistant MgO single crystals. Tartu, 2008.
63. **Veera Krasnenko.** Computational modeling of fluorescent proteins. Tartu, 2008.